A Novel Real Time Charging Approach for Electric Vehicles in Smart Grids

by

Abdoulmenim Bilh

A thesis
presented to the University of Waterloo
in fulfillment of the
thesis requirement for the degree of
Doctor of Philosophy
in
Electrical and Computer Engineering

Waterloo, Ontario, Canada, 2017

Examining Committee Membership

The following served on the Examining Committee for this thesis. The decision of the Examining Committee is by majority vote.

External Examiner	NAME:	Hossam Gaber
	Title:	Professor
Co-Supervisor	NAME:	Sagar Naik
	Title:	Professor
Co-Supervisor	NAME:	Ramadan El-Shatshat
	Title:	Professor
Internal Member	NAME:	Kankar Bhattacharya
	Title:	Professor
Internal Member	NAME:	Pin-Han Ho
	Title:	Professor
Internal-external Member	NAME:	Ali Elkamel
	Title:	Professor

I hereby declare that I am the sole author of this thesis. This is a true copy of the thesis, including any required final revisions, as accepted by my examiners.

I understand that my thesis may be made electronically available to the public.

Abstract

Integration of renewable energy sources (RES) into electric grids comes with significant challenges. The produced energy from renewable sources such as wind and solar is intermittent, non-dispatchable, and uncertain. The uncertainty in the forecasted renewable energy will consequently impact the accuracy of the forecasted net-load in the system. That, in turn, will increase the difficulties for the grid operators to meet the demand-supply balance in the grids. Fortunately, electric vehicles (EVs) are considered as a flexible load in the electric grids. The flexibility is due to the fact that vehicles in general are parked for longer time than needed to charge them. This flexibility in the EVs' load can potentially be used to counter the variations in the net-load.

This thesis proposes a novel charging algorithm for EVs. The algorithm uses the flexibility of EVs in order to absorb the unexpected fluctuations in the net-load caused mainly by the stochastic behavior of RES; therefore, it reduces the dependency on the expensive operational reserve needed otherwise to deal with these fluctuations.

The dissertation starts by evaluating the impact of the RES on the short-term forecast of the net-load in the electric grid. A stochastic model for the net-load forecast error is developed. The model captures the behaviour of the net-load forecast error for different penetration levels of wind power.

Second, a novel charging algorithm for EVs in smart grids is proposed. Unlike traditional charging methods, this algorithm is designed to exploit the flexibility of the EVs' load to absorb the unforeseen fluctuations in the net-load caused mainly by the intermittency of the RES (wind energy). A comprehensive performance evaluation of the proposed algorithm against a traditional Ahead-of-Time charging algorithm shows clear improvements achieved by the proposed algorithm in absorbing the unexpected fluctuations in the net-load caused by different penetration levels of wind power.

Third, the algorithm used, further, to provide regulation services to the grid. An aggregator server uses binary on-off commands to guide the EVs in order to provide the regulation service as opposed to adjusting the charging rates of the EVs to any value between zero and the maximum charging rate in most of the other studies in the literature. A unidirectional regulation method has been used as a benchmark to show the superiority of our method. Further, to realistically represent the plug-in time and plug-off (deadline) time of the EVs, data from the US Department of Transportation (DOT) have been used in the testing scenarios.

Fourth, an important aspect of the proposed algorithm is the fast response to the need of the electric system either to counter the variation in the net-load in the distribution system or to provide regulation service to the grid. Therefore, the thesis precisely evaluates the expected time delay from the instant when an aggregator server sends a command to n EVs to the instant when all the EVs' responses are received successfully by the server. To

achieve this goal, two steps are taken: **i)** a realistic communication structure between the aggregator server and the EVs is considered. **ii)** The wireless link between the access point (AP) and the EVs is accurately modeled in order to estimate the average delay. The model is based on Markov chain representation for the wireless IEEE 802.11 MAC protocol. The model has been validated by means of extensive simulation using the well-known Network Simulator 2 (NS2) tool.

Acknowledgements

My thanks and praise first and foremost go to Almighty God, for giving me the knowledge, opportunity, and the strength to accomplish this work.

Along the way, several people deserve sincere recognition. I am most grateful to my advisors, Pro. Sagar Naik and Dr. Ramadan El-shatshat, for their incomparable guidance and patience over the past years. They have been great mentors and friends. Over the years, they have always been available to guide my research in the right direction. Their valuable advice, generous help and time, and constant support were the secret of achieving all this work.

I would like also to extend my appreciation and thanks to my thesis committee members, Prof. Ali Elkamel, Prof. Kankar Bhattacharya, and Prof. Pin-Han Ho for sparing their time to review this research work.

I would like to acknowledge the Ministry of Higher Education of Libya for financially supporting this research work. Thanks to this generous fund, this thesis was made possible.

I would like to thank my family for their continuous and unconditional support for all my endeavors. My father, Ahmed Beela, My mother, Mahajouba Ekhrais, and my brothers and sisters, Taher, Amena, Maalooma, Omar, Hamdi, Mohammed, Yusra, Aisha, and Muraad, have been the greatest supporters in my life. I am grateful to them for their unconditional love, support, encouragement and the sacrifices they made to help me. Cordial thanks go to my beloved wife, Najat, for the endless understanding, support, patience and care she showed during this hectic period in my career. Despite being extremely busy, she has always been available to uplift me when I felt down and to congratulate me when I achieved. I am by all means indebted to her.

Finally, I thank all my teachers, colleagues and friends who helped and supported me in different ways throughout my work. God bless you all.

Dedication

This thesis is dedicated to my beloved children, Fatima, Ahmed, and Ali
I love you all

Table of Contents

List of Figures

List of Tables

List of Abbreviations

ACK	Packet Acknowledgement
AGC	Automatic Generation Control
AP	Access Point
CAISO	California ISO
CCC	Committee on Climate Change
CIRA	Canadian Internet Registration Authority
DCF	Distributed Coordination Function
DIFS	Distributed InterFrame Space
DOT	Department of Transportation
EMS	Energy Management System
EV	Electric Vehicle
FERC	Federal Energy Regulation Commission
G2V	Grid to Vehicle
ISO	Independent System Operator
MAC	Medium Access Control
NS2	Network Simulator 2
PJM	Pennsylvania, Jersey, and Maryland ISO
POP	Preferred Operating Point
RES	Renewable Energy Sources
SIFS	Short InterFrame Space
TOU	Time Of Use
V2G	Vehicle to Grid

List of Symbols

C	Battery's nominal capacity, same capacity for all EVs.
C_i^r	Requested amount of energy by i^{th} EV.
$d_i(t)$	Time left from t to the deadline.
$dead_i$	Deadline time of i^{th} EV.
$D(n)$	Average delay, including the transient time, for transmitting the confirmation message when n stations compete on the channel.
$\overline{D(n)}$	Average delay, including the transient time, for transmitting the confirmation message when one broadcast packet is sent to n stations.
e_i	Time elapsed since start of charging.
$E(.)$	Expectation function.
$E[d(n)]$	Average delay for transmitting the confirmation message when n stations compete on the channel in saturation state.
$E[\#Slots]$	Average number of time slots before a successful transmission.
$E[SlotLen]$	Average length of time slots.
$E_i(t)$	The amount of energy still needed by i^{th} EV at time slot t.
E_n	The total requested amount of energy by n^{th} EV.
$F_i(t)$	Flexibility of i^{th} EV estimated at time t.
$G(t)$	The utility's preferred overall load profile.
$l_i(t)$	Time needed to continuously charge the i^{th} EV to full battery estimated at time t.
$\hat{L}(t)$	Expected load in the system at time slot t.
$L_c(t)$	Conventional load at time t.
$L_{EV}(t)$	EVs load in the system at time slot t.

$L_N(t)$	Net load at time t.
$L_R(t)$	Produced power from renewable energy sources at time t.
$L_{oa}(t)$	Overall load in the system, net-load plus EV's load, at time t.
$\hat{L}_{oa}(t)$	Expected overall load in the system, expected net-load plus the optimized EVs' load.
MAE	Mean Absolute Error.
$N(\mu, \sigma^2)$	Normal distribution with mean μ and standard deviation σ.
$\mathcal{N}$	Set of indices of all EVs, $\forall n \in \mathcal{N}$.
p	Probability of transmission failure.
p_e	Probability of packet error due to the wireless lossy environment .
p_c	Probability of packet collision.
p_s	Probability of transmission success.
$plug_i$	Plug-in time of i^{th} EV.
P_{tr}	Probability of having at least one transmission from the n stations.
$P_{s\|tr}$	Probability of success when there is a transmission attempt.
$Pr(c\|f)$	Probability that the transmission failure is caused by collision of data packets.
$Pr(Ack_l\|f)$	Probability that the transmission failure is caused by ACK loss.
$POP(t)$	Preferred Operating Point of the EVs load at time slot t.
r	Charging rate, measured in Watt.
$r_i(t)$	Charging profile of i^{th} EV.
$r_i^*(t)$	Optimum charging profile of i^{th} EV according to Ahead-of-Time optimization.
$Reg(t)$	The value of needed regulation at time slot t.
RTO	Retransmission Time Out.
RTT_{int}	Round Trip Time of the internet link.
s_i	Time left to stop charging of i^{th} EV.
SOC_i	State Of Charge of i^{th} EV at plug-in time.
$SOC_i(t)$	State Of Charge of i^{th} EV at time t.
T_s	The period of time the channel is occupied due to a successful transmission.

T_f	The period of time the channel is occupied due to an unsuccessful transmission.
T_{data}	The period of time the channel is occupied due to transmitting data packet.
$T_i(n_i)$	Average time spent in the transient stage i for number of n_i stations.
T_D	Average time delay from when the aggregator server sends a command till the server receives the confirmation messages from all EVs.
T_{oa}	The overall time needed to get all targeted EVs (stations) responding to the regulation signal.
$U(a, b)$	Uniform distribution in range a, b.
W_{min}	Minimum contention window size.
W_{max}	Maximum contention window size.
$\bar{X}$	Average value of $X(t)$ over period of time T.
$\hat{X}(t)$	Forecasted value of $X(t)$ at future time t.
ε	Net-load forecast error.
ε_c	Conventional load forecast error.
ε_R	Renewable energy forecast error.
ζ	Idle time at server side.
τ	Probability of transmit in any time slot.
δ	Tolerance before interruption mode is triggered by the server.
λ	Average service rate of charging EVs in (EV/second).

Chapter 1

Introduction

1.1 General

The negative environmental impact of burning fossil fuels to produce energy has been a strong motive to invest in cleaner alternative of energy sources such as wind and solar in the recent years. In 2012, electricity sector and transportation sector have been reported as the largest contributors to greenhouses gas emission in USA [3]. As shown in Figure 1.1, 60% of the whole greenhouses gas emission is produced by electricity and transportation sectors combined. Therefore, a significant decrease in the emission from these two sectors will lead to a significant decrease in the whole emission figure. To achieve that goal, smart grid has emerged as the next generation of power grid with more renewable energy sources replacing the current fossil fuels sources. The deployment of these renewable sources will, consequently, have a positive impact on the reduction of greenhouses gas emission in the current electric grid. However, integration of these renewable sources into the smart grid comes with significant challenges. The produced energy from these renewable sources is intermittent, non-dispatchable, and uncertain. The uncertainty of the forecasted renewable energy will, consequently, increase the difficulties for the grid operators to meet the demand-supply balance in the grid.

On the other hand, Electric Vehicles (EVs) have emerged as a promising solution for the pollution caused by transportation sector. The Committee on Climate Change (CCC) projected the global annual sales of EVs in 2030 to be 60% of all cars' sale [4]. EVs rely, partially or completely, on the electricity to run their engines. However, the need for repeated charging for the batteries of these EVs will introduce another challenge to the electric grid. EVs load could potentially increase the demand at peak periods, power loss in the distribution system, and the randomness in the overall load in the system [21,66,68,70]. Fortunately, this type of load (EVs load) is considered as *deferrable* load, thus, manageable [72].

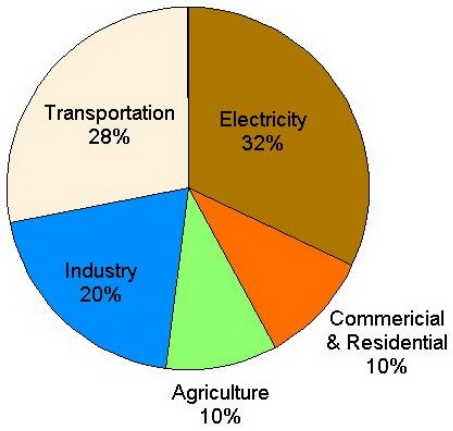

Figure 1.1: Sources of greenhouse gas emission in USA, 2012.

In this framework, this research is dedicated to efficiently manage EVs load in smart grid in order to not only shift this flexible load from peak period of the day to more desirable period, but also to reduce the impact of the uncertainty in the generation of the renewable energy sources in the gird.
In this study, it has been assumed that the distribution system is composed of a primary substation, renewable energy sources, conventional load, and EVs load as shown in Figure 1.2. Also, it is assumed that a utility (or an aggregator) server has the ability to command the charging EVs through two way communication link. Further, it is assumed that the distribution system is supplied by two types of energy sources; dispatchable (controlled) sources and non-dispatchable (uncontrolled) renewable sources and it has two types of load; conventional (uncontrolled) load and controlled EVs load. Finally, we assume that the renewable energy is fed directly to the distribution system to serve part of the load in the system. The remaining unserved load is served by the utility's conventional energy. Therefore, the power supplied by the substation is equal to the power demand minus the power generated by the renewable sources. In other words, the *net-load* seen by the substation is equal to the conventional load minus the generated power by the renewable sources [47].

1.2 Motivation and Challenges

Conventional power units are scheduled ahead of time to meet the expected demand in the electric grid. The schedule is decided based on the forecasted net-load demand. However, the forecasted net-load is not accurate due to the stochastic nature of renewable energy sources and the conventional load. Further, the forecasted net-load error is expected to

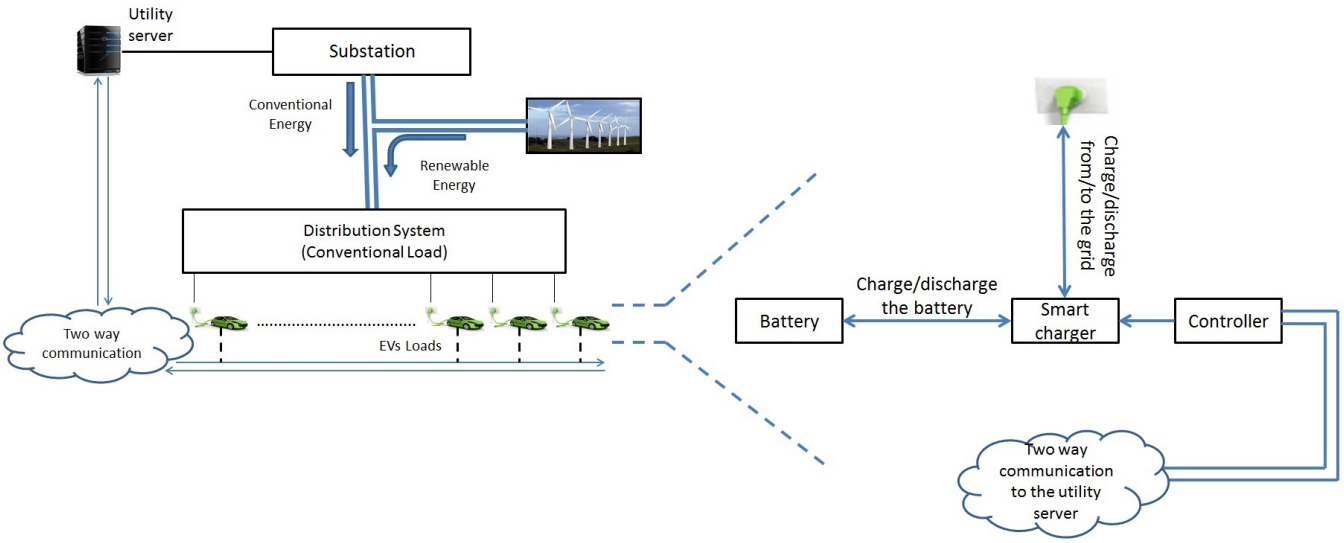

Figure 1.2: Distribution system with renewable source and EVs load

increase as the penetration level of the renewable energy sources increases. Traditionally, to encounter this unexpected variability in the load, enough regulation reserve and load-following reserve is maintained in the electric grid to compensate any unexpected increase or decrease in the load. This reserves give the grid operators the needed flexibility to immediately increase or decrease the supplied power to the grid to keep the delicate demand-supply balance in the system. These reserves are projected to increase in order to cope with higher variability in the net-load caused by higher penetration level of renewable energy sources. For example, Figure 1.3 shows the required increase in regulation reserve and load-following reserve in California Independent System Operator (CAISO) to deal with the increasing variability in the net-load caused by 20% and 33% renewable penetration projected in 2012 and 2020, respectively [35]. Considering the cost incurred by such increase in these reserves, it would be very beneficial to use the flexibility of deferable loads (*e.g.,* EVs load) to decrease this variability in the net-load and, consequently, decrease the amount of regulation and load-following reserves needed in the grid.

Apart from that, the new coming load of EVs could cause a problem in the grid if not dealt with carefully. This load, if not managed properly, will exacerbate the problem of peak demand in the system [24, 71]. Fortunately, EVs load is considered as a deferrable load, *i.e.,* this load has the flexibility to be deferred to another period of time if needed. In reference [72], it has been estimated that, on average, vehicles are parked somewhere for 90%-95% of the time. Considering the relatively shorter time for charging, the decision of start charging of these EVs could be deferred so that the overall load in the system is shaped in more desirable way for grid operators. In this research, besides shifting EVs load from peak periods to off-peak periods, our main focus is dedicated towards better use of the

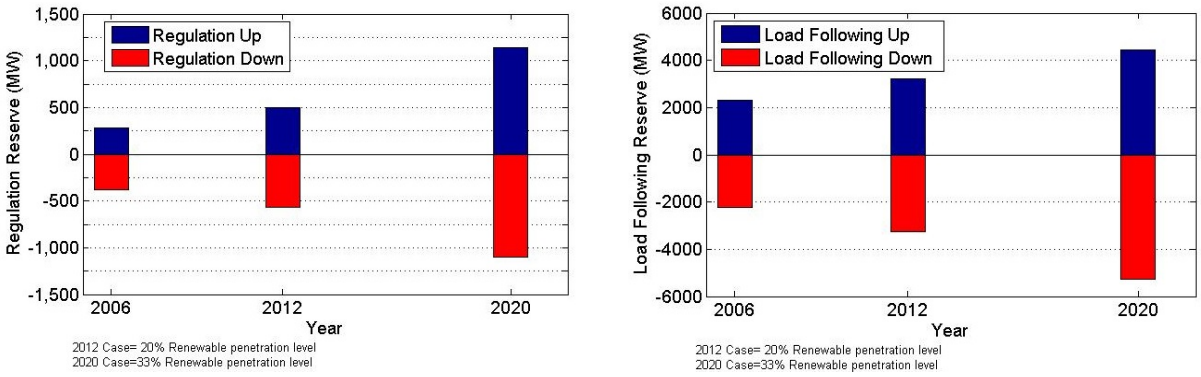

(a) Regulation Reserve

(b) Load Following Reserve

Figure 1.3: Regulation and Load Following reserves needed by CAISO to accommodate different penetration levels of renewable energy

flexibility of EVs load to encounter the stochastic behavior of the net-load which caused mainly by the stochastic behavior of RES in the smart grid. If the net-load forecast error is not addressed properly, it would cause severe operational difficulties especially when the penetration level of renewable sources is high. The objective in this study is to provide a charging algorithm for EVs in smart grid capable of decreasing the unexpected variability in the net-load in the grid, hence, improving the smart grid's efficiency.

1.3 Research Objectives

The main objective of this research is to introduce a novel charging algorithm for EVs in smart grid. On one hand, the algorithm manages the charging of EVs in the grid in order to satisfy the requirements and the constraints imposed by the customers, such as the amount of energy requested, plug-in time, and deadline (*i.e.,* plug-off)time. On the other hand, the algorithm effectively uses the flexibility of the EVs load in order to achieve two goals. First, shifting the charging time of the EVs from peak periods to off-peak periods as it is usually preferred by the distribution system and the grid operators. Also, charging during off-peaks periods benefits the customers as well since the energy cost is less. Second, the algorithm uses the flexibility of the EVs load further to absorb the unexpected fluctuations in the net-load or to participate in the regulation services in the grid.

1.4 Thesis Organization

This thesis is organized as follows:

- Chapter 2 provides a background on wind power and conventional load in the electric grid. The forecast methods and techniques of wind power and conventional load are investigated in this chapter. Importantly, the short-term forecast error of both the wind power and the conventional load is surveyed.

- Chapter 3 provides a review of the related work to charging EVs in the electric grid. The impact of uncontrolled charging of EVs on the electric grid is investigated. Also, the proposed methods and techniques to mitigate this impact are surveyed.

- Chapter 4 formally defines the net-load in the electric grid. The stochastic behaviour of the net-load represented by the forecast error is estimated. The effect of different penetration levels of wind power on the stochastic behaviour of the net-load is evaluated. Also, the inability of traditional scheduling algorithm for charging EVs to deal with the stochastic behaviour of the net-load is highlighted.

- Chapter 5 proposes a novel online charging algorithm for EVs. The algorithm shifts the EVs load from peak periods to off-peak periods. Additionally, the algorithm uses the remaining flexibility in the EVs load to absorb the unexpected variabilities in the net-load caused by the stochastic behaviour of the RES and the conventional load. Comprehensive analysis and evaluation of the proposed algorithm are provided in this chapter. Simulation results are used to compare the performance of the proposed algorithm to the performance of traditional scheduling algorithms.

- Chapter 6 uses approximately the same proposed technique in Chapter 5 to provide regulation services to the grid instead of absorbing the net-load variations. The performance of the proposed method is compared to the performance of a unidirectional regulation method used as a benchmark.

- Chapter 7 estimates the delay in the response time of the EVs to a command from the server. The communication link between the server and the EVs is accurately modeled. The packet loss probability of the wireless link is taken into consideration. Based on the model, the maximum number of EVs which can be supported by one access point (AP) to ensure a response time within a specific time limit is estimated.

- Chapter 8 summarizes the thesis work and provides interesting and challenging directions for future research.

Chapter 2

Background on Renewable Sources and Load in Electric Grid

In this chapter, we focus on the wind power as a representative for renewable energy sources. Specifically, the forecast methodology and uncertainty of the wind power will be reviewed. Also, as the other important component of the net-load in the system, the conventional load and its forecast error will be investigated.

2.1 Renewable Energy Sources (RES)

RES such as wind and solar are one of the main components of the future smart grid. The importance of these sources comes from the fact that these sources are considered as clean sources with zero greenhouse emissions in contrary to the traditional energy sources like nuclear, gas, and coal. However, these renewable sources are non-dispatchable and intermittent sources of energy. Unlike conventional power units, the amount of power produced from these sources at any point of time can not be dictated by the grid operator. Rather, the amount of power produced by these sources is related to their original source intensity at the moment, such as wind speed in case of wind power and sunlight in case of photovoltaic sources.
Noticeably, wind power as a clean source of electricity is in rise among other sustainable energy sources. That is due to the relatively lower cost compared to the other renewable sources. In USA, the wind power contributes to overall electricity production by nearly 3% in 2011 [58]. In Europe, wind energy currently contributes to whole consumed energy by 6%. Figure 2.1 shows the rapid increase in the generation of wind power among other renewable sources in USA in the last two decades [2]. Clearly, wind power growth is dominating the rest of renewable energy sources growth. For this reason, this work will use the wind power as a representative for RES in electric grid. The rest of discussion in this

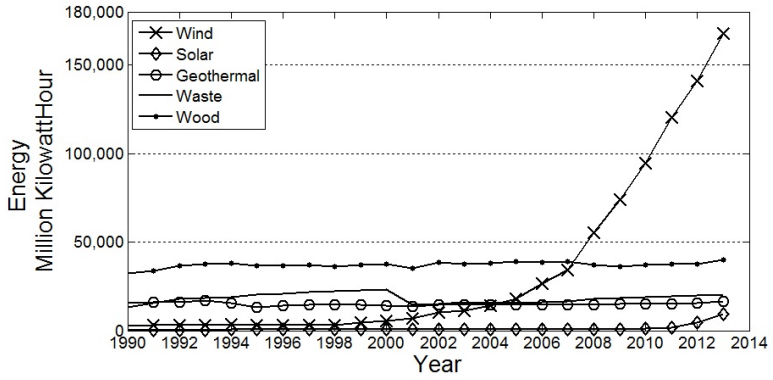

Figure 2.1: Electricity Net generation from Renewable sources in USA from 1990 to 2013

section will be divided into two main parts. First, general understanding of wind power generation. Second, wind power forecasting methods and their accuracies.

2.1.1 Wind Power Fundamentals

Wind power is a measure of the power in the wind. To convert this power into electricity, first, wind power is converted into mechanical energy and then this mechanical energy is converted into electricity. Wind turbines take this chain of processes to convert wind into electricity according to the following equation [5]:

$$P = \frac{1}{2}\rho A v^3 C_p \tag{2.1}$$

Where P is the extractable power from the wind in $watt$, ρ is the air density in kg/m^3, v is the wind speed in m/s, C_p is the power coefficient which represent the conversion efficiency of the turbine, and A is the cross-sectional area in square meter swept out by the wind turbine blades. Wind power efficiency C_p is limited by Betz limit or Betz' law. Albert Betz showed that, theoretically, $C_p \leq \frac{16}{27} \approx 0.59$. Practically, power efficiency C_p is between 0.35 and 0.45 for the most efficient turbines nowadays.
However, wind turbine starts to work typically at wind speed of 3-4 meters per second. This wind speed is known as cut-in speed as shown in Figure 2.2 [46]. At wind speed less than cut-in speed, there is no enough wind to rotate the blades of the wind turbine. As wind speed starts to pick up, the power produced from the wind turbine starts to pick up sharply. That is because of the cubic relationship between the wind speed and the extracted power in Equation (2.1). The power continues to increase as the wind speed increases until the wind speed reaches the rated output speed where the electric generator of the turbine reaches its limit. Typically, the rated output wind speed is around 12-14

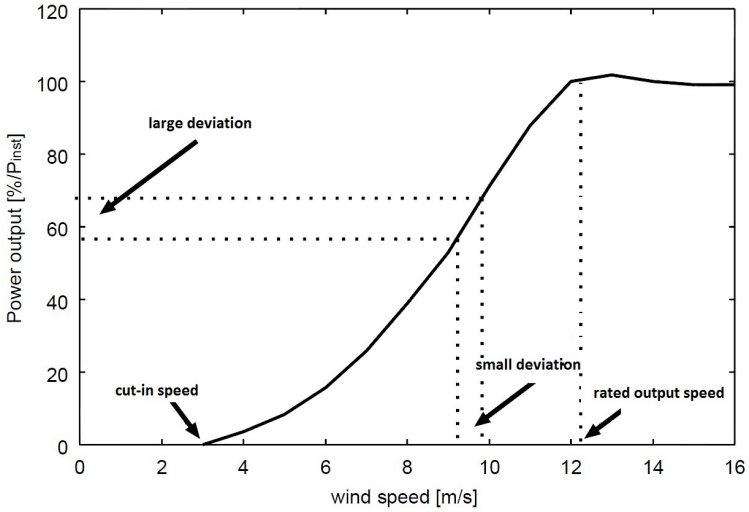

Figure 2.2: Power curve of wind turbine

meters per second. Worth mentioning that small deviation in the wind speed in the middle of the wind power curve would result in large deviation in the produced power. This makes the prediction of the wind power relies heavily on the accuracy of the wind speed forecast. This fact results in large wind power forecast error even when relatively small wind speed forecast error occurs as it will be discussed later.

2.1.2 Wind Power Forecast

With the increasing focus on integration of wind power into electric grid, the variability and uncertainty of the wind power is taken great amount of attention. One important tool to deal with this variability and uncertainty is wind power forecast. More accurate wind power forecast will help operating the electric grid more efficiently. Unit commitment and economic dispatch decision will rely heavily on the accuracy of the prediction of typically one day ahead wind power forecast especially when the wind power penetration level is high.
Time horizon of wind power forecast affects the accuracy and the methodology of forecasting. Generally, as time horizon increases, the forecast error tends to increase. Often, wind power forecast is divided into three categories according to the time horizon.

- *very short term.* The time range for this category is few hours. It could be for up to 4 hours as in [85] or 9 hours as in [59]. This forecast can be used to provide the grid operators with more accurate information about the wind power which will be produced in the near future. Also, if the wind power plants is participating in

electricity market, it can provide the seller with the appropriate information to play in real time market.

- *short term.* The time ranges starts from very short term, few hours, to two or three days ahead. This kind of forecast can be used in unit commitment and economic dispatch scheduling in electric grid.

- *medium term.* the time horizon of this category is 3-7 days. This forecast can be used for unit commitments scheduling and for maintenance planing for turbines or transmission lines of electric grid.

Ranging from using pure statistical models to using pure Numerical Weather Prediction (NWP) models, the forecast of the mentioned three category can be done. As this work concerns about the impact of integrating wind power on the operational side of the electric grid, briefly, we will go through the first two wind power forecast categories.

1. **Very-Short Time Wind Power Forecast.** In very short-term wind forecasting approach, statistical models are usually used. These statistical models such as Auto-Regressive Moving Average (ARMA), Kalman Filters, and Auto-Regressive with Exogenous Input (ARX) are time series models. These models take past and present observed values, like wind speed and generated wind power, as an input to the model to produce an estimate for the future values. This can be depicted mathematically as follows:

$$\hat{P}_{t+k} = f(P_t, P_{t-1}, ..., P_{t-n}, x_t, x_{t-1}, ..., x_{t-n}) + \varepsilon \tag{2.2}$$

   where $\hat{P}_{t+k}$ is the predicted wind power at future time (t+k) given that the current time is t. $P_t, P_{t-1}, ..., P_{t-n}$ are the recorded past and present values of wind power and $x_t, x_{t-1}, ..., x_{t-n}$ are other past recorded values which affect the wind power production such as wind speed, temperature, ..*etc.*The error of forecasting in Equation (2.2) is represented by the random variable ε, often called white noise. The smaller the variance of this random variable, the better forecast accuracy. The mean of this random variable is usually zero or close to zero. The function $f(.)$ which represents the model is a generic function and it could be linear or non-linear.
   The very-short forecasting models avoid the costs of using Numerical Weather Prediction as an input to the models. Because of the assumption of stability of the weather in very short time span, these models spare the cost of requesting weather prediction values from weather forecast centers. That is exactly why these models are useful only for a very short time, minutes or very few hours.

2. **Short Time Wind Power Forecast.** As the time horizon increases, the error of the wind power forecast using very-short time forecast methods increases. Current short

time forecast methods are used to forecast the wind power up to 72 hours. Unlike very-short time forecast methods, short time forecast methods require Numerical Weather Prediction (NWP) values as an input. Weather prediction models is a mathematical model takes some of the current atmospheric variables as an input and produce future estimation for atmospheric variables as an output. These atmospheric variables include temperature, pressure, wind speed and direction, and rainfall. By using NWP values in wind power prediction alongside with the past statistical values like wind power and wind speed, the wind power forecast accuracy can be significantly increased.

Mainly, there are two groups of short-time wind power forecast, physical approach and statistical approach. The physical approach forecasts the wind speed at the turbine hub's height first, then, it uses the manufacturing turbine power curve to convert the forecasted wind speed to wind power forecast. In statistical approach, the raw inputs, NWP values and past recorded wind power, are converted directly to wind power through statistical models. Further, a combination of the two approaches is used in some systems to take the advantages of both approach aiming to better forecast. Many short time wind power forecast methods can be found in [22,45,48,92].

(a) *Physical approach.* In this approach, three different inputs are needed. Atmospheric variables NWP, SCADA data, and the wind farm specification like terrain characteristics. NWP is needed to know the atmospheric variables prediction such as wind speed and wind direction. Supervisory Control and Data Acquisition (SCADA) system provides the most recent information of the wind speed and wind power from the site. The terrain specifications are used to refine the wind speed suggested by NWP model.

As shown in Figure 2.3, these inputs go through first stage of "Downscaling". In this stage, NWP and SCADA data are used to predict the wind speed and wind direction at the best predictable height at the targeted site. Then, the terrain characteristics like roughness, orography, and obstacles are used to refine the wind speed and direction at the turbine hub's height. The next stage uses the wind turbine power curve to convert the predicted wind speed into wind power. However, as shown in Figure 2.2, small error deviation in wind speed prediction can be translated into significant error deviation in the wind power prediction. Therefore, the first stage of physical approach which converts the raw input data to wind speed at turbine hub's height is considered the most critical stage in improving wind power forecast.

(b) *Statistical approach.* This approach uses statistical models to draw the desired output directly from the effective raw inputs in one stage. NWP and SCADA data are used as inputs to these models which in turn gives the estimated wind power forecast as an output as depicted in Figure 2.4. Note that the terrain characteristic of the wind farm is excluded from the inputs to these models

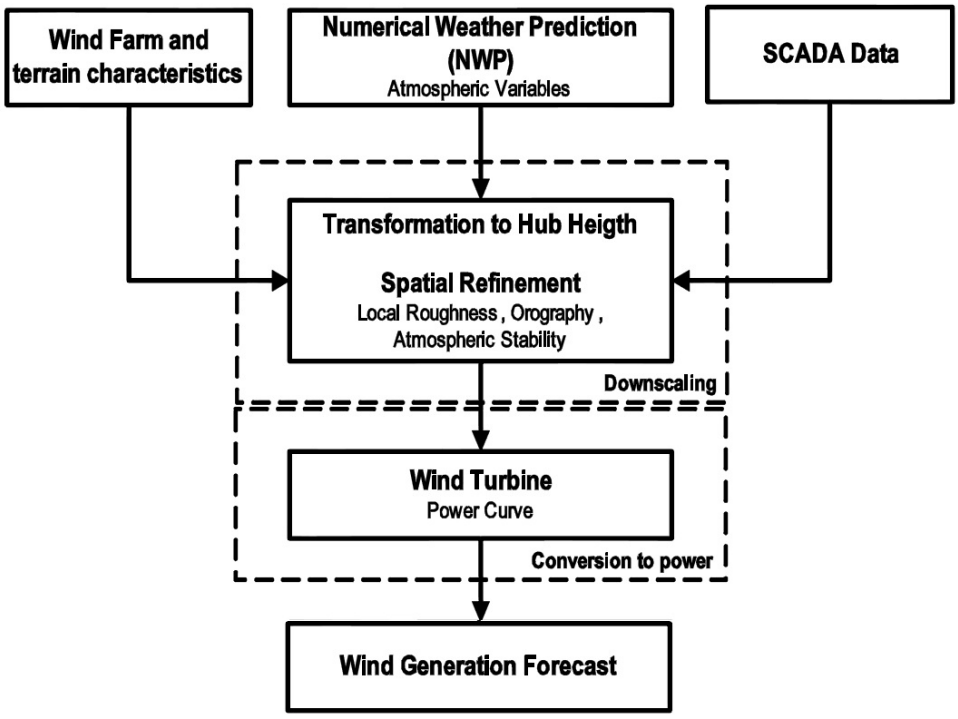

Figure 2.3: physical approach of short-time wind power forecast

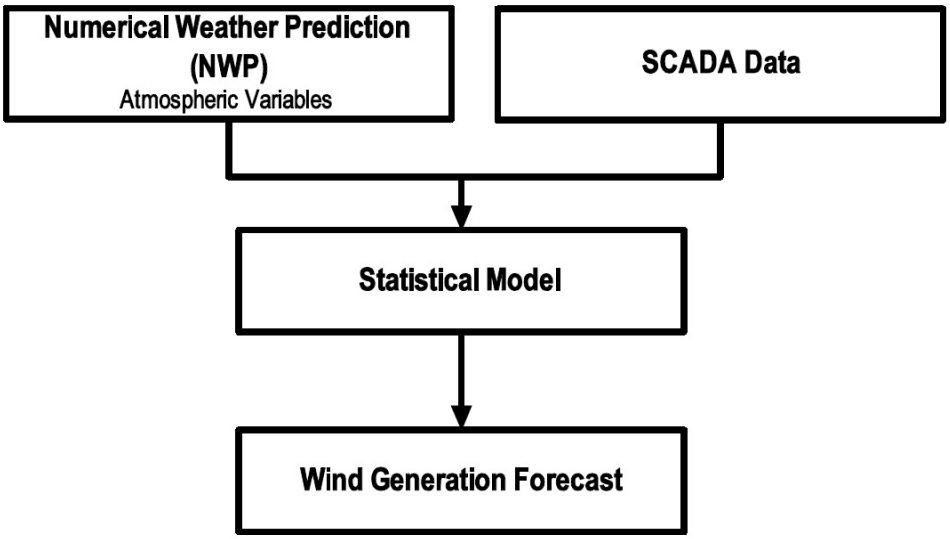

Figure 2.4: statistical approach of short-time wind power forecast

compared to the physical models. In fact, the effect of the terrain is still included in these models, but, indirectly. Most of these models use training technique in the beginning in order to teach the model the relationship between the inputs and the outputs. These training techniques tune the model's parameters in order to get the right output for any input. When a model is trained by the data from a specific wind farm, the parameters of this model will be adjusted in a way that reflects the effect of any terrain characteristic of that wind farm site.

Different statistical techniques are used in this area. Artificial Intelligence based techniques such Neural Networks (NNs) and Support Vector Machines (SVMs) are among most sophisticated techniques adopted by this approach. Also, expert system models can be used to map the inputs to the outputs. In these systems, data base of recorded (inputs, outputs) pairs are used to match the input to the appropriate output.

It is important to notice that the statistical models often need enough historical data to train the models before these models are ready to be used in prediction. For a new wind farm, for example, it would be difficult to get this record of (inputs, outputs) data since the farm is new. Also, although this approach may seem to avoid the problem of the sensitivity of wind power curve in the physical approach, in fact, the problem is still there and can be seen in the relationship between the raw inputs, NWP and SCADA, and the wind power prediction as an output. Small error in the raw inputs can result in larger error in the output.

2.1.3 Wind Power Forecasting Error

To adequately integrate the wind power into smart grid, it is essential to understand the uncertainty of wind power prediction. The uncertainty of wind power generation is the inability of predicting the exact amount of wind power to be generated in the future time, often within 48 hours. This uncertainty can be measured by the forecast error, $e(.)$. Electric grid's operators and wind power generation companies always prefer less error in the wind power forecast to give them a stronger base on which they can take more accurate operational decisions. Generally, there are many factors and characteristics affect the accuracy of wind power forecast [60]:

1. Terrain complexity of the wind farm's site. The mountains and any physical obstacles can have a significant impact on predicting of the wind speed and direction at the site which will, in turn, affect the accuracy of the wind power forecast.

2. Size of the wind farm in terms of number of wind turbines and their arrangement on the site. Obviously, more turbines mean higher wind power capacity for this farm which will lead to higher forecast error. For this reason, it is beneficial to report the normalized wind power forecast error by installed capacity rather than just the error itself. Also, the layout of wind turbines on the site should be engineered well in order to decrease the disturbance of wind flow caused by one turbine on another.

3. Quality of NWP forecast. The error in NWP forecast will definitely affect the accuracy of wind power forecast.

4. Quality of SCADA data measurements.

5. Site climatology conditions.

There are many metrics to quantify the wind power forecast error in the literature. To explore some of these metrics, we adapt the notations used in [53] which are commonly used in wind power forecasting community.

P_{inst}	: Wind farm installed capacity
$k = 1, 2, .., k_{max}$	: Prediction horizon (No. of time-steps)
k_{max}	: Maximum prediction horizon
N	: Number of data used for the model evaluation
$P(t+k)$	: Measured power at time $t+k$
$\hat{P}(t+k\|t)$	: Power forecast for time $t+k$ made at time origin t
$e(t+k\|t)$	: Error corresponding to time $t+k$ for the prediction made at time origin t
$\varepsilon(t+k\|t)$	: Normalized prediction error (normalized with the installed capacity)

The basic definition for forecast error at time $t+k$ can be expressed as follows:

$$e(t+k|t) = P(t+k) - \hat{P}(t+k|t) \tag{2.3}$$

It is important to normalize the error by the size of produced wind power to keep the errors related to the magnitude of forecasted power. Conventionally, wind power community normalize the wind power forecast error by the installed capacity of wind power.

$$\varepsilon(t+k|t) = \frac{1}{P_{inst}}(P(t+k) - \hat{P}(t+k|t)) \tag{2.4}$$

The error generally consists of two types of errors, systematic error μ and random error ξ.

$$e = \mu + \xi \tag{2.5}$$

μ is a constant representing the bias in the forecasting. Ideally, the forecast methods are unbiased, $\mu = 0$. However, this can be practically difficult. Therefore, forecast methods compete to have as less bias as possible. Having positive bias, $\mu > 0$, means that the forecast method is systematically over-forecasting the wind power. On the other hand, if $\mu < 0$, the method is consistently under-forecasting the wind power.
The other component of the forecast error is a random error ξ. This error has zero mean. However, it usually has a variance. The forecasting method is considered better when this variance is smaller.
Statistical measurements from recorded error $e(t+k|t)$ for $(t = 1, 2, ..., N)$ can be used to characterize the forecast error. The bias error can be estimated as follows:

$$BIAS(k) = \hat{\mu}(k) = \frac{1}{N}\sum_{t=1}^{N} e(t+k|t) \tag{2.6}$$

This estimation is considering one part of the forecast error, the bias only. Mean Absolute Error (MAE) is considering both components of the error forecast. This metric is expressed as follows:

$$MAE(k) = \frac{1}{N}\sum_{t=1}^{N} |e(t+k|t)| \tag{2.7}$$

Also, Mean Square Error (MSE) is another metric which is used in the literature alongside MAE.

$$MSE(k) = \frac{1}{N}\sum_{t=1}^{N} (e(t+k|t))^2 \tag{2.8}$$

Sometimes the square root of MSE are used instead of MSE. This metric is called Root Mean Square Error (RMSE).

$$RMSE(k) = \sqrt{MSE(k)} \tag{2.9}$$

These metrics are used heavily in the literature to describe the forecast error. For example, MAE and/or RMSE can be used to compare the performance of two wind power forecast methods. Less MAE or RMSE is better. However, more comprehensive representation of the forecast error can be achieved by reporting the distribution of the error instead of just one value representation. In a case study published in [53], multi-MW wind farm data are used to illustrate the distribution of the produced wind power forecast error. This data are taken over 3-months winter period of 2003.

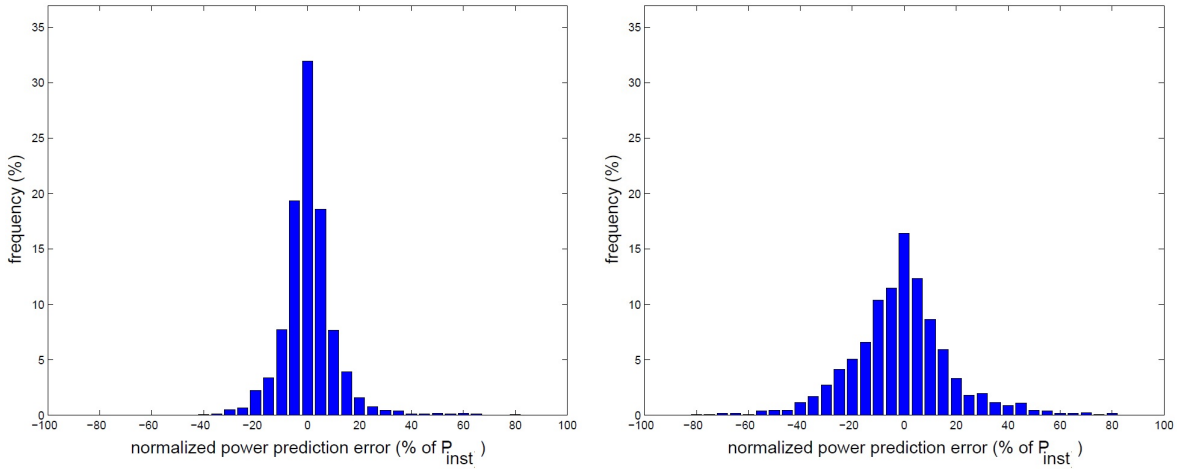

(a) Error distribution of 1-hour ahead prediction (b) Error distribution of 24-hour ahead prediction

Figure 2.5: Distribution of wind power forecast error [53]

Figure 2.5 shows the distributions of the forecast error of one-hour ahead time and 24-hour ahead time. From the figure, the mean values of both distributions are approximately zero. However, the spread of the error in both cases are different. Clearly, the one-hour ahead distribution is more concentrated around the mean. While, 24-hour ahead error distribution is relatively widely spread around the mean. This agrees with the assumption that the forecast accuracy decreases as the time horizon increases. That spread can be statistically represented by the variance of the distribution. This distribution can represent the error in more comprehensive way compared to the previous forecast error measures. Moreover, the distribution of wind power forecast can easily fit a normal (Gaussian) distribution. In fact, it has been shown in previous studies that the forecast error follows a Gaussian distribution [11, 23, 55, 65]. Only the first and the second moments of normal distribution, mean and variance, are needed to completely describe the distribution.

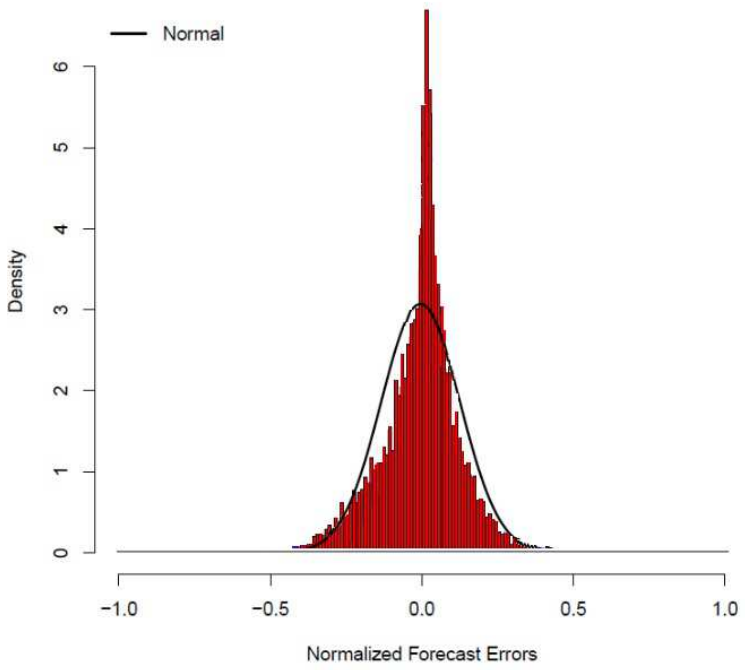

Figure 2.6: CAISO day-ahead wind power forecast error, normalized by wind farm capacity [36]

Therefore, in this work, we will used the normal distribution to describe the forecast error whenever it is possible. For example, in [36], day-ahead forecast error data were taken from California Independent Operator System (CAISO) for the year 2011. The results are taken from wind farm with installed capacity of 940 MW. The results show that the mean and the standard deviation of the normalized errors are $\mu_w = -0.004, \sigma_w = 0.130$. Figure 2.6 shows the histogram of the error distribution.

2.2 Electric Load

To understand the operational challenges in the power grid, it is important to understand the conventional load in the grid. The whole purpose of any electric gird is to satisfy the load in the system. Therefore, this section will be dedicated to study the fundamentals of electric load and forecast methods of the load in the literature.

2.2.1 Load Definition

The load is usually defined as the sum of all power required by all customers in the electric grid at any point of time. Usually, load is measured in Watt. Supply-demand balance is important goal to be achieved in the electric grid. Therefore, the electric grid operator needs to know how much load "demand" in the grid to supply the necessary power in order to keep the system balanced.
In fact, load profile in distribution system is affected by many factors:

1. *Type of the customers*. The load profile tends to have different shape and behavior according to type of the customer. Accordingly, customers in the distribution systems are divided into three different types; residential, commercial, and industrial. For example, the energy consumption by residential area seems to start to rise in the morning when people usually wake up. The peak demand for this category often at 8:00 PM when most of residents return from their work to their houses and starts to use the electricity more. During the early morning 1:00 AM- 7:00 AM, the residential area consumption hits the lowest level as most of the residents are sleeping. Commercial area and industrial area are more systematic in their consumption according to their working time.

2. *Time*. The amount of electric load tends to be different in different time period. During one day, in the residential areas, the early morning load is usually the lowest, while the load significantly increases in evening when people arrive to their houses. While in the industrial areas, the load is at highest at the working hours' period. Also, different electric load profiles are recorded for different seasons of the year. In the winter, the load is generally higher compared to summer in cold places.

3. *Weather*. Weather has noticeable effect on electricity consumption. Temperature and humidity can influence the usage of heating and cooling systems which will, consequently, influence the power consumption.

There is a need for estimating the load in the system in the future time. This estimation is used by the electric operator to make short-time operational decisions, maintenance scheduling, and power grid upgrading plan. As a result, the development of load forecast methods took a significant attention. In the next section, we will briefly describe the common load forecasting methods.

2.2.2 Load Forecasting

As mentioned earlier, load forecasting helps the utility for making decisions on how much power to purchase or generate for the coming short-term or Long-term future. Also, the

load forecasting helps for load switching, infrastructure developments and maintenance planning [26]. Load forecast categorized into three categories:

1. *Short-term forecasting.* Usually from one hour to one week.
2. *Medium-term forecasting.* Usually from a week to a year.
3. *Long-term forecasting.* Usually for more than one year.

According to [26], different factors affect different load forecast categories:

1. Factors for short-term forecasting
   (a) Time factor. Time of the year, day of the week, hour of the day are important factors for short-term load forecasting. Also whether the day is holiday or not is another important factor. The behavior of the load is changing according to these time factors.
   (b) Weather factor. Temperature and humidity are important factors in influencing the consumption of the electricity. Therefore, taking these factors into consideration is important. Fortunately, in short-time, the prediction of these weather factors is possible.
   (c) Customers' type. Every type of the three types of the customers has a different load characteristic which has to be taken into consideration when we try to predict the load in the system.
2. Factors for medium- and long-term forecasting.
   (a) Historical data of the load and the weather.
   (b) Future forecast for weather.
   (c) Number of the customers in every class.
   (d) The appliances characteristics including ages.
   (e) Appliances sales rates.
   (f) Economic growth in the area..*etc.*

2.2.3 Load Forecasting Methods

In general, statistical models are often used for forecasting. Electric load can be forecasted using these methods. There are mainly two statistical models have been used for forecasting, additive method and multiplicative method. The difference between the two is in the

way the forecasted load is expressed. In the additive methods, the load, L, is represented as a sum of group of factors. While the multiplicative models represent L as multiplication of group of factors. The following two equations represent the additive and multiplicative methods consequently.

$$\begin{aligned} L &= L_n + L_w + L_s + L_r, \\ L &= L_n \times F_w \times F_s \times F_r, \end{aligned} \tag{2.10}$$

where L_n is the "normal" (base) part of the load which represents the shape (cycle) of the load in each day of the year. L_w, L_s, and L_r represent the weather factor, special events (*i.e.,* holidays) factor, and the random factor respectively. Similarly, F_w, F_s, and F_r represent the weather factor, special events factor, and the random factor respectively for multiplicative model. For instance, [18] introduced forecasting methods based on additive methods while [69] used the multiplicative method for short-term forecasting.

However, as the short-term forecasting is sensitive to different factors compared to medium- and long-term forecasting, different models have been developed to suit both types of forecasting.

1. *Medium- and long-term forecasting methods.*
   End-use models and **Econometric models** are most used models for medium- and long-term forecasting.
   In End-use model, extensive information at the end use is the main factor in this model. The type of appliances used in the house, the size of the house, and the expected age for the current appliances are some of the information used in such a model. Also, this model takes into consideration the type of the customer. This model accuracy depends on the accuracy of such factors. However, the difficulty of collecting such information and the confidence in its accuracy is the main problem in this approach.
   Econometric models, on the other hand, combine economic theories and statistical techniques in an attempt to forecast the demand on medium and long-term.
   Also, statistical methods for medium-term forecasting have been used in the literature. For example, in [27, 28] a multiplicative model has been used to represent the load as follows:

   $$L(t) = F(d(t), h(t)) \times f(w(t)) + R(t), \tag{2.11}$$

   where $L(t)$ is the load at time t. And $d(t), h(t)$ is the day and the hour at time t. $w(t)$ is the weather factor at time t. Finally, $R(t)$ is the random error. This model shows a good convergence and accurate results according to the authors.

2. *Short-term forecasting methods.*

Significant numbers of methods have been developed for short-term forecasting. The level of accuracy needed in short-term forecasting is higher compared to medium-term and long-term forecasting. Both Statistical and artificial intelligence techniques are used in this range. Briefly, we list the common techniques used for short-term load forecasting adapted from [26].

(a) **Similar-day approach.** This approach emerges from the intuition that the same day with the same circumstances for the same area would result in the same load profile. Through historical data for the last two or three years, we search for a day has the same characteristics like the day we want to forecast. These characteristics can be the weather factor, date of the day, day of the week, and if it is holiday or normal day. If we could find such a day from the historical data, then we can use the load profile of that day as a forecast for our targeted day. However, it is important to not go too far into the past and assume that would always mimic the current situation. There are changes in the load consumption through the time and that should be taken into consideration.

(b) **Regression methods.** One of the most used statistical techniques in load forecasting. This technique uses the relationship between the load and some factors like weather and day type and customers' class to forecast the load in the future given the estimation of the effective factors in the future.

(c) **Time series.** This technique is based on the assumption that any time series has a structure in itself. Therefore, the time series techniques try to detect this structure. Once the structure is discovered, the series can be extended based on that structure, hence, forecasting. Auto-Regressive Moving Average (ARMA) model for stationary time series and Auto-Regressive Integrated Moving Average (ARIMA) for non-stationary time series are among the most famous models of this technique. To include the effects of some factors from outside the series of data itself, ARIMAX was developed as new model which includes along the time series, some other effective factors on the behavior of data series. For load forecasting, ARIMAX has been used as a model which takes the historical load data as the time series and the weather and the type of the day as effective factors.

(d) **Neural networks.** The artificial neural network (ANN) has demonstrated the ability for curve fitting. ANN works as a non-linear function that maps a group of inputs to desired output. This network has the capability of learning which helps the network to adapt the non-linear function of the inputs to the desired output. A set of training data used to train the network to learn and to establish the target function. This technique has been used since 1990s to forecast the electricity load [42]. One of the most used learning techniques for load forecast purpose is the supervised back propagation technique. In this technique, the

weights (i.e. parameters of the mapping function) are adjusted every time a new sample of training data set used. The weights will be eventually set to, hopefully, the optimum values and then the network will be ready for forecasting.

(e) **Expert systems.** This technique uses a group of rules set by experts in order to reach appropriate decision. Load forecasting expert system is a software program implemented based on rules established by experts in the field of load forecasting to forecast the electricity load.

(f) **Support vector machines.** This technique is the most recent technique for classification. This powerful technique can solve the problem of classification by transforming the difficult classification problem from its original space into another space where the classification becomes easier, then, bringing the results back to the original space. A function called kernel, $K(.,.)$, is the key for such a transform. This technique depends on finding the right kernel for the problem. If the right kernel is obtained, this technique can be the best technique among other classification technique.

2.2.4 Load Forecasting Error

Load forecast is crucial for operational decisions and upgrading plans in electric grid. Therefore, the error in load forecasting would have a direct impact on the accuracy of all these decisions.

All wind power forecast error metrics explained in Section 2.1.3 are used to measure the load forecast error in the literature. Similar to wind power forecast error, the load forecast error is assumed to follow Gaussian distribution [11, 23, 55, 65]. Unlike wind power forecast error, however, the load forecast error is not as sensitive to the time horizon due to highly repetitive nature of daily load profile [23]. Also, the forecast error of electrical load is relatively less than the forecast error of wind power. In [36], the load forecast error of CAISO for year 2011 is evaluated. The results represent the day-ahead forecast error of 2011 normalized by average load of 26297 MW. The error distribution is shown in Figure 2.7. Mean value of the normalized error is $\mu_l = -0.002$ and the standard deviation is $\sigma_l = 0.026$.

The spread of load forecast error, $\sigma_l = 0.026$, is noticeably less compared to the spread of wind power forecast error taken from the same system, CAISO, for the same year, 2011, which was $\sigma_w = 0.130$ as mentioned in Section 2.1.3. This states clearly that the error in the day-ahead wind power forecast is significantly higher than the error in the day-ahead load forecast.

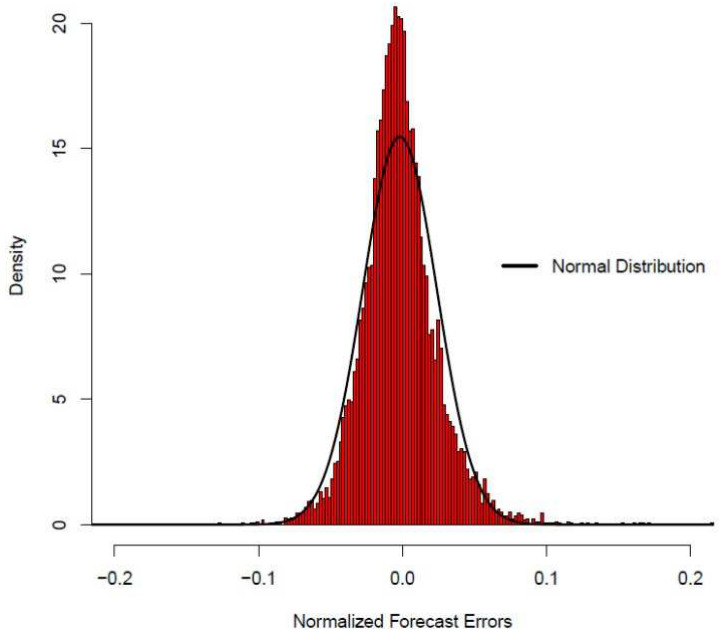

Figure 2.7: CAISO day-ahead load forecast error, normalized by the average load in the system [36]

2.3 The Net-Load Forecast Error

The combination of load and wind power in the electric grid result in so called "Net-load". Net-load is defined as the load minus the wind power. Thus, we define the *Net-Load*, $L_N(t)$, as follows:

$$L_N(t) = L_c(t) - L_w(t), \tag{2.12}$$

where, $L_c(t)$ is the conventional load in the grid at time t, and $L_w(t)$ is the produced wind power, *the negative load*, at time t.

In this case, the operational decisions of unit commitments and operational reserve should be designed to meet the Net-load instead of the load itself. These decisions are usually taken day-ahead based on the forecasted Net-load. However, this net-load forecast can suffer from significant forecast error, especially when the wind power penetration level is high.

Many studies have shown that in order to cope with the increasing net-load forecast error due to the increase in wind power penetration level, the operational reserves need to be increased [7, 35, 84]. In [35], a report from CAISO shows that both regulation reserve and follow up reserve need to be increased in order to keep the the electric grid reliable as wind power penetration level increases as shown previously in Figure 1.3.

2.4 Summary

In this chapter, the two components of the net-load in the electric grid, RES and conventional load, are reviewed. Mainly, the forecast methods and techniques of wind power, as a representative for RES, and conventional load are summarized. However, it has been shown that these forecast methods are not accurate especially for wind power. In the literature, the forecast errors of conventional load and wind power are statistically modeled as random variable. This random variable often follows Gaussian distributions.

The main findings of this literature review can be summarized in the following points:

1. More operational flexibility is needed in the system to cope with the intermittent RES penetration.
2. As the penetration level of the intermittent RES increases, the net-load forecast error increases. Consequently, more operational reserved is needed to operate the electric grid.

Chapter 3

Literature Review on Electric Vehicles

Electrification of transportation sector has recently attracted a significant attention in academic and industrial societies. This is due to the fact that there would be a tremendous reduction in the greenhouses gas emission had this electrification of transportation sector achieved. In USA, the transportation sector alone contributes by 28% of the whole figure of greenhouses gas emission in the country [3].

This chapter reviews the literature of charging the electric vehicles (EVs) in the grid. The impact of uncontrolled charging of the EVs on the distribution system is discussed. Also, the proposed solutions for the problems of the uncontrolled charging of the EVs are thoroughly reviewed. Finally, the shortcomings of the proposed charging algorithms in the literature are summarized.

3.1 Electric Vehicle

There are mainly two types of EVs: Battery Electric Vehicle (BEV) and Plug-in Hybrid EV (PHEV) [56]. BEVs are completely relying on the electricity to function. Battery is used to store the necessary energy to power the vehicle. This battery is chargeable and the electric grid is used as a source of energy to recharge the vehicle's battery. On the other hand, PHEV is partially electrical. PHEV is powered by both Internal Combustion Engine (ICE) and electric engine. Therefore, the battery in PHEV is often smaller compared to the battery in BEV.
The future vision of EVs and its interaction with the grid is bidirectional. That is, the EVs can charge from the grid and, also, can provide support energy to the grid by discharging to the grid. This capability is also referred to as grid-to-vehicle (G2V) and vehicle-to-grid (V2G) [39].

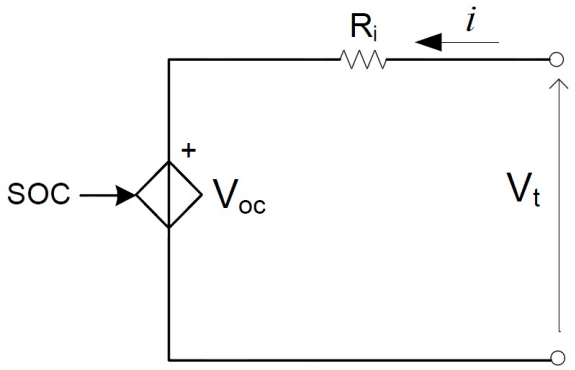

Figure 3.1: EV battery model [57]

3.1.1 Electric Vehicle Battery

1. **Battery model.** According to [34], more than 70% of EVs in 2015 will use Li-ion battery. In comparison to other types of batteries, Li-ion batteries have important advantages [6]. Li-ion batteries have a greater energy to weight ratio compared to other batteries. Also, this type of batteries have no memory effects. Memory effect is defined as gradually losing of maximum energy capacity of the battery if it is repeatedly recharged after being only partially discharged. Also Li-ion batteries have low discharge rate when it is not in use.
   Li-ion battery's model, as in reference [57], represents the battery by two components: battery internal impedance R_i and State Of Charge (SOC) as variable voltage source, V_{oc}, as depicted in Figure 3.1.

   SOC is expressed as follows:

$$SOC = \frac{Q}{Q_{nom}}, \tag{3.1}$$

   where Q is the actual capacity stored in the battery in Ah, and Q_{nom} is the nominal capacity of the battery in Ah.
   The EV charging model in Figure 3.2 represents the complete model when EV is connected to the grid. V_c and i_c represent the grid voltage and the absorbed current from the grid respectively. Therefore, the power absorbed from the grid side, P_{ac} can be expressed as follows:

$$P_{ac} = V_c \times i_c \tag{3.2}$$

   The consumed power from the grid to charge the battery, P_{ac} is constant most of the time. In Figure 3.3, experimental results show the behavior of absorbed power and SOC of a particular Li-ion battery during the time of charging [57]. Charging power was 3.7 KW of single phase charger. The charging is started with SOC=60%.

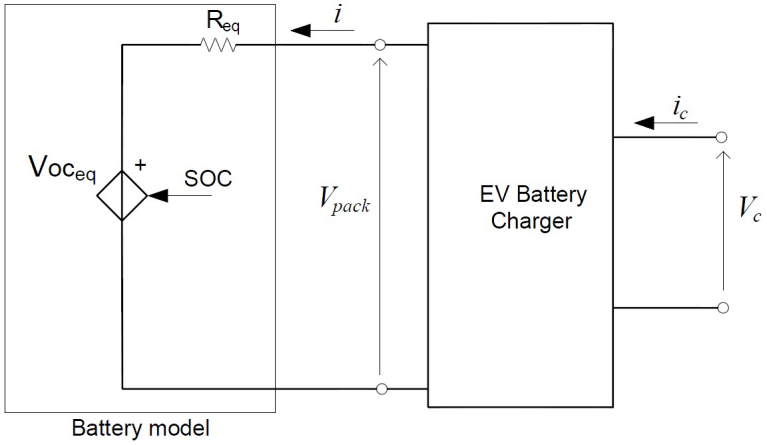

Figure 3.2: EV model [57]

Clearly, the power profile of the battery is constant until the battery is above 95% fully charged. In the last stage, the charging current starts to decrease and, consequently, the power starts to decrease until the battery is fully charged and no more current absorbed.
Generally, in the literature, the battery's charging power profile is assumed to be variable and can be set to any level of power within the maximum allowed limit. The assumption is that the chargers, of *level 2 and 3*, are smart enough to be set to any level at any interval of time. Li-ion batteries have so called memoryless property which assumes that the life time of the battery would not be affected by variable charing profile.

2. **charging levels.** Three different charging levels have been suggested by the Electric Power Research Institute to charge EVs [61]. Level 1 uses the standard voltage for houses in USA with 120 VAC, 12 amp or 16 amp. Therefore, this charging level will support maximum charging power of 1.4kW- 1.9kW. With this level of charging a battery with energy of 16kWh, for example, will need between 8.4h-11.4h to be charged from 0% to 100%. The advantage of this method of charging is that it does not need any extra infrastructure installation as it uses the existing houses's plugs. However, the time of charging is significantly large. On the other hand, level 2 is considered to be the preferable charging level with 240 VAC and 15 amp. The charging power of this method is around 3.3 kW. That will reduce the charging time of 8 kWh battery from 8 hours, using level 1 charger, to 4.8 hours. Special equipments required to ensure higher level of safety in this level compared to level 1. Finally, level 3 is the fast charging level with 60-150 kW charging power. Batteries can be charged to 50% just in 10 to 15 minutes. The expense of practically install such a powerful charger is high. For that reason, level 3 is not considered to be feasible in

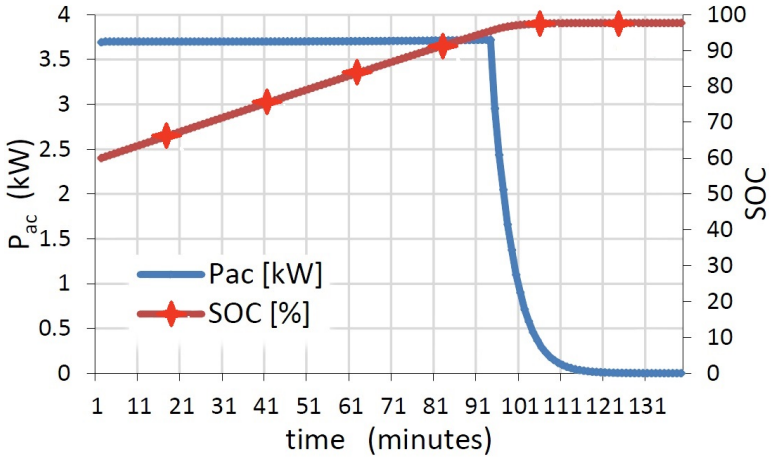

Figure 3.3: Absorbed power from the grid during charging

the near future. As a result, level 2 is considered the most reasonable compromise between slow and fast charging methods.

3.1.2 Communication and Control

The communication between the electric utility and the vehicle most likely will be conducted between the utility and the smart charger instead of the vehicle itself as the it is fixed in one place. The location of the vehicle could be defined by the position of the charger itself; therefore, there will be no need to send information about the location of the vehicle. However, since the standardization of communication between the charger and the utility is not fully developed yet, different pathways between the charger and the utility are possible:

1. **Wireless Network:** In this approach, transceiver is installed in the charger to wirelessly connect to an access point and through to the utility server. This approach assumes that the communication between the vehicle and the utility is not critical. Therefore, delay can be tolerated. The data rate can be relatively low, (9.6 to 56 kb/s) [78], but enough for EVs communication.

2. **Power Line Carrier (PLC):** Although power lines are originally created to carry electricity, the power line could also carry data. However, due to the noise and signal fading, PLC is limited to carry data with less than 14 Mb/s [54]. This rate is enough for exchanging EVs related information. Nevertheless, the security and reliability of PLC need more investigation.

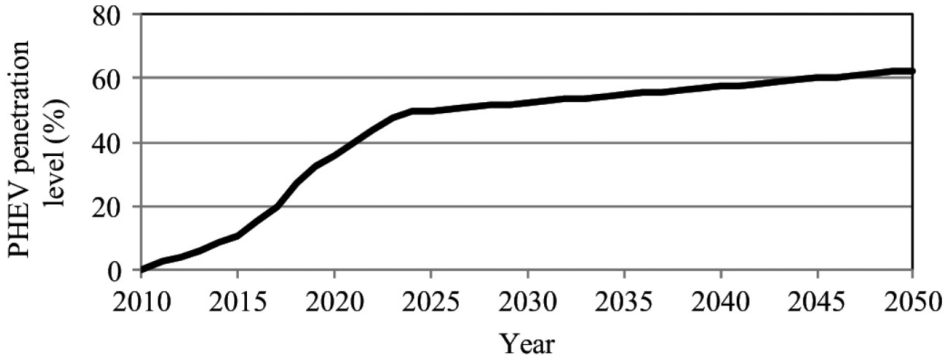

Figure 3.4: The penetration level of EVs on distribution system [74]

3. **Internet Protocol (IP):** This method is most promising method. It is available in most places and offered with reasonable cost. The charger needs an access to the local network which facilitates the connection to any other terminal in the internet. The smart charger can connect through cable or wirelessly to the nearby network. Using the internet, however, may risk the security of the delivered data between the EVs and the utility. Also, the reliability of the communication will depend on the reliability of the internet provider which the smart charger is connected to.

3.1.3 Charging EVs

Charging EVs from electric grids adds a new load to the grid. The penetration level of EVs is an important factor to determine the EV's impact on the electric grid. According to [74], the current average of vehicles per house in USA is 2.3. The prediction of the penetration level of EVs in USA is depicted in Figure 3.4.

With level 2 charging power of 3.7-4 KW, the impact of EVs on the distribution system should be considered carefully. Many specification of the distribution system can be affected by this load. Voltage deviation, power loss, peak load, and overloading transformers and cables are important issues should be considered when studying the impact of high penetration level of EVs .
In general, there are two charging scenario in the literature: uncontrolled charging and controlled/coordinated charging.

A) Uncontrolled Charging

uncontrolled charging means that there are no scheduling to the time of charging. Once the EV is plugged into the charger, the charging starts until the battery is fully charged

or the charger is plugged off. Many studies have been dedicated to measure the impact of uncontrolled charging on the distribution systems.

As early as 1993, study of the impact of EVs on the distribution system is published in reference [70]. The study uses electricity demand data from town of Blacksburg in Virginia. In this study, the charging time is assumed to start at 8:00 PM when the off-peak interval starts. The study shows that 10% penetration level of EVs could cause a new peak in the starting of off-peak period in residential area. This new peak is even bigger than the daily load peak without EVs' load. As a solution to this problem, the authors suggest incentives to the customers to distribute their charging time throughout the off-peak period.

In [66], a study shows the impact of uncontrolled charging of EVs on the winter load curve in UK. The study shows increase of about 18% in the peak load for 10% penetration level of EVs. In this study, the authors assumed that customers will plug in their EVs to the charger when they arrive from work at around 6:00 PM. Charging is assumed to be for six hours with constant current of 10 A. This increase in the system's peak load has noticeable effect on the voltage deviation in the system. Also, the increase in the peak load could challenge the technical limitation of the distribution system which may necessitate an expensive upgrade to the distribution system to cope with this new peak.

The effect of uncoordinated charging of EVs on the distribution equipment, particulary, the distribution transformers, has been demonstrated in simulation study in [62]. The study used Western Australia 1200-node test system as a base for the simulation. The results show that even with low penetration level of EVs, 17%-31%, significant surge in the transformers' current, from 37% to 74%, is measured which effectively consume the lifetime of these transformers.

Work in [68] took the stochastic nature of SOC of the battery and starting time into consideration to measure the impact of the uncoordinated EVs charging on a typical UK distribution system. A probability density function for starting time of charge is developed based on electricity tariff structure and the pattern of vehicle usage. Also, the initial SOC of EV's battery is assumed as a random variable. The density function representing this random variable is determined from the travelled distance distribution. The simulation results for 10% penetration level of EVs with uncoordinated charging scenario shows 17.9% increase in the daily peak in residential areas, while 20% penetration level would increase the daily peak demand by 35.8%. Also, the study shows increase in the peak demand in the commercial and industrial areas when uncoordinated charging scenario is assumed. According to the paper, it is important to study different areas, (*i.e.,* residential, commercial, or industrial), separately rather than studying the overall load profile. The aggregated load profile results may mask a problem in one of these areas.

Also, study on the impact of uncoordinated EVs' charging on typical distribution system in Belgium published in [21]. Results show increase in both power loss and voltage deviation in the distribution system as number of EVs increases. At EVs' penetration level of 30%, the power loss doubled compared to the recorded power loss without EVs' load. Also, the voltage deviation reached its allowed limit, 10%, at peak load period on typical winter

night in Belgium.
Other studies and surveys on the impact of uncoordinated EV's charging can be found in [32, 33, 80, 88, 89, 96]. In general, the uncontrolled EV's charging can lead to the following undesirable effects:

1. Increase in the peak demand. This increase will stress the whole grid and infrastructure upgrades may become necessary to cope with this increase.

2. Increase in the energy cost. The increase in demand during the peak period due to the uncontrolled EVs' charging will increase the cost of energy $/Kwh for the utility. In turn, the utility will charge the customers more to compensate.

3. Increase in the power loss in the distribution system.

4. Increase in the voltage deviation in the distribution system.

5. Increase in the surge current in the transformers and other distribution systems' equipment. This will stress these equipment which, consequently, will decrease the lifetime of these expensive equipment.

To mitigate or at least decrease the negative effects of uncontrolled EVs' charging, the charging should be controlled. For example, shifting the time of charging from the peak period to off-peak period can be beneficial for utilities and customers alike. In fact, in most of the studies of the uncontrolled EVs' charging, the coordinated EVs' charging is suggested to decrease the negative effects of uncontrolled charging on the distribution systems.

B) Coordinated Charging

Coordinated charging of EVs can shift the charging time of EVs from the undesired period of time to more suitable period where the distribution system can accept more load. This optimization is known as coordinating charging. For example, late night valley when the load is at its minimum is a good choice for charging EVs since most of vehicles are parking at houses' parking lots and available for charging. At that period, electricity prices at its lowest rate which can work as an incentive for the customers to let their vehicles participate in these coordinating protocols. Under this notion of coordination, significant work in the literature has been published.

Authors in [17] suggested charging algorithm uses Time Of Use (TOU) prices to schedule the charging power and time of EVs. This scheduling should result in minimum charging cost for the customers. That also would shift the charging time from peak period to off-peak period as TOU prices are less in the off-peak period compared to peak period, thus, this scheduling will result in better load curve for the utility. The problem is formulated as an optimization problem as follows:

$$\begin{aligned} \text{minimize} \quad & C = \sum_{i=1}^{N} M(t_i) P(t_i) \Delta t \\ \text{subject to} \quad & 0 \leq P(t) \leq P_{battery}(t), \end{aligned} \tag{3.3}$$

where the total charging time for each vehicle is divided into N time slots with length of Δt for each time slot. $M(t_i)$ is the price of energy for the time slot t_i. $P(t_i)$ is the charging power at time slot t_i. This charging power can be adjusted to any level between zero and maximum allowed charging power, $P_{battery}(t)$. Adopted from [64], $P_{battery}(t)$ is changing nonlinearly with SOC of the battery according to given curve. The paper used this curve to determine the value of $P_{battery}(t)$ at any given SOC. due to nonlinearity of maximum charging power, heuristic algorithm is designed to solve this optimization problem. Finally, this paper includes a case study of charging Li-ion battery equipped in Nissan Altra EV. The start charging time is assumed normally distributed around 6:00 PM with standard deviation of 5. Also, initial SOC is assumed normally distributed around 0.5 with standard deviation of 0.3. Actual TOU prices in Beijing is used in this study. The results show that the average reduction in the cost using this optimization is 39.67% for 5% penetration level of EVs in Beijing compared to uncontrolled charging scenario. However, this study used TOU prices which are fixed for long period of time, typically for many months. This pricing system does not respond to the dynamic behavior of EVs load. EVs can easily create a new peak in the system especially in the beginning of the cheap period of time.

In [75], the authors investigated the effect of Time Of Use (TOU) prices strategy on a residential area representing average residential area in USA, Washington DC. By measuring the customers' response to the change in the electricity prices, TOU prices model can be built in order to shift deferrable load (*i.e.,* PHEV) from peak period to off-peak period. Typically, increasing the electricity prices during peak period compared to off-peak period can drive the customers to shift their usage from peak to off-peak period. However, the paper recommends careful design of TOU prices rate. Too much prices difference between peak and off-peak period can push too many customers to use off-peak period which may lead to a new peak load, especially in the beginning of off-peak period.

A work in reference [29] proposes a decentralized protocol to shift the EVs load to fill the valley in electric load profile. The problem is formulated as optimization problem as follows:

$$\begin{aligned} \text{minimize} \quad & \sum_{t=1}^{T} U\Big(D(t) + \sum_{n=1}^{N} r_n(t)\Big) \\ \text{s.t.} \quad & 0 \leq r_n(t) \leq r_n^{max} \\ & \sum_{t=1}^{T} \left(r_n(t) \times \Delta T\right) = R_n, \end{aligned} \tag{3.4}$$

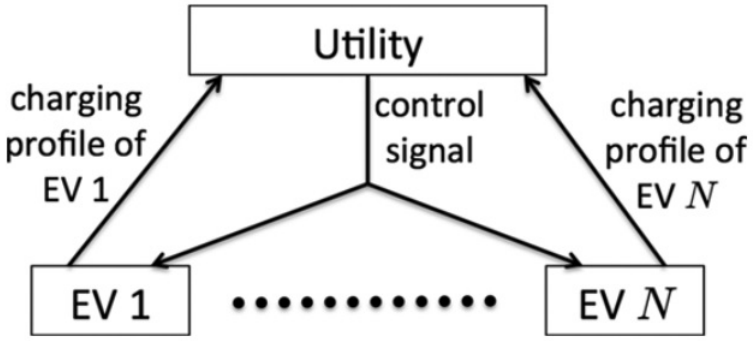

Figure 3.5: Information exchange between utility and EVs [29]

where, N is the number of EVs to be charged in period of T time slots of length ΔT. $D(t)$ denote the base load at time slot t, $r_n(t)$ denote the charging rate of EV n at time slot t, and $r_n := (r_n(1), r_n(2), ..., r_n(T))$ denote the charging profile of the n^{th} EV during all T time slots. $U(.)$ is a convex function. The charing rate at any time slot, $r_n(t)$ can not exceed the maximum allowed charing power r_n^{max}. Finally, R_n is the total energy needed by the n^{th} EV by the end of the charging period. The solution of this optimization will be the optimum charging profiles for all EVs which makes the overall load profile as flat as possible. The authors in this paper proposed a decentralized protocol to solve this optimization iteratively. In each iteration, the utility sends control single to all EVs. This signal can be interpreted as price single for all time slots. On receiving this signal, each EV adjust its charing profile in order to minimize the total charing cost. Then, every EV sends back its new charing profile to the utility. Utility calculates the overall EVs load profile and it adjusts its pricing signal by increasing the prices at the time slot where more load is pile up and decreasing the prices in the time slot where the load is light. After that, the utility sends a new signal for the second iteration. This process continue until the optimum load profile is achieved. Figure 3.5 illustrates the information flow between the utility and EVs. This algorithm aims to schedule EVs charging times in order to achieve better load profile in the system. However, the algorithm is depending on knowing the base load in the system in advance. This knowledge can be taken from the load forecast. But, the load forecast, especially when intermittent RES are used in the system, can be subjected to significant forecast error. This error can negatively affect the resultant overall load profile in the system.

Reference [20] proposes coordinated charging algorithm for EVs to minimize the power loss in the distribution system during a future period of time T. The algorithm uses the forecasted load in the system and the specification of EVs to be charged as inputs to calculate the optimum charging profiles for the EVs. This period of time is divided into t_{max} intervals, $t \in (1, 2, ..., t_{max})$, with length of Δt. The algorithm minimizes the power

loss in the system by solving the following optimization problem.

$$\begin{aligned} \text{minimize} \quad & \sum_{t=1}^{t_{max}} \sum_{l=1}^{lines} R_l \times I_{l,t}^2 \\ \text{s.t.} \quad & \forall t, \forall n \in nodes : 0 \leq P_{n,t} \leq P_{max} \\ & \forall n \in nodes : \sum_{t=1}^{t_{max}} P_{n,t} \times \Delta t \times x_n = C_{max} \\ & x_n \in \{0, 1\} \end{aligned} \tag{3.5}$$

The distribution system is divided into lines, $l \in (1, 2, ..., lines)$. The loads are attached to N nodes, $n \in (1, 2, ..., N)$. EVs are distributed randomly on the nodes. The binary variable x_n in the optimization formula serve as an indicator for the existence of an EV at node n, $x_n = 1$ means there is an EV attached to the distribution system at node n and $x_n = 0$ means no EV at that node. R_l is the impedance of the line l. Quadratic programming is used to solve this problem. Then, the resultants EVs' load is combined with the forecasted load to determine the overall load profile in the system. Next, the backward-forward sweep method is used to determine the power loss in the system. This procedure is repeated until power loss based stopping criterion is reached.
However, the paper is mainly using the day-ahead load forecast as a deterministic variable. To capture the stochastic behaviour of the day-ahead forecasted load in the system, the authors suggest using stochastic optimization where different possible scenarios of the day-ahead load is optimized and the expected value of the power loss evaluated.

Distributed algorithm to optimize the charging of EVs is proposed in [30]. In this algorithm, iteratively, EVs receive a control signal from the utility to guide these EVs to choose their own charging profiles to achieve the overall flat load profile in the system. The broadcasted signal from the utility works as an intimidating pricing signal. First, the EVs sends their complete charging profiles to the utility during the period T. Then, the utility calculates the overall load profile in the system during the period T from EVs charging profiles plus the forecasted load during that period. To flatten this overall load profile in the system, the utility broadcast guiding single, *i.e.,* pricing single, to all EVs so they adjust their charging profiles accordingly. The single stochastically reduce the overall EVs charging load during the interval Δt where the overall load profile is high and shift that load to another interval where the load is lower. After this adjustments, EVs send the new charging profiles again to the utility. the utility repeats this procedure until the best overall load in the system is achieved.
Again, the load forecast has been used as a base to optimize the charging of EVs. This forecast, however, can have significant error which may affect the real overall load in the system.

In [49], the paper is trying to mitigate the effect of uncontrolled EVs charging by

proposing a decentralized charging algorithm. The aim is to flatten the load curve in the system as much as possible to improve the chance of the distribution system to cope with higher penetration level of EVs. This work is avoiding the optimization methods used in other scheduling algorithms since the hours-ahead load forecast is not accurate. On-line algorithm is proposed to work on small intervals of time, 15 minutes, where the prediction is more accurate. In the beginning of each interval, command signal is sent to all plugged in EVs to turn on the needed EVs' load during that interval. This signal can be sent more than once in the beginning of each interval until the right number of EVs are on. Every time, the signal is adjusted according to the resulted EVs' load from the previous signal until the right number of EVs' load achieved. However, the paper did not show how the utility knows the right amount of EVs' load at each interval of time. Instead, the authors used variable , β, which effect the decision of right number of EVs put to charge at any point alongside the net-load at that time interval. In a case study in this paper, β is given different values with different penetration levels without justification. Also, the deterministic behavior of turning EVs on according to reference number in the command signal can lead to very difficult situation when cluster of EVs have the same specification. If group of EVs have close specifications, they can turn on or off together when the utility needs just some of them to be on at that moment.

An ant-based swarm algorithm to coordinate EVs charging is proposed in [93]. The task of this algorithm is to fill the load valley within specific time period with EVs load. The algorithm uses the load forecast to optimize the charging times of the EVs. The authors tried to tackle the problem of load forecast error by rerunning the algorithm repeatedly every time a better forecast is produced. However, this repetition can be computationally expensive and timely consuming.

3.2 Summary

In the literature, the works on smart charging of EVs can be divided into three categories: charging influenced by the tariffs; controlled charging by a central utility; and controlled charging in distributed manner. Under the first category, Time Of the Use (TOU) pricing is used as an incentive to the EVs' owners to shift the charging time of their EVs to off-peak periods [17, 75]. One shortcoming of this approach is the possibility of forming a new peak in the beginning of the off-peak period when many EVs are likely to start charging simultaneously. The second category of charging algorithms depends on a centralized unit coordinating the charging times of all participating EVs [20, 41, 51, 77]. For example, in reference [20], a coordinated charging algorithm is proposed to minimize the power loss and to maximize the grid's load factor. This charging coordination is managed entirely by a centralized utility server. Consequently, the centralized server needs to be powerful enough to manage all scheduling tasks such as solving the optimization problem of charging

time of EVs and communicating with each EV whenever it is necessary. The scalability problem of this approach has led to the third category of charging algorithms. In this category, charging decisions are shared between a centralized unit and the EVs. This would decrease the pressure on the centralized unit especially when the penetration level of EVs is high. Motivated by their scalability, many decentralized algorithms for charging have been proposed in the literature [29, 30, 49, 91, 93].

In general, in both the centralized and distributed charging categories, the strategy was to use the flexibility of EVs' loads to schedule the EVs charging time into more suitable periods of time. This charging schedule is optimized ahead of time based on the short-term forecast of the load in the system. However, in the presence of RES, the forecasted *net-load* is not accurate due to the stochastic nature of RES. Some studies tried to deal with this problem but in a naive way. Works in references [93] and [63] suggested rescheduling whenever more accurate net-load forecast comes. This strategy can be easily overwhelmed by the speed of the unexpected fluctuations in the net-load. Other studies used stochastic optimization techniques to solve the optimization problem [20, 41]. However, their stochastic optimizations generally consider minimizing *the expected* value of the objective function. These stochastic optimizations do not deal with each scenario individually. Rather, they give one optimized solution for all possible scenarios.

The work in this dissertation is motivated by the findings in this chapter and the pervious chapter. First, the stochastic behaviour of RES and its impact on the forecast error of the net-load in the system should be carefully modeled. Also, the impact of different penetration levels of intermittent RES on the net-load forecast error has to be measured. Next, the flexibility of the EVs' load will be exploited further in order to absorb the unexpected fluctuations in the net-load at real time. Most of the works in the literature optimize the charging time of the EVs ahead of time to, for example, flatten the overall load in the distribution system. These works assume that the flexibility of the EVs load is exhausted by this optimization. This thesis shows that the EVs load flexibility can be used twice; first, to shift the EVs load from peak periods to off-peak periods. Second, the flexibility of the EVs load is used further to counter the unexpected fluctuations in the net-load at real time.

Chapter 4

Evaluation of the Net-load Forecast Error

. In this chapter, we formally define the net-load forecast error in the system. Next, the net-load forecast error is modeled carefully to capture the behaviour of the unexpected fluctuations in the net-load at real time. Also, the impact of different penetration levels of wind power on the net-load forecast error is measured by the model. Finally, the ahead-of-time optimization adopted by most of scheduling methods in the literature is formulated. Then, the impact of the net-load forecast error on these scheduling methods is demonstrated.

4.1 The Net-Load

Figure 4.1 shows the system model of this study. The generated power from the sustainable (renewable) energy sources is fed directly to the consumers. The remaining unserved load, the net-load, is served by the utility's conventional power units. In this work, we treat the generated power from sustainable energy sources as a "*negative*" load in the electric grid. Thus, we define the *Net-Load*, $L_N(t)$, as follows:

$$L_N(t) = L_c(t) - L_R(t), \tag{4.1}$$

where, $L_c(t)$ is the conventional load in the grid at time t, and $L_R(t)$ is the produced power from the renewable energy sources at time t. In the rest of our discussion, without any loss of generality, we will use wind power as a representative of renewable energy sources.

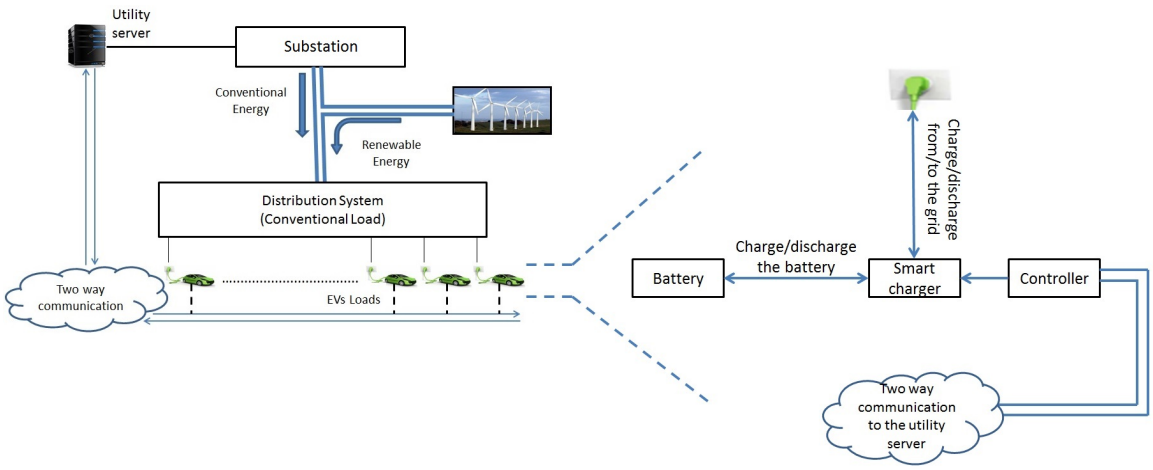

Figure 4.1: System Model

4.2 The Net-Load Forecast Error

Based on Equation (4.1), the *forecasted* net-load $\hat{L}_N(t)$ at a future time t can be expressed as follows:

$$\hat{L}_N(t) = \hat{L}_c(t) - \hat{L}_R(t), \tag{4.2}$$

where, $\hat{L}_c(t)$ is the forecasted load at time t, and $\hat{L}_R(t)$ is the forecasted wind power at time t. However, both the forecasted loads, $\hat{L}_c(t)$ and $\hat{L}_R(t)$, suffer from forecast error. Therefore, the actual net-load at a future time t can be written as follows:

$$L_N(t) = (\hat{L}_c(t) + \varepsilon_1) - (\hat{L}_R(t) + \varepsilon_2), \tag{4.3}$$

where, ε_1 is the forecast error of the conventional load and ε_2 is the forecast error of the generated wind power. It has been shown in previous studies that both the forecast errors follow a Gaussian distribution [11,23,55,65]. Therefore, ε_1 and ε_2 can be formally expressed as follows:

$$\begin{aligned} \varepsilon_1 &\sim N(\bar{L} \times \mu_1, (\bar{L} \times \sigma_1)^2) \\ \varepsilon_2 &\sim N(c \times \mu_2, (c \times \sigma_2)^2), \end{aligned} \tag{4.4}$$

where, $\bar{L}$ is the average load, and μ_1 and σ_1 are mean and standard deviation of load forecast errors normalized by $\bar{L}$, respectively. Also, c is the installed wind power capacity, and μ_2 and σ_2 are the mean and standard deviation of wind power forecast errors normalized by c, respectively.
As an example in this study, we use data taken from California Independent System Operator (CAISO) for the year 2011 to quantify the parameters of the two forecast errors (*i.e.,*

μ_1, σ_1 and μ_2, σ_2) [36]. Day-ahead forecast data for both wind power and load in CAISO system are compared to the real wind power and load values in the system to estimate these parameters. The results show that $\mu_1 = -0.002, \sigma_1 = 0.026, \bar{L} = 26297MW$ for the conventional load, and $\mu_2 = -0.004, \sigma_2 = 0.130, c = 940MW$ for wind power. However, in this study, we assume that the means of both errors go to zero as the examined data points increases: $\mu_1 \to 0$ and $\mu_2 \to 0$. In other words, we assume that the forecasting is unbiased (*i.e.,* the chance of over forecasting is equal to the chance of under forecasting). Also, since it is generally assumed that both the errors are uncorrelated [11], Equation (4.3) can be rewritten as follows:

$$\begin{aligned} L_N(t) &= (\hat{L}_c(t) - \hat{L}_R(t)) + (\varepsilon_1 - \varepsilon_2) \\ &= \hat{L}_c(t) - \hat{L}_R(t) + \varepsilon, \end{aligned} \tag{4.5}$$

where,

$$\begin{aligned} &\varepsilon \sim N(\mu, \sigma^2), \text{ where} \\ &\mu = \bar{L} \times \mu_1 - c \times \mu_2, \\ &\sigma^2 = (\bar{L} \times \sigma_1)^2 + (c \times \sigma_2)^2 \end{aligned} \tag{4.6}$$

Equation (4.6) represents the net-load forecast error as normal distributed random variable. That is because adding two independent normal distributions results in another normal distribution. This representation of the net-load error captures the full extent of the relationship between the net-load forecast error with the wind power forecast error and the conventional load forecast error. Additionally, graphical relationship can be drawn from this equation to illustrate the relationship between the net-load forecast error, ε, and the penetration level of wind power represented by the installation capacity c as it will be shown later in this section.

Further, it is beneficial to represent the net-load forecast error as normalized error. To achieve this, we will normalize the net-load forecast error, ε, by the average net-load ($\bar{L}_N$) in the system. To estimate $\bar{L}_N$, we take the expectation of the first part of Equation (4.5) as follows:

$$\begin{aligned} E(L_N(t)) &= E(\hat{L}_c(t)) - E(\hat{L}_R(t)) + E(\varepsilon_1) - E(\varepsilon_2) \\ \Rightarrow \bar{L}_N &= \bar{L} - \bar{L}_R + \mu_1 - \mu_2 \\ &= \bar{L} - \bar{L}_R \end{aligned} \tag{4.7}$$

where, $\mu_1 = 0$ and $\mu_2 = 0$ according to our assumption, and $\bar{L}_R$ is the average generated wind power. However, instead of normalizing by $(\bar{L} - \bar{L}_R)$, we will normalize the net-load forecast error ε by $(\bar{L} - c)$. This change will not affect the trend of the normalized error since $\bar{L}_R$ and c are in a linear relationship to each other. We have chosen to use c over $\bar{L}_R$ to comply with the convention in the literature [36]. Thus, the normalized net-load

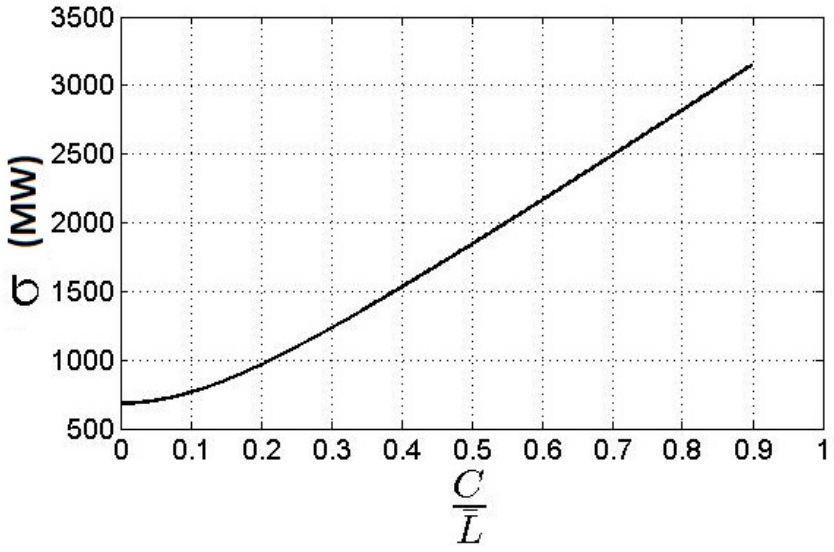

Figure 4.2: The change in σ with wind power capacity

forecast error can be represented as follows:

$$\begin{aligned} &\varepsilon_{norm} \sim N(\mu_n, \sigma_n^2), \text{ where} \\ &\mu_n = \frac{\bar{L}}{\bar{L}-c} \times \mu_1 - \frac{c}{\bar{L}-c} \times \mu_2, \\ &\sigma_n^2 = (\frac{\bar{L}}{\bar{L}-c} \times \sigma_1)^2 + (\frac{c}{\bar{L}-c} \times \sigma_2)^2 \end{aligned} \tag{4.8}$$

It should be noted that the mean, μ_n, of normalized error ε_{norm} is equal to zero (*i.e.*, $\mu_n = 0$) since $\mu_1 = 0$ and $\mu_2 = 0$.

To illustrate the effect of the penetration level of wind power on the net-load error, we will use the numerical results mentioned earlier in this section for CAISO system for σ_1 , σ_2, and $\bar{L}$. First, we use Equation (4.6) to show the behavior of σ with different penetration levels of the wind power. Figure 4.2 represents the increase in the standard variation of the net-load error, σ, versus the increase in the penetration level of wind power, c. The x-axis represents $\frac{c}{\bar{L}}$ changing from 0.1 to 0.9. This change represents the change of the penetration level of wind power in the system. The vertical axis shows the corresponding value of σ.

Clearly, the net-load forecast error is significantly increasing as the penetration level of wind power increases. Also, it is important to notice that the net-load forecast error is increasing as the average net-load itself decreases. This is due to the fact that the increase in penetration level of wind power will decrease the net-load and, at the same

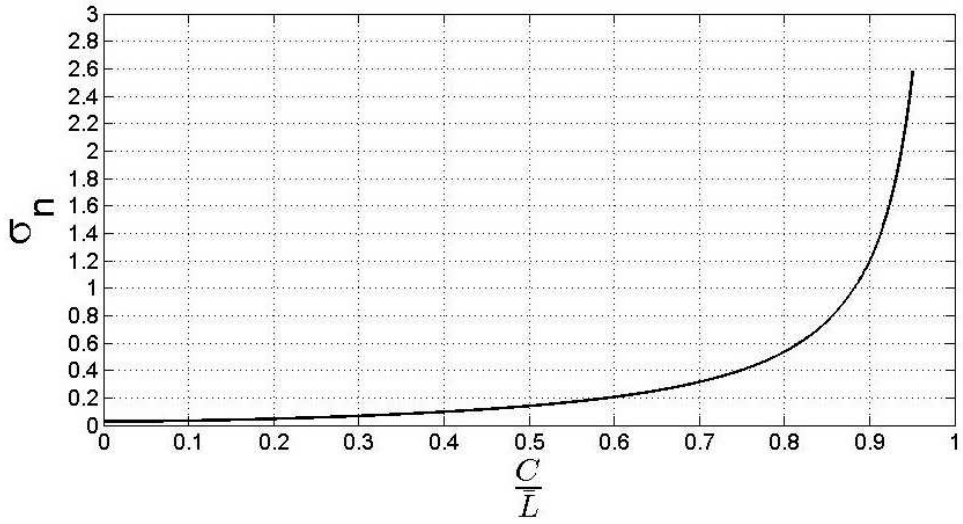

Figure 4.3: The change in σ_n with wind power capacity

time, will increase the net-load forecast error.This can be seen clearly in the behavior of the normalized net-load error against different penetration levels of wind power. Figure 4.3 shows the relationship of the normalized net-load forecast error, σ_n described in Equation (4.8), versus different penetration levels of wind power, $\frac{c}{\bar{L}}$.

It is clear from the graph that the increase in σ_n is exponential. Thus, although higher penetration level of wind power in the grid will decrease the net-load and, consequently, will decrease the need for fossil fuel power plants, more operational reserve will be needed to meet the increasing net-load forecast error. This explains the reported need by CAISO to increase the regulation and load following reserves to accommodate higher penetration levels of RES in the system as shown in Figure 1.3.

4.3 Impact of The Net-Load Forecast Error on Traditional Ahead-Of-Time Scheduling Methods For Charging EVs

Several studies have been dedicated to examine the impact of charging EVs on the power system [12, 31, 52, 67, 90]. In these studies, it has been concluded that uncoordinated charging of EVs will result in new peak load in the power grid, possible voltages deviation problems in the system, and/or increase in the power losses. To mitigate these effects, coordinated charging methods have been proposed [20, 29, 51]. In general, the proposed methods distribute the time of charging of these EVs over future period of time $\mathcal{T}$ in order

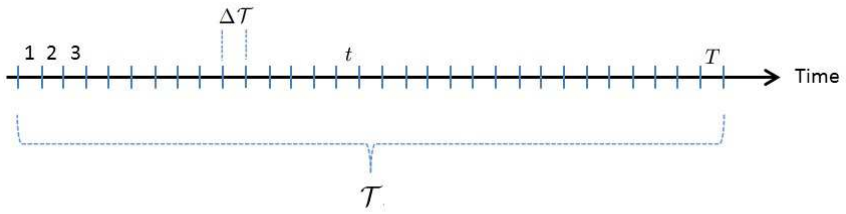

Figure 4.4: Time slots of width $\Delta\mathcal{T}$ within period $\mathcal{T}$

to smooth the overall load in the power system assuming that all EVs are available to be charged at any period of time within $\mathcal{T}$. This charging mechanism optimizes the charging times of the EVs in order to shift the EVs load from peak periods to off-peak periods as much as possible. To explain this ahead-of-time optimization method, we consider a scenario where we have N EVs, $\mathcal{N} := \{1, 2, ..., n, ..., N\}$, to be scheduled for charging over future span of time $\mathcal{T}$. This period of time divided into T time slots of length $\Delta\mathcal{T}$, $\mathcal{T} := \{1, 2, ..., t, ..., T\}$, where $\sum_{t=1}^{T} \Delta\mathcal{T} = \mathcal{T}$. Figure 4.4 shows T time slots within the time horizon $\mathcal{T}$.

Also, the utility is assumed to have the forecast of the base load in the system, $\hat{D(t)}$, during this period of time $\mathcal{T}$. $\hat{D(t)}$ represents all conventional load in the system, excluding the EVs load. Each EV needs to be charged by pre-determined amount of energy, E_n, during its available time which assumed to be $\mathcal{T}$. Eventually, the charging method should guarantee a charging profile for each n^{th} EV $r_n := \{r_n(1), r_n(2), ..., r_n(T)\}$ so that $\sum_{t=1}^{T} r_n(t) \times \Delta\mathcal{T} = E_n$, $n \in \mathcal{N}$. Where $r_n(t)$ is the charging power rate of the n^{th} EV during the time slot t. Importantly, $r_n(t)$, $\forall t$, should not exceed the maximum allowed charging power r_n^{max}. Thus, the constrain $0 \leq r_n(t) \leq r_n^{max}, \forall t \in \mathcal{T}, \forall n \in \mathcal{N}$ should be met.

In this study, we choose the objective function of the optimization to be the flattening of the overall load in the system. This optimization has many benefits to the distribution system, such as decreasing the peak demand, decreasing the power loss in the distribution system, decreasing the voltage deviation, and decreasing the surge current in the transformers and other distribution systems' equipment. Also, this choice benefits the customers since it shifts the charging time of EVs to off-peaks periods when the cost of the energy is usually less. More generally, we say that the utility's goal is to track the preferred load profile $G(t)$.

Given this layout, the scheduling problem can be mathematically formulated as an

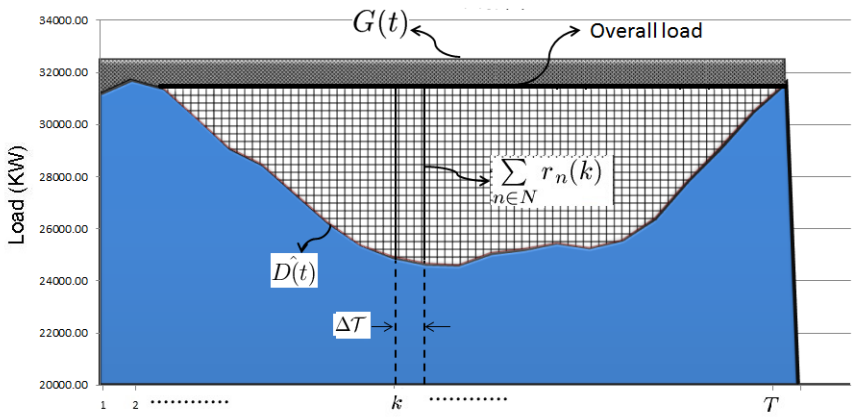

Figure 4.5: Graph showing the optimization for the overall load without error

optimization problem as follows:

$$\begin{aligned} \underset{r_n(t)\forall n\forall t}{\text{minimize}} \quad & \sum_{t=1}^{T}[(\hat{D(t)} + \sum_{n=1}^{N} r_n(t)) - G(t)]^2 \\ \text{s.t.} \quad & 0 \leq r_n(t) \leq r_n^{max}, \forall t \in \mathcal{T}, \forall n \in \mathcal{N} \\ & \sum_{t=1}^{T} r_n(t) \times \Delta\mathcal{T} = E_n, \forall n \in \mathcal{N} \end{aligned} \tag{4.9}$$

In this optimization problem, the overall load $(\hat{D(t)} + \sum_{n\in\mathcal{N}} r_n(t))$, $t \in \mathcal{T}$, needs to be as close as possible to the target load profile $G(t)$, $t \in \mathcal{T}$. This is achieved by minimizing the square difference between the two values, $\sum_{t\in\mathcal{T}}[(\hat{D(t)} + \sum_{n\in\mathcal{N}} r_n(t)) - G(t)]^2$, $t \in \mathcal{T}$. Figure 4.5 shows graphically this layout. The decision variables of this optimization are the charging profiles of the EVs, $r_n(t)$, $\forall n \forall t$. Therefore, the result of this optimization problem will be the optimum charging profiles to all EVs r_n^*, $\forall n \in \mathcal{N}$.
However, in this formulation, there is a fundamental assumption that the utility has the knowledge of the base load $D(t)$. In fact, the utility has the forecast of the base load $\hat{D(t)}$, not the exact $D(t)$. The exact base load can be expressed as follows:

$$D(t) = \hat{D(t)} + \varepsilon, \tag{4.10}$$

where, ε is the forecast error. This error can be significant especially when the penetration level of RES increases as explained in Section 4.2.

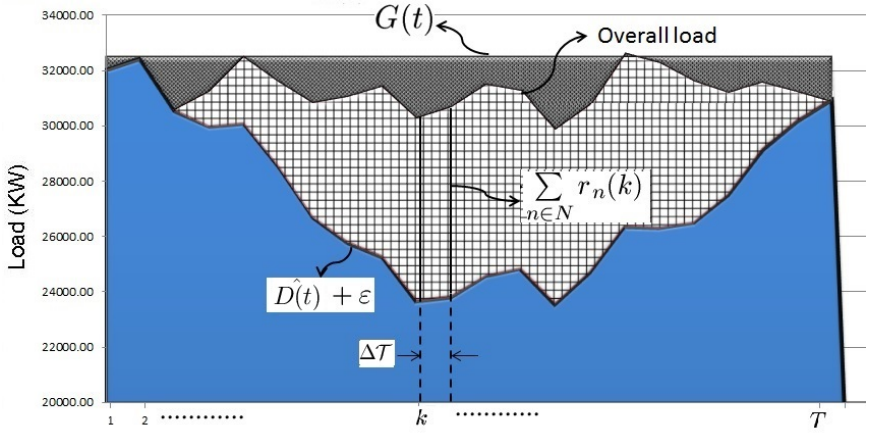

Figure 4.6: Graph showing the effect of forecast error on the optimized overall load

As a consequence of not taking this error into consideration, the optimized overall load in the system will be susceptible to this error. Thus, the targeted load profile, $G(t)$, will not be fully achieved. Actually, more significant the net-load forecast error is, farther the real overall load profile is from the targeted overall load. To illustrate this effect graphically, Figure 4.6 shows the expected overall load in the system when including the forecast error in comparison to the expect overall load without the forecast error in Figure 4.5. In Figure 4.5, the EVs charging profiles are optimized to achieve flat load profile in the system, $G(t)$. As a result from this optimization, the overall load profile is flat as promised given the forecast error is zero. But we know that the forecast error is not zero. Rather, it could be very significant especially when the penetration level of RES is high. Therefore, this forecast error will affect the overall load profile as shown in Figure 4.6.

Finally, it is important to understand that the deviation of the real overall load from the targeted profile is not caused by the optimized EVs load; instead, it is a result of the stochastic behavior of the net-load in the system. However, we believe that EVs load has the flexibility to encounter this error had it been exploited in better way.

4.4 Summary

In this chapter, we investigated the nature of the net-load forecast error in the electric grid. Based on the load forecast error and the wind energy forecast error, the net-load forecast error is modeled as a random variable. It has been shown that this random variable follows Gaussian distribution. As an example, real data from CAISO have been used to estimate the parameters of this Gaussian distribution, (μ, σ^2). Also, the impact of different penetration levels of RES (represented in this study by the wind energy) on σ^2

is illustrated. Finally, the inability of the traditional ahead-of-time scheduling algorithms of charging EVs to deal with the variability in the net-load caused by the forecast error is explained.

Chapter 5

A Novel Online Charging Algorithm for EVs Under Stochastic Net-Load

.

In this chapter, we propose a novel charging algorithm for Electric Vehicles (EVs) in smart grids. Unlike traditional charging methods, this algorithm is designed to exploit the flexibility of the EVs' load to absorb the unforeseen fluctuations in the net-load caused mainly by the intermittency in wind energy. In this chapter, we first formulate the problem with traditional charging algorithms in the presence of renewable energy sources (RES). Second, we show that the overall energy consumed by the overall load in the system can be estimated ahead of time despite the stochastic behavior of the net-load. Third, a detailed description of our online algorithm shows how EVs' charging decision is taken by the utility server in real time—not ahead of time—according to the current situation of the net-load. Also, unlike most of the charging algorithms in literature, our proposed algorithm considers keeping the charging rates constant, thus, imposing less technical and engineering requirements and complexity on the EVs' charging infrastructure. Finally, to test the performance of our online charging algorithm, a tool has been developed in Java to simulate our algorithm. A comprehensive performance evaluation of our algorithm against a traditional Ahead-of-Time charging algorithm shows clear improvements achieved by our algorithm in absorbing the unexpected fluctuations in the net-load caused mainly by the stochastic behavior of the produced wind power.

In general, most of charging algorithms in the literature use the flexibility of EVs' loads to schedule the EVs charging time into more suitable periods of time. This charging schedule is optimized ahead of time based on the short-term forecast of the load in the system. However, in the presence of RES, the forecasted *net-load* is not accurate due to the stochastic nature of RES. As explained in Chapter 4, the net-load is the difference between the conventional load and the generated power from RES in the distribution system. In

most of the previous works in the literature, the uncertainty in the forecasted net-load is not considered. Some studies tried to deal with this problem but in a naive way. Works in references [93] and [63] suggested rescheduling whenever more accurate net-load forecast comes. This strategy can be easily overwhelmed by the speed of the unexpected fluctuations in the net-load. Other studies used stochastic optimization techniques to solve the optimization problem [20, 41]. However, their stochastic optimizations generally consider minimizing *the expected* value of the objective function. These stochastic optimizations do not deal with each scenario individually. Rather, they give one optimized solution for all possible scenarios. In contrast, we propose a novel charging algorithm deals with the stochastic fluctuations in the net-load as it happens. The algorithm uses the flexibility of EVs' load to adjust the overall load to more desirable load profile by the utility. The proposed algorithm absorbs the unexpected fluctuations in the net-load caused mainly by the stochastic behavior of wind power; therefore, it reduces the dependency on the expensive operational reserve needed otherwise to deal with these fluctuations.

The contribution of the work in this chapter is summarized in four points:

1. We define and formulate the problem with traditional Ahead-of-Time charging algorithms in the presence of RES.

2. We show that the energy consumed by the overall load in the system can be estimated ahead of time despite the stochastic behavior of the net-load and that this estimation gets more accurate as the period of time over which this estimation is done increases.

3. We propose a novel online charging algorithm which uses the flexibility of EVs' load not only to shift the EVs' loads from peak-periods to off-peak periods similar to other charging algorithms, but also to counter the unexpected variability in the forecasted net-load in real time.

4. In our proposed algorithm, the charging power rate to the batteries is assumed to be constant. In contrast, the other charging algorithms usually treat the charging power as a variable which can be set to any value between zero and maximum allowed value in every small interval of time. To apply such charging profiles to the batteries, the smart chargers have to be equipped with such a capability. However, this capability will impose more technical and engineering requirements and complexity on the charging infrastructure compared to the simpler charging infrastructure needed by our charging strategy.

The rest of the chapter are organized as follows. The system model is briefly described in Section 5.1. The problem with the Ahead-of-Time optimization approach for charging EVs is formulated in Section 5.2. Our proposed solution and the description of the proposed algorithm are given in Section 5.3. We show the performance of our algorithm against traditional Ahead-of-Time scheduling algorithm in Section 5.4. Finally, the chapter is summarized in Section 5.6.

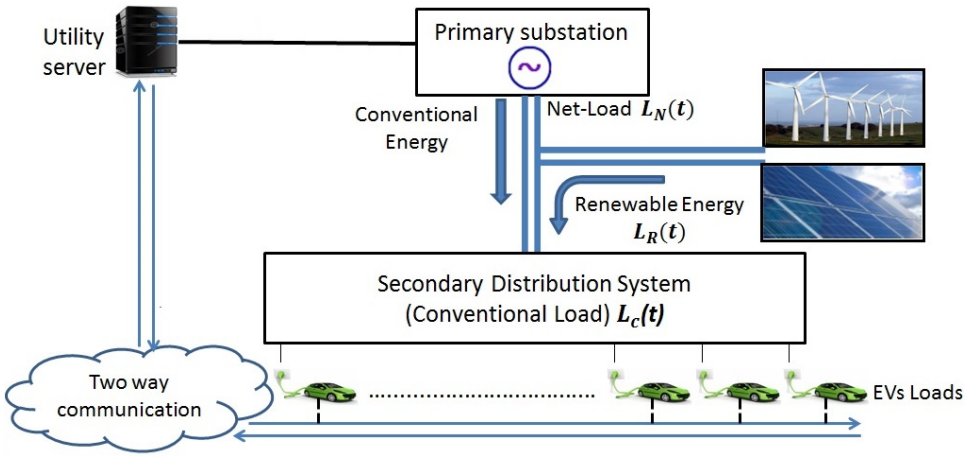

Figure 5.1: The system model

5.1 System Model

Figure 5.1 shows the system model considered in this study. In this model, the distribution system has three types of loads. First, the conventional load, $L_c(t)$, represents the uncontrolled daily load in the system. The second type of load is the charging profiles of EVs, $r_i(t)$, $\forall i \forall t$. Here, $r_i(t)$ represents the charging rate of i^{th} EV at time slot t. The utility server can command any EV to start charging or stop charging at any time as long as the EV is connected to the smart charger. Third, the power produced by RES, $L_R(t)$, is considered as a negative load in the system. Although $L_R(t)$ is not dispatched, it can be forecasted, however, with less accuracy compared to the forecast of $L_c(t)$. Also, in this work, as explained in Chapter 4, we define the net-load, $L_N(t)$, as follows:

$$L_N(t) = L_c(t) - L_R(t). \tag{5.1}$$

The primary substation keeps the system balanced by producing enough conventional energy to feed the net-load at all times.

5.2 Problem Formulation

In the literature on charging algorithms for EVs, the charging time of EVs is generally scheduled ahead of time in order to mitigate the problem of creating new peaks or exacerbating existent peaks in the system. To explain the problem with this approach, assume that n EVs are available for charging during a period of time T. This period is divided into m slots of length Δt so that $m \times \Delta t = T$. The i^{th} EV is plugged-in at time slot

$plug_i$ and will be unplugged at time slot $dead_i$ by which the customer needs his vehicle to be fully charged. Both $plug_i$ and $dead_i$ are decided by the customer. Also, the state of charge of the battery of the i^{th} EV at $plug_i$ is denoted by SOC_i. If $SOC_i = 0$, it means that the battery is empty at $plug_i$ time, while $SOC_i = 0.5$ means the battery is half full. The value of SOC_i differs from one customer to another based on their driving behavior. Without loss of generality, we assume that the batteries of all n EVs have the same nominal capacity denoted by C. In this work, we assume that all batteries are charged with a constant charging rate, r. Thus, the scheduling of the charging times of these EVs can be formulated as an optimization problem as follows [29]:

$$\begin{aligned} &\underset{r_i(t),\forall i}{\text{minimize}} \sum_{t=1}^{m} \Big((\hat{L}_N(t) + \sum_{i=1}^{n} r_i(t)) - G(t) \Big)^2, \\ &\text{subject to} \\ &\qquad \sum_{t=plug_i}^{dead_i} (r_i(t) \times \Delta t) = C_i^r, i = 1, 2, ..., n. \\ &\qquad C_i^r = (1 - SOC_i) \times C, \end{aligned} \tag{5.2}$$

where, $r_i(t)$, $\forall i$, are the charging profiles of EVs, the subject of this optimization. In every time slot, t, between plug-in and deadline times, $plug_i \leq t \leq dead_i$, $r_i(t)$ can be either "on" with charging rate r or "off" with charging rate 0. In addition, the constraints of this optimization should be met, *i.e.,* delivering the required energy, C_i^r, to the battery of the i^{th} EV before the deadline. In the objective function, $G(t)$ represents the desired overall load in the system. For example, if the utility prefers to have the overall load in the system as flat as possible, then $G(t)$ can be replaced by a constant. It is worth noting that, in traditional Ahead-of-Time charging algorithms [20, 29, 30], the net-load used in the optimization is the expected net-load, $\hat{L}_N(t)$—and not the real net-load, $L_N(t)$, as the optimization is done ahead of time. In this context, two main problems arise.

First, the optimization uses $\hat{L_N}(t)$ which deviates from $L_N(t)$ by a random variable ε. This random variable can be characterized by a normal distribution with a mean μ and a variance σ^2, $\varepsilon \sim N(\mu, \sigma^2)$, as explained in Chapter 4. Although the mean of this forecast error is zero ($\mu = 0$), the variance, σ^2, can be significant especially when the penetration level of RES is high. Thus, having the solution of the optimization problem in (5.2), $r_i^*(t)$, $\forall i$, we define the *expected* overall load in the system as follows:

$$\hat{L}_{oa}(t) = \hat{L}_N(t) + \sum_{i=1}^{n} r_i^*(t), \forall t. \tag{5.3}$$

However, the *real* overall load in the system, $L_{oa}(t)$ is affected by the net-load forecast

error, ε, as follows:

$$L_{oa}(t) = \hat{L}_N(t) + \varepsilon + \sum_{i=1}^{n} r_i^*(t), \forall t. \tag{5.4}$$

This means that although the optimization guarantees the closeness of the expected overall load in the system, $\hat{L}_{oa}(t)$, to the desired overall load by the utility, $G(t)$, the real overall load, $L_{oa}(t)$, is not as close. In fact, $L_{oa}(t)$ deviates from $\hat{L}_{oa}(t)$ by the net-load forecast error ε as it is clear from Equations (5.3) and (5.4). It is important to note that this difference between $\hat{L}_{oa}(t)$ and $L_{oa}(t)$ has to be dealt with when it appears in the system. This is usually done by maintaining an appropriate operational reserve in the grid. Therefore, the increase in ε should be met by an increase in the operational reserve in the system. As shown in Chapter 4, ε increases as the penetration level of RES increases, and, consequently, the operational reserve must be increased. However, the flexibility of the EVs' loads can help in absorbing part of this error in the real overall load had it been better exploited and, hence, reducing the dependency on the operational reserve. In Equation (5.4), the optimized EVs' loads, $r_i^*(t)$, are not rigid loads. These loads, in fact, can be used to accommodate part of the fluctuation in the real overall load. Some EVs' charging profiles, $r_i^*(t)$, can be further shifted before or after their assigned time slots to absorb this error. Nevertheless, traditional EVs' charging optimization approach represented by Equation (5.2) does not consider this possibility, even though the EVs' load have the flexibility to do so.

Second, in most of the charging algorithms in the literature, the batteries charging rate, $r_i(t)$, is allowed to take any value between 0 and r_{max}, *i.e.*, $0 \leq r_i(t) \leq r_{max}$, $\forall i \forall t$. However, to apply such variable charging profiles to the batteries, the smart chargers have to be equipped with such a capability which, consequently, will impose more technical and engineering requirements and complexity on the charging infrastructure. Thus, in this work, we are considering a constant charging rate, r, which would require a simpler charging infrastructure.

5.3 Proposed Solution

This section will be divided into three subsections. First, we show that an optimum overall load reference can be determined ahead of time. This overall load reference can be used then by the utility server to adjust $L_{oa}(t)$ at real time. Second, the flexibilities of EVs will be defined. Knowing these flexibilities are essential to deciding which EVs should start charging first in order to meet the charging deadlines imposed by the customers. Third, our proposed online charging algorithm will be explained in details.

5.3.1 The Predetermined Overall Load Reference

This load reference should be calculated ahead of time to be used by our algorithm to adjust the real overall load in the system during the active charging period T.

Now, consider the expected overall load, $\hat{L}_{oa}(t)$, and the real overall load, $L_{oa}(t)$, during the optimization period T, which are calculated earlier in Equation (5.3), and Equation (5.4), respectively.

Theorem : The difference between the average consumed energy by the expected overall load, $\hat{L}_{oa}(t)$ in Equation (5.3), over all m time slots and the average consumed energy by the real overall load, $L_{oa}(t)$ in Equation (5.4), over all m time slots goes to zero as the period of time, T, increases. Mathematically,

$$\frac{1}{m}\sum_{t=1}^{m} L_{oa}(t) \times \Delta t - \frac{1}{m}\sum_{t=1}^{m} \hat{L}_{oa}(t) \times \Delta t = 0, T \to \infty, \tag{5.5}$$

where,

$$m = \frac{T}{\Delta t}$$

.

Proof. From Equation (5.3), by taking the expectation of both sides:

$$\begin{aligned} E(\hat{L}_{oa}(t)) &= E(\hat{L}_N(t)) + E(\sum_{i=1}^{n} r_i^*(t)) \\ &= \overline{\hat{L}_N} + \sum_{i=1}^{n} \bar{r_i^*}, \end{aligned} \tag{5.6}$$

where $\overline{\hat{L}_N}$ represents the average of the forecasted values of the net-load during the time period T, $\overline{\hat{L}_N} = \frac{1}{m}\sum_{t=1}^{m} \hat{L}_N(t)$. And $\bar{r_i^*}$ represents the average value of charging rates of i^{th} EV of all slots of time in the time period T, $\bar{r_i^*} = \frac{1}{m}\sum_{t=1}^{m} r_i^*(t)$. Similarly, from Equation (5.4), we get:

$$\begin{aligned} E(L_{oa}(t)) &= E(\hat{L}_N(t)) + E(\varepsilon) + E(\sum_{i=1}^{n} r_i^*(t)) \\ &= \overline{\hat{L}_N} + \hat{X} + \sum_{i=1}^{n} \bar{r_i^*}, \end{aligned} \tag{5.7}$$

where $\hat{X}$ is a random variable represents the average of m samples from ε, and m is the number of time slots in the time period T. According to central limit theorem, $\hat{X}$ can be represented by normal distribution with mean equal to mean of ε, which is zero, and

variance equal to $\frac{\sigma^2}{m}$, $\hat{X} \sim N(0, \frac{\sigma^2}{m})$, where σ^2 is the variance of ε. Thus, from Equations (5.6) & (5.7):

$$\begin{aligned}
& E(L_{oa}(t)) - \hat{X} = E(\hat{L}_{oa}(t)) \\
\Rightarrow & \frac{1}{m}\sum_{t=1}^{m} L_{oa}(t) - \hat{X} = \frac{1}{m}\sum_{t=1}^{m} \hat{L}_{oa}(t), \\
\Rightarrow & \frac{1}{m}\sum_{t=1}^{m} L_{oa}(t) \times \Delta t - \hat{X} \times \Delta t = \frac{1}{m}\sum_{t=1}^{m} \hat{L}_{oa}(t) \times \Delta t, \\
\Rightarrow & \frac{1}{m}\sum_{t=1}^{m} L_{oa}(t) \times \Delta t - \frac{1}{m}\sum_{t=1}^{m} \hat{L}_{oa}(t) \times \Delta t = \hat{X} \times \Delta t
\end{aligned} \tag{5.8}$$

Clearly, as T increases, m increases and, therefore, the variance of $\hat{X}$, $\frac{\sigma^2}{m}$, goes to zero. Thus:

$$\frac{1}{m}\sum_{t=1}^{m} L_{oa}(t) \times \Delta t - \frac{1}{m}\sum_{t=1}^{m} \hat{L}_{oa}(t) \times \Delta t = 0, \quad T \to \infty. \tag{5.9}$$

□

Based on that, $\hat{L}_{oa}(t)$ can be used as a reference to which $L_{oa}(t)$ can be adjusted at real time during the time period T using the flexible EVs load. That is, when $L_{oa}(t)$ is less than the reference, $\hat{L}_{oa}(t)$, $L_{oa}(t)$ will be increased by increasing the EVs' load. Similarly, when $L_{oa}(t)$ is greater than $\hat{L}_{oa}(t)$, $L_{oa}(t)$ will be decreased by decreasing the EVs' load. According to the theorem, the average energy deficit in every time slot, Δt, between $L_{oa}(t)$ and $\hat{L}_{oa}(t)$ goes to zero as T goes to infinity. In fact, the result in Equation (5.8) shows that even for a limited period of time T, the energy deficit, $\hat{X} \times \Delta t$, is getting smaller as T increases. Thus, by adjusting $L_{oa}(t)$ to $\hat{L}_{oa}(t)$ at real time, most of the demands in the system will be satisfied by the end of the period of time T. The remaining deficit between $L_{oa}(t)$ and $\hat{L}_{oa}(t)$ will be satisfied by the operational reserve. Nevertheless, this deficit will be less than the deficit between $L_{oa}(t)$ and $\hat{L}_{oa}(t)$ using the traditional optimization methods. The energy deficit in each time slot, Δt, in case of traditional optimization methods can be estimated directly from Equations (5.3) and (5.4) by $\varepsilon \times \Delta t$. Definitely, this deficit, $\varepsilon \times \Delta t$, is greater than the deficit, $\hat{\mu} \times \Delta t$, since the variance of ε, σ^2, is greater than the variance of $\hat{X}$, $\frac{\sigma^2}{m}$. Therefore, if the EVs load is flexible enough to allow this adjustments for the $L_{oa}(t)$ at real time, this will help in decreasing the amount of operational reserve needed in the system otherwise.

5.3.2 Load Flexibility of EVs

In this work, the flexibility of the i^{th} EV, denoted by $F_i(t)$, is defined as follows:

$$\begin{aligned} F_i(t) &= d_i(t) - l_i(t), \qquad plug_i \leq t \leq dead_i, \\ l_i(t) &= \frac{(1 - SOC_i(t)) \times C}{r}, \\ d_i(t) &= (dead_i - t) \times \Delta t, \end{aligned} \tag{5.10}$$

where $d_i(t)$ is the time left for the i^{th} EV to the deadline, $l_i(t)$ is the time needed to continuously charge the i^{th} EV to full capacity, and $SOC_i(t)$ is the state of charge of the battery at time t. $F_i(t)$ indicates how much time the i^{th} EV can wait before the charging must start in order to be fully charged before the deadline. Therefore, we have the choice to delay the start of charging of the i^{th} EV as long as $F_i(t) > 0$ but not beyond that. Also, we say that the i^{th} EV has more flexibility than the j^{th} EV if $F_i(t) > F_j(t)$.

Note that the overall flexibility of the EVs' load ($\sum_{\forall i} F_i(t)$) directly affects the ability of our algorithm to adjust the overall load in the system. A larger flexibility in the EVs' load gives more ability to manipulate the overall load. Therefore, to maintain the flexibility of the EVs load in the system at its highest, our charging algorithm must serve the EVs with the lowest flexibilities first. The departure of the EVs with the lower flexibilities first will maintain the overall flexibility of the EVs load at its highest as opposed to the departure of EVs with larger flexibilities first. In other words, the EVs with lower flexibility should be charged first in order to maintain the overall flexibility of the waiting EVs at the highest. Worth noting that the flexibilities of EVs are affected by the deadline time, $dead_i$, imposed by the customers as shown in Equation (5.10). That is, increasing $dead_i$ will increase $F_i(t)$. Therefore, since the flexibility of an EV is essential to the performance of our algorithm, the utility should encourage the customers to move their deadline, $dead_i$, farther in exchange of some rewards.

5.3.3 The Details of The Proposed Algorithm

The proposed algorithm manages the number of the EVs being charged in the distribution system in real time. Control signals will be sent from the utility server to the smart chargers to guide them to start charging or, sometimes, stop charging as needed. For ease of understanding, the algorithm is divided into two stages, offline stage and online stage, as shown in Figure 5.2.

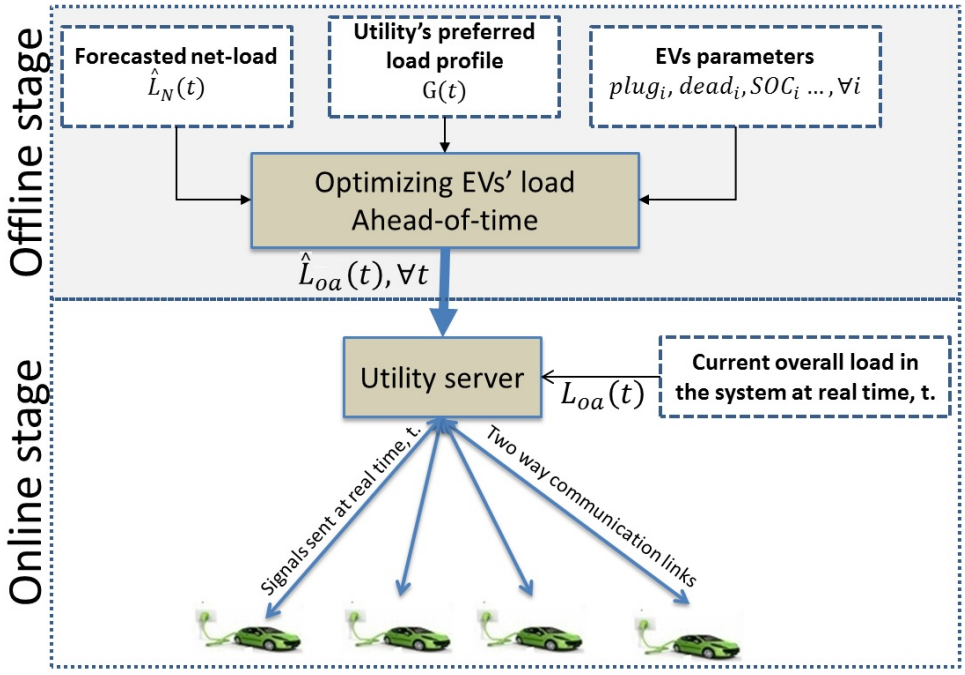

Figure 5.2: Algorithm structure

A) Offline Stage

In this stage, $\hat{L}_{oa}(t)$ will be calculated ahead of time, before starting the active charging period of time, T. We assume that the server has all the needed inputs to perform the optimization problem in Equation (5.2), such as, $\hat{L}_N(t)$, $G(t)$, $plug_i$, $dead_i$, SOC_i, $\forall i$ $\forall t$. The charging profiles, $r_i(t)$, for all EVs will be optimized in order to make the overall load profile during the time period T as close to the desired load profile $G(t)$ as possible. Then, the expected overall load profile, $\hat{L}_{oa}(t)$, will be determined using $\hat{L}_N(t)$ and the optimum EVs charging profiles, $r_i^*(t)$, as shown in Equation (5.3).
It may be noted that the expected overall load profile, $\hat{L}_{oa}(t)$, is subject to normally distributed error, ε, as shown in Equation (5.4). However, $\hat{L}_{oa}(t)$ will be used as a reference load profile to which $L_{oa}(t)$ can be adjusted at real time. Contrary to Ahead-of-Time charging algorithms, our online algorithm will not use the "optimum" charging profiles, $r_i^*(t), \forall i$, as charging profiles for the EVs, instead, they will be used only to determine $\hat{L}_{oa}(t)$ ahead of time. The decision to start charging the EVs will be controlled by the utility server at real time as will be explained in the online stage. Note that the daily driving behavior of people can be statistically measured and, therefore, predicted especially when the number of vehicles is statistically significant [73]. Thus, the charging parameters of EVs such as, $plug_i$, $dead_i$, and SOC_i, $\forall i$, can be estimated according to these statistics and, based on that, the load reference, $\hat{L}_{oa}(t)$, can be drawn. This will make our algorithm

more practical since the individual charging parameters such as, $plug_i$, $dead_i$, and SOC_i, $\forall i$, are not needed ahead of time any more.

B) Online Stage

In this stage, the utility server will keep monitoring the real overall load, $L_{oa}(t)$, during the time period T and compare it with the predetermined reference load, $\hat{L}_{oa}(t)$, obtained from the offline stage. Both loads, $L_{oa}(t)$ and $\hat{L}_{oa}(t)$, are shown as inputs in **Step (1)** of the flow chart of the server's algorithm in Figure 5.4. Every short interval of time, ζ in **Step (2)**, the server compares $L_{oa}(t)$ to $\hat{L}_{oa}(t)$ in **Step (3)**. If $L_{oa}(t)$ is less than $\hat{L}_{oa}(t)$, then the utility server will send signals to specific EVs to start charging in order to adjust the real overall load back to the reference load as in **Step (4)**. On the other hand, if $L_{oa}(t)$ is higher than $\hat{L}_{oa}(t)$, the utility server will let the departure of the fully charged EVs to compensate as shown in the transition from **Step (3)** to **Step (2)**, or, if needed, the utility server will force some EVs to interrupt their charging in order to get $L_{oa}(t)$ in the system down to $\hat{L}_{oa}(t)$ as shown in **Step (6)**. These EVs' load's ramp-up and ramp-down mechanisms are essential in controlling the EVs' loads in the distribution system in real time.

B).1 Ramping-up EVs' load: Given the needed information about plugged-in EVs at the server side, $plug_i$, $dead_i$, SOC_i, $\forall i$, the flexibility of each plugged-in EV can be calculated at the server side from Equation (5.10). When $L_{oa}(t) - \hat{L}_{oa}(t) < 0$, the server calculates the number of EVs, N_{EV}, needed to start charging in order to set $L_{oa}(t)$ back to $\hat{L}_{oa}(t)$ as follows:

$$N_{EV} = \left\lceil \frac{\hat{L}_{oa}(t) - L_{oa}(t)}{r} \right\rceil \tag{5.11}$$

Then, the server will choose flexibility value, $\mathcal{F}(t)$, so that only N_{EV} number of EVs have flexibility values less than $\mathcal{F}(t)$ among the rest of the waiting EVs. Mathematically, if we define a set S:

$$S = \{i^{th}EV : F_i(t) < \mathcal{F}(t)\}, i = 1, 2, ..., n, \tag{5.12}$$

then, $\mathcal{F}(t)$ should be chosen such that $|S| = N_{EV}$. This value, $\mathcal{F}(t)$, will be included in a data packet and this packet will then be broadcast to all waiting EVs as shown in **Step (4)** in Figure 5.4. Upon receiving this packet, the EVs will extract $\mathcal{F}(t)$ and compare it to their individual flexibility $F_i(t)$ as shown in **Step (1)** through **Step (3)** of the flow chart of the algorithm running on EVs in Figure 5.5. If $F_i(t) < \mathcal{F}(t)$, then the EV will start charging and report its start action back to the server, as shown in **Step (4)** and **Step (5)** in Figure 5.5; otherwise, the EV goes to **Step (1)** and it keeps waiting for the next broadcast from the server. The newly added EVs' load should increase $L_{oa}(t)$ to match $\hat{L}_{oa}(t)$. The server keeps monitoring $L_{oa}(t)$ and compares it with $\hat{L}_{oa}(t)$ every ζ interval of

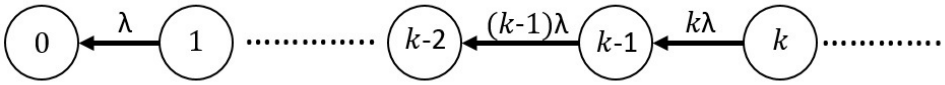

Figure 5.3: Departure model of fully charged EVs

time, as shown in **Step (2)** and **Step (3)** in Figure 5.4, and, thus, repeats this ramp-up mechanism as needed.

B).2 Ramping-down EVs' load: When $L_{oa}(t)$ is higher than $\hat{L}_{oa}(t)$, the currently charging EVs' load should be reduced to decrease $L_{oa}(t)$ back to $\hat{L}_{oa}(t)$. A straight forward way to achieve this is to just wait for the departure of the fully charged EVs. This passive approach will eliminate the interruption of charging of EVs. For a deeper insight into this mechanism, we model this departure of the fully charged EVs as a pure-death model as shown in Figure 5.3. In this model, the states represent the number of EVs being charged at the moment. In general, the charging time l_i for the i^{th} EV given in Equation (5.10) is a random variable since SOC_i is a random variable. However, the expected charging time, $E(l_i)$, for a randomly picked i^{th} EV can be expressed as follows:

$$E(l_i) = \frac{(1 - E(SOC_i)) \times C}{r} = \frac{1}{\lambda} \tag{5.13}$$

Therefore, the service rate, which is also known as the departure rate, of k EVs being charged at a given moment is $k\lambda$. Clearly, the larger the rate of departure $k\lambda$, the faster the ramp-down of EVs' load. This rate depends on two parameters. First, it depends on the number of EVs, k, being charged at the moment. The higher this number is, the faster is the departure rate. In general, we expect that the number of simultaneously charging EVs increases when the number of EVs requiring to be charged during the time period T increases. Therefore, the higher the penetration level of EVs is, the faster will be the ramp-down speed. Second, the average charging time, $\frac{1}{\lambda}$, also effects the departure rate, $k\lambda$. This average charging time depends on the rate of the charge r, which is assumed to be fixed, the capacity of the battery C, and the expected value of the initial state of charge $E(SOC_i)$ as shown in Equation (5.13). If we want uninterrupted charging for every EV, then this charging time cannot be controlled by the server.

However, in our proposed charging algorithm, some of the EVs being charged at the moment can be *temporarily* interrupted to increase the departure rate $k\lambda$, when needed. This happens when the normal departure rate is not fast enough. In our algorithm, when $L_{oa}(t)$ is higher than $\hat{L}_{oa}(t)$ by a specified limit δ, the server will broadcast an interrupting signal to all EVs which are being charged at the moment as shown in **Step (6)** in Figure 5.4.

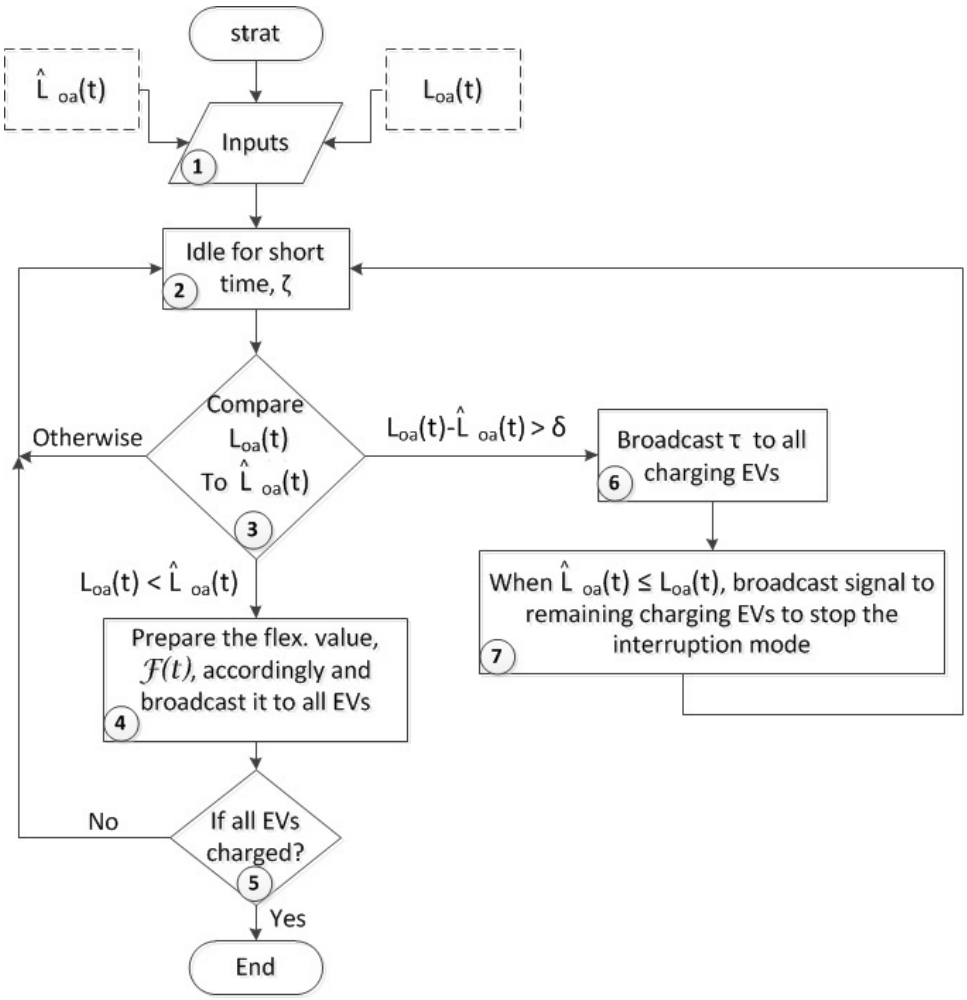

Figure 5.4: Charging Algorithm running on the server

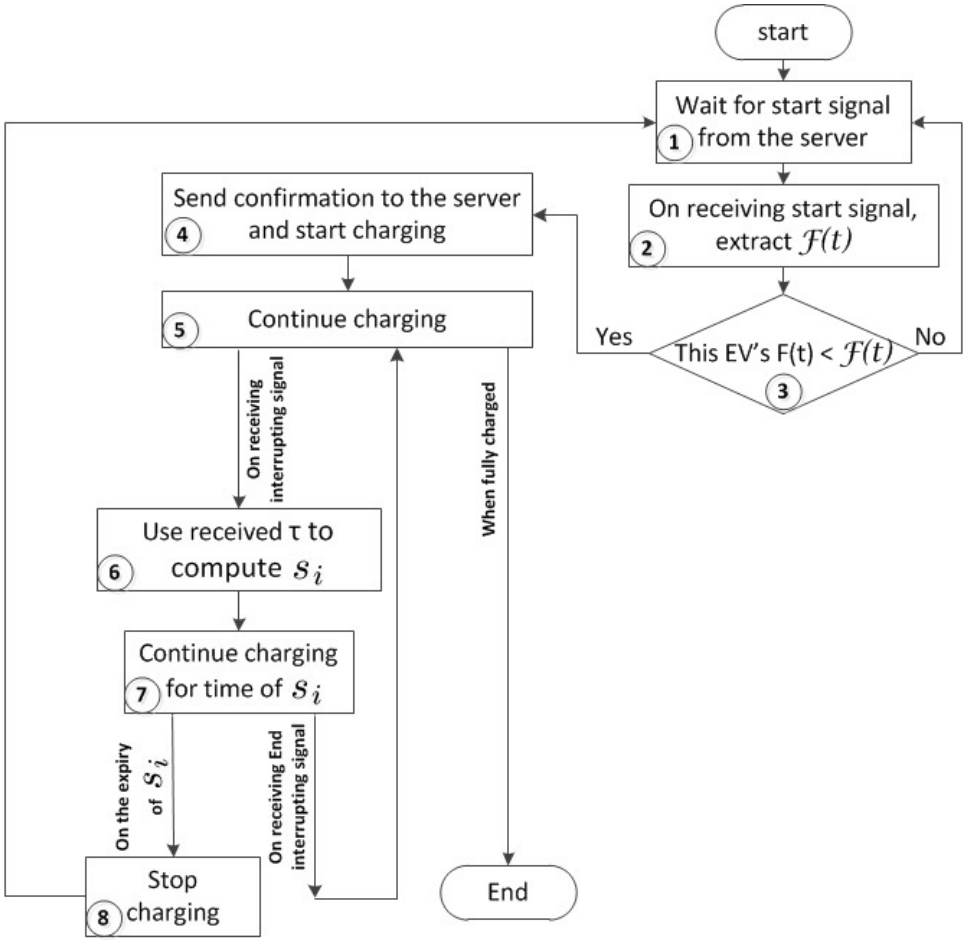

Figure 5.5: Charging Algorithm running on the EVs

This signal carries an interruption time, denoted by τ, chosen by the server to guide some of charging EVs to temporarily stop charging. However, the charging of the interrupted EVs will be resumed later as it will be explained. This interruption time, τ, should be less than $E(l_i)$ in order to increase the departure rate $k\lambda$. Upon receiving this signal, the actively charging i^{th} EV will use the received τ to calculate how much time, s_i, it continues charging before it should stop charging as shown in **Step (5)** through **Step (7)** in Figure 5.5. The i^{th} EV calculates s_i as follows:

$$s_i = \left\lceil \frac{e_i}{\tau} \right\rceil \times \tau - e_i, \tag{5.14}$$

where e_i is the time for which the i^{th} EV is being charged so far. The estimated stoppage time s_i for the i^{th} EV is illustrated graphically in Figure 5.6.

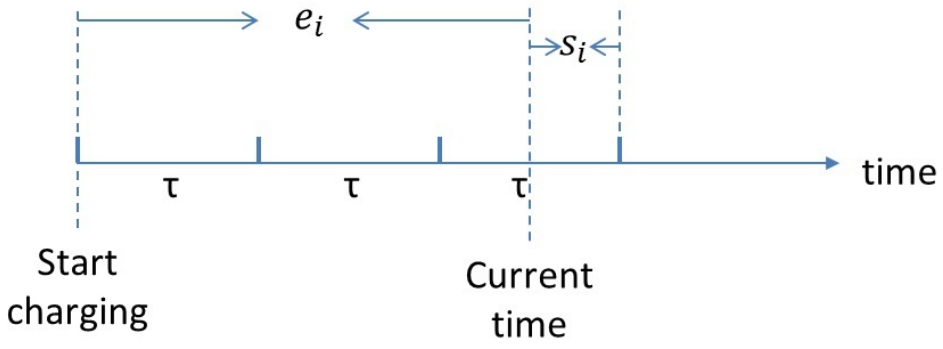

Figure 5.6: Estimation of stoppage time s_i

Clearly, the EVs which started charging at different times will have different s_i. Once an EV determines its own s_i, it will continue charging for a time of s_i before it stops charging as shown in the transition from **Step (7)** to **Step (8)** in Figure 5.5. However, the server will keep monitoring $L_{oa}(t)$, and when it is back to $\hat{L}_{oa}(t)$, the server will broadcast a signal to all remaining charging EVs to let them continue charging without interruption as shown in **Step (7)** in Figure 5.4. Upon receiving this signal, the EVs which have unexpired s_i will set their charging mode back to the normal charging mode without interruption as shown in the transition from **Step (7)** to **Step (5)** in Figure 5.5. It is important to note that the server can increase the ramp-down speed by decreasing τ. Also, this mechanism offers a gradual decrease in the EVs' load which can be stopped at the right moment, when $L_{oa}(t) = \hat{L}_{oa}(t)$, and restore the normal departure rate. This would keep the charging interruptions to the participating EVs to the minimum. Also, it is important to note that the charging interruption of EVs is a temporary. This can be seen in the transition from **Step (8)** to **Step (1)** in Figure 5.5. After the interruption, the EV will wait for a new signal from the server to resume charging according to its new flexibility.

5.4 Performance Evaluation

To evaluate the performance of our online charging algorithm, a special Java tool has been developed to simulate the algorithm. The performance of our algorithm will be tested against the performance of the Ahead-of-Time scheduling algorithms, such as the one in reference [29].

First, the algorithm will be tested under three different penetration levels of wind power, namely, 10%, 20%, and 30%. These different penetration levels of the intermittent wind power represent different levels of net-load forecast error in the system.

Second, as shown in Section 5.3.3, the number of participating EVs is expected to affect the ramp-down speed of the EVs' load. Specifically, as the number of the participating EVs increases, the ramp-down speed in the EVs' load increases, thus, a better performance in terms of the closeness of $L_{oa}(t)$ to $\hat{L}_{oa}(t)$ is expected. Therefore, different penetration levels of EVs will be considered in this evaluation.

Third, the algorithm will be tested with different charging interruption time, τ. In the beginning, we will test our algorithm with no charging interruption against the Ahead-of-Time scheduling algorithm. Then, different values of interrupting time, τ, will be used to examine their effects on the performance of the algorithm.

Fourth, different swings levels of the stochastic net-load will be considered. These swings will be simulated by applying the net-load error to the expected net-load at different time intervals, namely, 15-minutes, 10-minutes, and 5-minutes. The performance of our algorithm under these different levels of fluctuations will be evaluated.

Finally, to eliminate the requirements of submitting the charging parameters such as, $plug_i$, $dead_i$, and SOC_i, ahead of time, and, therefore, make our algorithm more practical, a common load reference will be generated from the assumed distributions of these charging parameters. Then, the performance of our algorithm using this common load reference will be evaluated as well.

5.4.1 Simulation Setting

For more realistic representations of the daily load profile, data has been collected from CAISO website [1]. The data represents the recorded load profile in CAISO from 8:00 PM, 15 December 2013, to 12:00 PM, 16 December 2013. This CAISO load profile is measured in Megawatts (MW) for this large system. However, in our experiment, we will scale this load profile down to Kilowatts (kW) to suit our much smaller distribution system load profile. This load profile will be used to represent the forecast of the conventional load, $\hat{L}_c(t)$, for the 8:00PM-12:00PM period. Then, the real conventional load, $L_c(t)$, will be derived using Equation (5.15):

$$L_c(t) = \hat{L}_c(t) + \varepsilon_c, \tag{5.15}$$

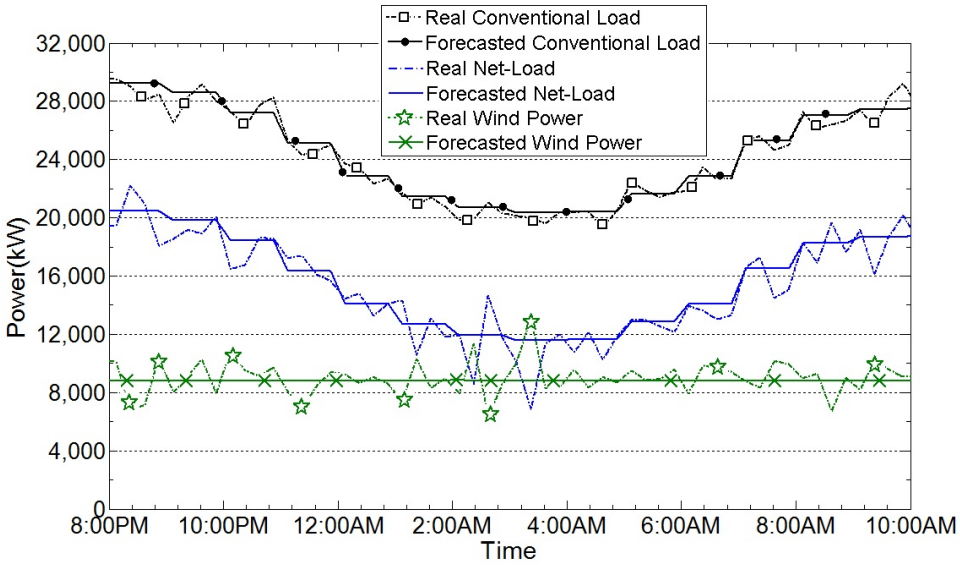

Figure 5.7: Real Net-Load vs forecasted Net-Load for 30% wind power penetration

where ε_c is a random variable representing the forecast error of the conventional load in the system. The distribution of this random variable is approximated as normal distribution as shown in Chapter 4. The estimated parameters of the normalized ε_c for CAISO system are shown in Table 5.1.

Also, we assume that the wind power forecast, $\hat{L}_R(t)$ for the same period of time is fixed throughout this period and is proportional to the average conventional load in the system according to the assumed penetration level of wind power. For example, for 10% penetration level of wind power, $\hat{L}_R(t) = 0.1 \times \bar{L}_c, \forall t$, where, $\bar{L}_c = \frac{1}{m}\sum_{t=1}^{m} \hat{L}_c(t)$. However, due to the error in the wind power forecast, ε_R, the real wind power, $L_R(t)$, is represented as follows:

$$L_R(t) = \hat{L}_R(t) + \varepsilon_R, \tag{5.16}$$

where ε_R is normally distributed as shown in Chapter 4. The estimated parameters of the normalized ε_R for CAISO system are shown in Table 5.1. It is worth noting that the net-load forecast error, ε, is the combination of the two forecast errors ε_R and ε_c [10]. Figure 5.7 shows an example case of all these settings. It is important to keep in mind that only the forecasted net-load is known ahead of time.

Additionally, in this experiment, we assumed that the participating EVs will be plugged-in to the charger at random time between 6:00PM-10:00PM when people usually arrive at home. Also, we assumed that the deadlines dictated by the customers are distributed randomly between 6:00AM-10:00AM in the morning when people usually start their trips. Therefore, the plug-in time and deadline time are considered uniformly distributed random

Table 5.1: Parameters used in the experiment

Paramater	The value
Normalized ε_c	$\varepsilon_c \sim N(-0.002, (0.026)^2)$
Normalized ε_R	$\varepsilon_R \sim N(-0.004, (0.13)^2)$
C, $\forall EVs$	8 kWh
r, $\forall EVs$	3 kW, Level II charging standard [61]
SOC_i, $\forall i$	$SOC_i \sim U(0, 0.6)$
$plug_i$, $\forall i$	$plug_i \sim U(6:00PM, 10:00PM)$
$dead_i$, $\forall i$	$dead_i \sim U(6:00AM, 10:00AM)$
δ	$\delta = \infty$, for non-interrupting mode, δ=5 kW, for interrupting mode
Idle time, ζ	10 seconds

variables within the described intervals as shown in Table 5.1. Also, the initial state of charge of the batteries, SOC_i, $\forall i$, is assumed to be uniformly distributed between (0.0-0.6).

Finally, in all scenarios in this experiment, we assume that the utility prefers to flatten the overall load in the system as much as possible. Therefore, we treat the preferred load profile, $G(t)$, in Equation (5.2) as a constant. The rest of the setting and parameters of the experiment are shown in Table 5.1.

5.4.2 Simulation Results

For all combinations of different penetration levels of EVs with different penetration levels of wind power, we solve the optimization problem in Equation (5.2) to get the *optimum* charging profiles, $r_i^*(t)$, $\forall i$. In case of the Ahead-of-Time algorithm which is used as a benchmark in this evaluation, the EVs will schedule their charging according to these charging profiles. However, in case of our algorithm, these charging profiles will be used only to calculate the reference load, $\hat{L}_{oa}(t)$, as explained in the offline stage of our algorithm in Section 5.3.3.A.

A) Charging Without Interruption

In this part, once an EV starts charging, it continues charging without any interruption. This is achieved by setting the parameter δ to ∞ in the server algorithm shown in Figure 5.4. Remember, the departure rate of the fully charged EVs, $k\lambda$, will limit the ramp-down average speed of the EVs' load as explained earlier in Section 5.3.3.B. Also, in this part, the penetration level of EVs is assumed to be 8000 EVs. The non-interrupted charging of these 8000 EVs is tested under three different penetration levels of wind power, 10%, 20%, and

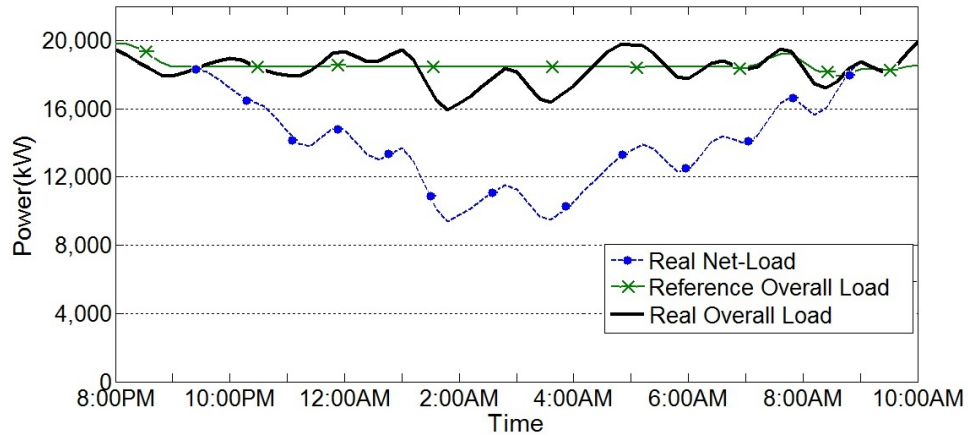

(a) Ahead-of-Time Algorithm

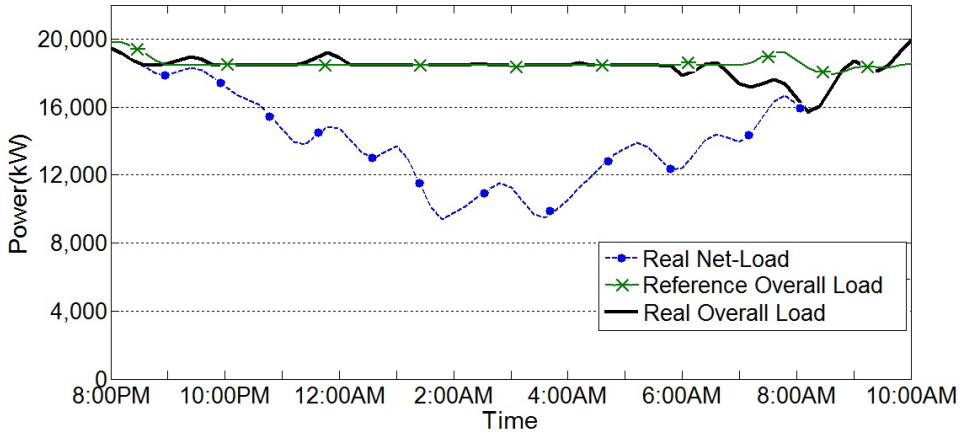

(b) Our Algorithm

Figure 5.8: Performance of our algorithm vs Ahead-of-Time algorithm with 30% wind power penetration

30%. The results from our algorithm are compared with the results from Ahead-of-Time charging algorithm in all scenarios.

Figure 5.8 shows the results from one scenario of 30% penetration level of wind power. The real overall load of the Ahead-of-Time algorithm, $L_{oa}(t)$, is clearly fluctuating around the reference overall load, $\hat{L}_{oa}(t)$. This is due to the fact that the forecast of the net-load is subject to the forecast error, ε. This error appeared at real time or close to real time causing $L_{oa}(t)$ to deviate from $\hat{L}_{oa}(t)$. On the other hand, our algorithm displayed better response to these fluctuations due to its online mechanism. Clearly, the resultant $L_{oa}(t)$ of our algorithm is much closer to $\hat{L}_{oa}(t)$ most of the time. However, the limitation of the

ramp-down speed due to insistence of our algorithm to continuously charge EVs without interruption, $\delta = \infty$, results in a deviation of $L_{oa}(t)$ from $\hat{L}_{oa}(t)$ around 12:00 AM. This deviation can be reduced by interrupting some of the actively charging EVs as will be shown later. Also, around 6:30AM, all EVs are either fully charged or already started charging and, thus, our algorithm lost the ramp-up ability. That is why $L_{oa}(t)$ of our algorithm starts to drop from $\hat{L}_{oa}(t)$ at that time to eventually match $L_N(t)$. To precisely measure the deviation of $L_{oa}(t)$ from $\hat{L}_{oa}(t)$ for both algorithms, we use the Mean Absolute Error (MAE) between the two loads as follows:

$$MAE = \frac{1}{j}\sum_{t=1}^{j}|\hat{L}_{oa}(t) - L_{oa}(t)|, \tag{5.17}$$

where j is the number of samplings from the time period 10:00PM to 10:00AM. In this work, the sampling was every minute through out the whole period. In the scenario shown in Figure 5.8, our algorithm achieved a smaller MAE of 320 kW compared to MAE of 694 kW achieved by the Ahead-of-Time algorithm.

The result of this scenario alongside results from other 49 scenarios for 30% penetration level of wind power are shown in Figure 5.9(a). In every scenario, the same settings have been used but with different seeds for the normal distribution representing the net-load forecast error, ε. On average, our algorithm achieved an improvement of 42% over the traditional Ahead-of-Time scheduling algorithm. The same procedure is repeated for 10% penetration level of wind power and 20% penetration level of wind power. Figures 5.9(c) and 5.9(b) show the results of the 50 different scenarios of 10% and 20% penetration level, respectively. On average, our algorithm achieved improvements of 51% for 20% penetration level and improvements of 49% for 10% penetration level.

B) The Effect of The Number of Participating EVs on The Performance

In this part, we demonstrate the effect of the penetration level of EVs on the performance of our algorithm. Seven different penetration levels of EVs are considered, namely, 8000 EVs, 6000 EVs, 4000 EVs, 2000 EVs, 1000 EVs, 500 EVs, and 250 EVs. Figure 5.10 shows the results of the average MAE achieved for every penetration level of EVs. Each point in every curve represents the average MAE of 150 runs each with different seeds for our normally distributed net-load forecast error, ε. To test our algorithm under a significant net-load forecast error, 30% penetration level of wind power is considered in this part. From the results, the Ahead-of-Time algorithm achieved approximately the same average MAE, around 817 kW, for all different penetration levels of EVs as shown in Figure 5.10. Obviously, this is expected since the Ahead-of-Time algorithm does not actively react to the net-load forecast error, ε. Thus, this error will fully impact the real overall load in the system, as shown in Equation (5.4), regardless of the number of EVs being charged. On

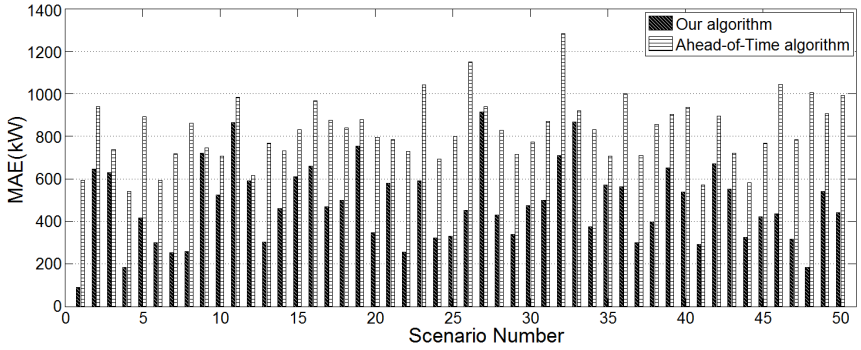

(a) 30% wind power penetration level

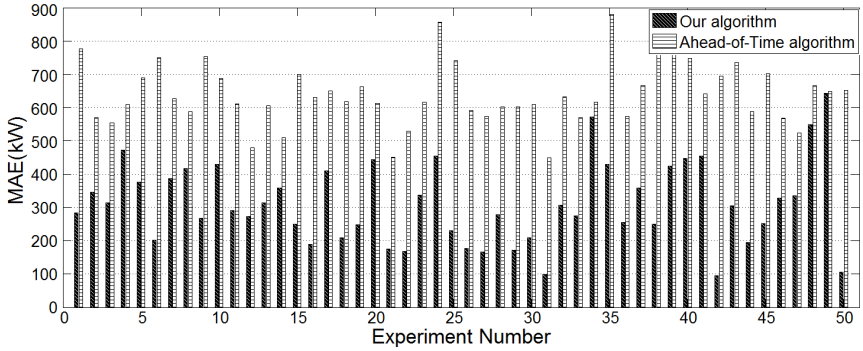

(b) 20% wind power penetration level

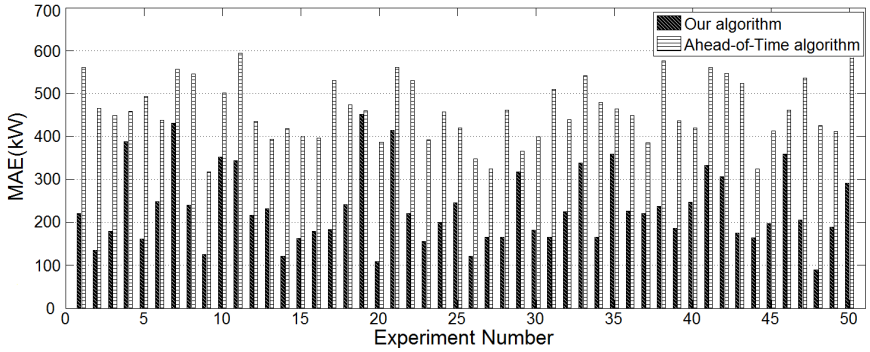

(c) 10% wind power penetration level

Figure 5.9: Performance of our algorithm vs Ahead-of-Time algorithm with different wind power penetration levels

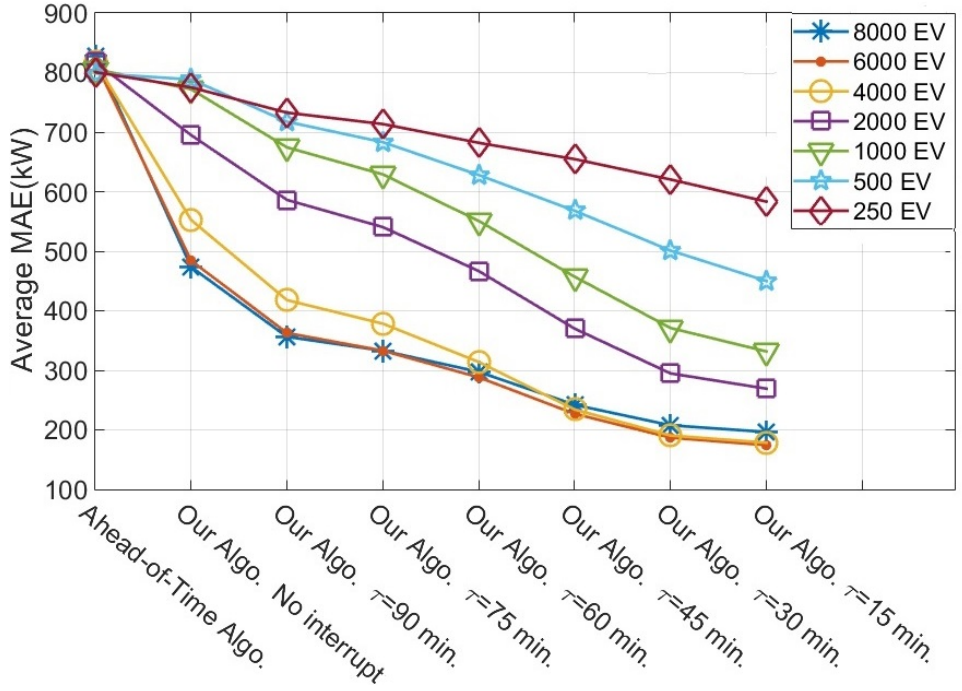

Figure 5.10: Performance of different penetration levels of EVs with different interruption time τ

the other hand, our algorithm shows better performance compared to the Ahead-of-Time algorithm in all penetration levels of EVs. However, the performance of our algorithm varies based on the number of participating EVs. In general, the larger the number of participating EVs is, the better is the performance. For instance, in the case of charging without interruptions, the 8000 EVs group achieved the best performance with average MAE of 473 kW, while the 250 EVs group achieved average MAE of 775 kW, barely beating the Ahead-of-Time algorithm. The influence of the number of participating EVs on the performance is due to two reasons. First, as the number of EVs increases, the load's flexibility in the system increases, and, thus, the ability to absorb the fluctuation in the real overall load increases. Second, the ramp-down speed of EVs' load is proportional to the number of EVs charging at the moment as explained in Section 5.3.3.B. Thus, when the number of participating EVs is smaller, the ramp-down speed is slower which consequently decreases the performance.

C) The Effect of Interruption Time τ on The Performance of Our Algorithm

The performance of our algorithm with different interruption times, $\tau = \{90, 75, 60, 45, 30, 15\}$ min, for all penetration levels of EVs is shown in Figure 5.10. Consistently, our algorithm achieved better performance as the interruption time τ gets smaller. This is a direct result of having better ramp-down speed in the EVs' load when τ is decreased, as explained in Section 5.3.3.B. However, it is worth noting that the impact of a smaller τ on the performance is different as the numbers of participating EVs differ. For example, the improvement in the performance when τ is decreased from 30 min to 15 min in the 8000 EVs group is not as significant compared to the improvement achieved in the 500 EVs or 250 EVs groups for the same change in τ. This is due to the fact that at the same τ, the average ramp-down rate, $k\lambda$, is higher when the number of participating EVs is larger. Therefore, the effect of smaller τ on smaller group of EVs is more significant compared to bigger groups of EVs. It is worth mentioning that although the decrease in the interruption time τ results in better performance in terms of matching $L_{oa}(t)$ to $\hat{L}_{oa}(t)$, the average number of interruptions during the charging of the participating EVs increases. In general, as τ gets smaller, more interruptions are expected. Table 5.2 shows the average number of interruptions per EV for all the different penetration levels of EVs with different interruption time τ. The results show a consistent increase in the average number of interruptions per EV as the interruption time τ decreases for all groups. This indicates that our algorithm achieves a better performance in terms of getting $L_{oa}(t)$ close to $\hat{L}_{oa}(t)$ but that achievement comes at the expense of having more charging interruptions per EV. It is important to note that the charging interruptions per EV does not affect the amount of energy delivered to the EV by the end of charging period T. All EVs have been charged with the requested amount of energy within their specified deadline. The number of interruptions per EV refers to the number of temporary interruptions in charging during the whole charging period of the EV.

Table 5.2: Average number of interruptions per EV

	Number of participating EVs						
τ(min.)	**8000**	**6000**	**4000**	**2000**	**1000**	**500**	**250**
90	0.12	0.15	0.18	0.23	0.31	0.34	0.36
75	0.16	0.19	0.24	0.33	0.44	0.49	0.53
60	0.23	0.27	0.34	0.48	0.63	0.69	0.73
45	0.36	0.41	0.48	0.65	0.82	0.90	0.93
30	0.60	0.65	0.74	0.92	1.12	1.14	1.15
15	1.39	1.35	1.42	1.60	1.72	1.50	1.41

D) The Response of Our Algorithm to Different Fluctuation Levels in The Net-Load

In the previous results, our algorithm demonstrated the ability to absorb the unexpected fluctuations in the net-load. This ability will be tested further with different fluctuation levels in the real net-load. These different levels will be implemented by applying the net-load forecast error, ε, to the expected net-load at different interval lengths. Clearly, applying the forecast error, ε, at smaller intervals of time results in more volatile net-load. Three different interval lengths are considered in this section: 15-minutes, 10-minutes, and 5-minutes. Figure 5.11 illustrates how well our algorithm manages to absorb the fluctuations in the real net-load during the active charging period for all these time resolutions. Remember, these fluctuations are not known to our algorithm ahead of time. Instead, the algorithm responds to these fluctuations as they appear at real time. As shown in the figure, the real overall load in the system is kept flat as much as possible during the active charging period as preferred by the utility.

For more representative results, 100 different seeds for the net-load error, ε, for each of the three fluctuation levels are tested. Table 5.3 summaries the average MAE achieved by our algorithm compared with MAE achieved by the conventional (Ahead-of-Time) algorithm for all of these scenarios. Clearly, our algorithm achieved smaller MAE, closer $L_{oa}(t)$ to $\hat{L}_{oa}(t)$, compared to MAE achieved by the Ahead-of-Time algorithm. Also, as expected, the average number of charging interruptions per EV increases as the intensity of the fluctuations in the net-load increases as shown in Table 5.3. This is due to the fact that our algorithm adjusts the interruption time, τ, to smaller values as the fluctuations in the net-load increases. Consequently, the average number of charging interruptions per EV increases as explained in Section 5.4.2.C.

In fact, this special ability of our algorithm to absorb these fluctuations in the net-load promotes our algorithm as a candidate to provide ancillary services in the system. In general, two types of ancillary services are dedicated to balance generation and load under normal conditions in the electric system, namely, regulation and load-following services.

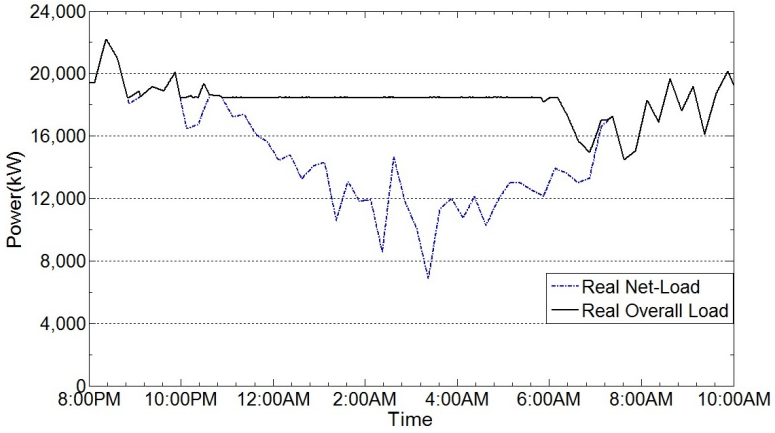

(a) 15-min. fluctuation level

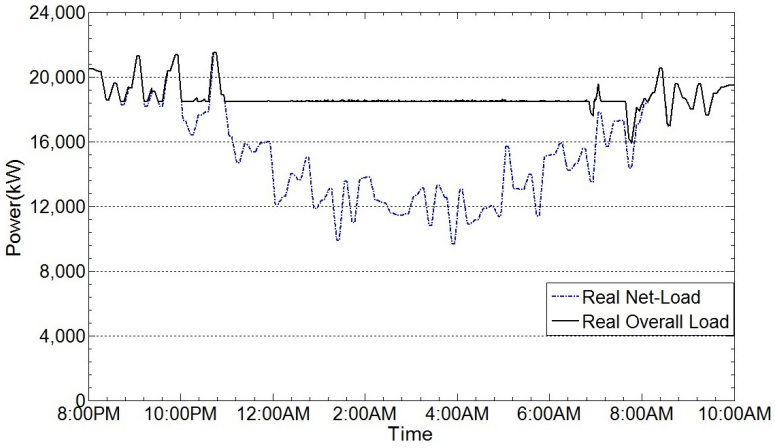

(b) 10-min. fluctuation level

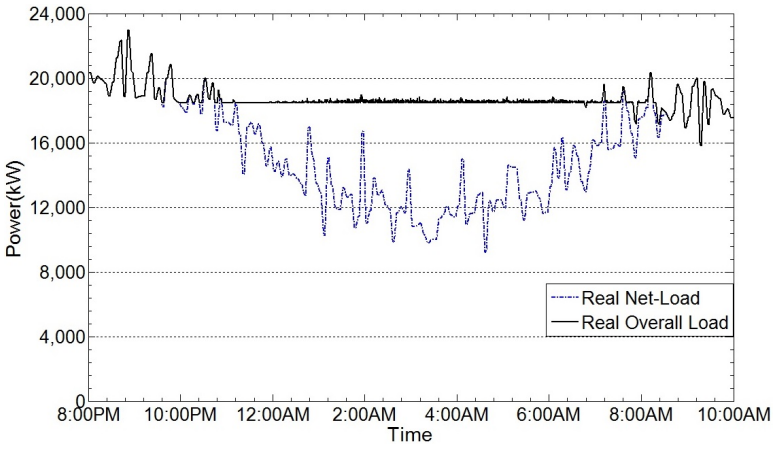

(c) 5-min. fluctuation level

Figure 5.11: Performance of our algorithm with different fluctuation levels

Table 5.3: Performance of our algorithm vs Ahead-of-Time(Conv.) algorithm with different fluctuations' levels

Net-Load Resolution	MAE (kW) (Conv. Algo)	MAE (kW) (Our Algo.)	Average Number of Interruptions per EV
15 min.	916.1	236.4	3.5
10 min.	915.8	237.9	7.2
5 min.	919.5	262.0	18.3

Both of these services are required to swiftly balance any fluctuation in the load. According to reference [43], the response speed required by regulating reserve is around 1 minute and the response speed required by load-following reserve is around 10 minutes. Clearly, our algorithm demonstrates a fast response to different level of fluctuations in the system. Thus, the algorithm can easily participate in providing ancillary services to the grid and, thus, relieve the pressure on the regulation and load-following reserves in the system.

E) Performance of Our Algorithm Using Common Load Reference

In this section, we use stochastic optimization to determine a *common* load reference, $\hat{L}_{oa}^{com}(t)$, for all possible scenarios of charging parameters, $plug_i$, $dead_i$, and SOC_i, $\forall i$. As discussed in Section 5.3.3.A, the advantage of having a common load reference is that the individual charging parameters will not be needed ahead of time to determine the load reference anymore, and, thus, making our algorithm more practical. To estimate $\hat{L}_{oa}^{com}(t)$, we used a simple stochastic programming approach adopted from the work in reference [20]. For that purpose, 500 different scenarios have been created for a group of 8000 EVs. In each scenario, the values of charging parameters, $plug_i$, $dead_i$, and SOC_i, of each of the i^{th} EV have been generated by sampling their corresponding distributions shown in Table 5.1. The wind power penetration level is assumed to be 30% in all scenarios. For each scenario, $\hat{L}_{oa}(t)$ has been determined as before using Equations (5.2) and (5.3). We refer to the resultant $\hat{L}_{oa}(t)$ of scenario sc as $\hat{L}_{oa}^{sc}(t)$, $sc = 1, 2, ..., 500$. Finally, $\hat{L}_{oa}^{com}(t)$ is calculated as follows:

$$\hat{L}_{oa}^{com}(t) = \frac{1}{500} \sum_{sc=1}^{500} \hat{L}_{oa}^{sc}(t), \forall t. \tag{5.18}$$

Using $\hat{L}_{oa}^{com}(t)$ as load reference, the performance of our algorithm is examined using 100 different scenarios. In each scenario, the net-load error, ε, and the charging parameters, $plug_i$, $dead_i$, and SOC_i, $\forall i$, are randomly selected according to their distributions in Table 5.1. The performance of our algorithm is measured in terms of the mean absolute error (MAE) between $L_{oa}(t)$ and $\hat{L}_{oa}^{com}(t)$ for each scenario as shown in Figure 5.12. Also, the Ahead-of-Time algorithm performance for each scenario is shown in the figure as well. However, since the Ahead-of-Time algorithm uses the "*optimised*" charging profiles, $r_i^*(t)$,

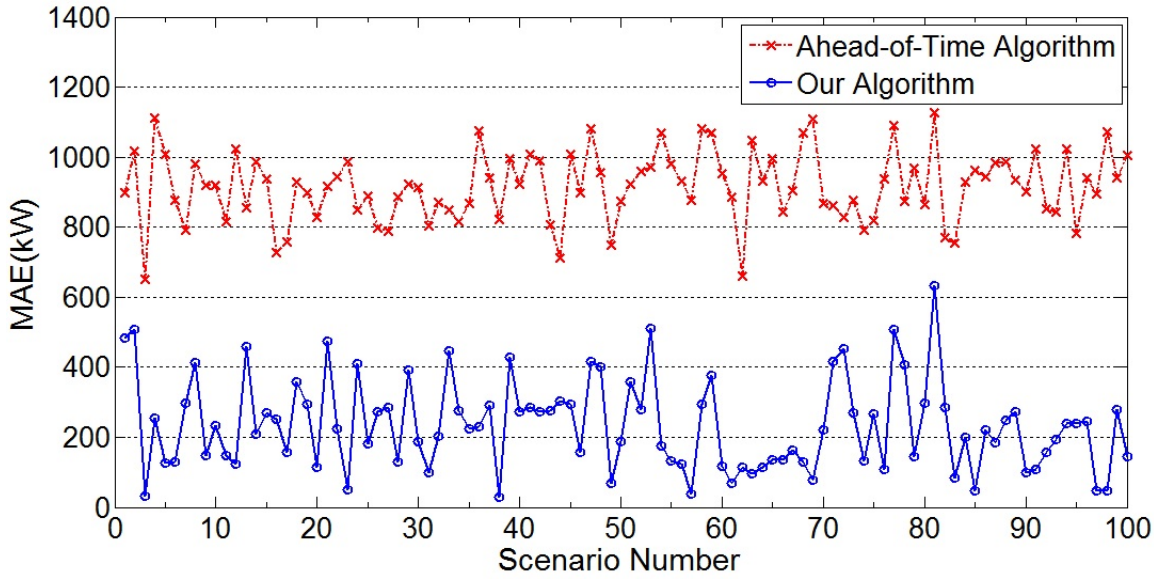

Figure 5.12: Performance of our algorithm with common load reference versus the performance of Ahead-of-Time algorithm

$\forall i \forall t$, obtained from Equation (5.2) directly as charging profiles for EVs, we assume that all charging parameters are known to the Ahead-of-Time algorithm ahead of time. Thus, the performance of the Ahead-of-Time algorithm is measured in terms of MAE between $L_{oa}(t)$ and $\hat{L}_{oa}(t)$ for each scenario. Although our algorithm was tested under two stochastic behaviors, the net-load forecast error and the charging parameters of EVs, yet, it demonstrates a better performance compared to the Ahead-of-Time charging algorithm which was subjected to only one stochastic behavior, the net-load forecast error.

5.5 The Integration of The Algorithm in The System

The services provided by the proposed charging algorithm work on different time horizons varying from hours/day to seconds as follows:

Hours/Day: The algorithm optimizes the charging times of the EVs according to preferred load profile, $G(t)$, as shown in the offline stage of the algorithm in Section 5.3.3.A. This optimization is done ahead of time since $G(t)$ can be decided ahead of time based on some preferences, such as flattening the overall load in the system as shown in this study. Further, $G(t)$ can be designed based on the energy prices during the day, such as Time-Of-Use (TOU) prices. TOU prices are known ahead of time, thus, $G(t)$ can be designed ahead of time in order to minimize the charging cost for the participating EVs.

Minutes: The forecast of the energy produced by RES (often with a resolution of less

than an hour) is not accurate due to the stochastic nature of RES. Consequently, the short term forecast of the net-load in the distribution system is not accurate especially when the penetration level of RES is high. The proposed algorithm can help in integrating RES to the distribution system by absorbing any unexpected fluctuations in the net-load due to the forecast error. The results in Section 5.4.2.D demonstrate the ability of our algorithm to respond fast enough to any fluctuation within few minutes. However, the utility server should be able to monitor the net-load in the distribution system at real time. Therefore, a coordination at the level of distribution system is needed.

Seconds: Also, the proposed algorithm is capable of providing ancillary services to the electric grid such as regulation reserve. Regulation reserve gives the grid operators the ability to fine-tune the supply-demand balance in the electric grid within short time (every 4 seconds typically) [13]. Traditionally, such a service is provided by power plants. These power plants are adjusted to provide a specific power output called the preferred operating point (POP) [14]. When the grid operator needs an instant increase or decrease in the power to adjust the supply-demand balance in the grid, it sends Automatic Generation Control (AGC) signal to these power plants to increase or decrease their power output accordingly. This service can be provided by the proposed algorithm since decreasing EVs loads is equivalent to increasing the produced power in the system and vice versa. The optimized EVs load, $r_i^*(t), \forall t \forall i$, is equivalent to the POP in the power plants. The inherent mechanism of ramp-up and ramp-down of EVs load in the proposed algorithm can be used to follow AGC dispatch signals instead of adjusting $L_{oa}(t)$ to $\hat{L}_{oa}(t)$. However, providing this service needs coordination at the grid level. The provider of this service (aggregator or utility) needs to pass a test to assure that it is able to respond within a specific time [43]. Also, a communication infrastructure is needed to carry AGC dispatch signals from the grid operator to our algorithm's server.

It is worth mentioning that the integration of these services into the system should be coordinated at different levels. The first service (Hours/Day level) does not need any coordination with the system operators since it optimizes the charging profiles of EVs ahead of time based on chosen preference, $G(t)$. However, providing the second and the third services (Minutes and Seconds levels) need a close coordination with the system operators at distribution system level and at electric grid level, respectively. Also, it is important to note that while the optimization in the offline stage ensures providing the first service (*i.e.,* Hours/Day level), the online stage can only provide one of the other two services (*i.e.,* Minutes or Seconds level). That is because committing to responding to the fluctuations in the net-load in the distribution system conflicts with committing to following AGC signals from the grid operator. Therefore, our algorithm can provide the first service with either the second or the third service. Consequently, a choice has to be made between the latter two services, perhaps, based on their profitability. In this study, we have demonstrated the ability of the proposed algorithm in providing the first and the second services. In the literature, the proposed charging algorithms for EVs are typically designed to provide the first service only (the ahead of time optimization for charging time of EVs in order to

achieve some benefits such as filling the load valley in the system) [17, 20, 41, 51, 75, 77]. As for providing ancillary services to the grid, most of the works in the literature consider using the energy in the batteries of EVs (V2G) to provide such services [15, 37, 40]. On the other hand, our algorithm provides, at the same time, the first and either the second or the third service using only charging of EVs (G2V) with simpler technical requirements for the smart chargers (constant charging rates).

5.6 Summary

In this Chapter, a novel online charging algorithm for EVs in smart grids is proposed. The algorithm increases or decreases the EVs' load at real time as needed in order for the real overall load to match the forecasted overall load as most of the utilities prefer. This work is started by defining the shortcomings of traditional Ahead-of-Time charging algorithms especially when RES penetration level is high in the system. Then, we showed that the energy consumed by the load in the system can be estimated ahead of time despite the stochastic behavior of the net-load. Also, the flexibility of the EVs' loads is precisely defined in order for the proposed algorithm to exploit it effectively. Then, a novel online charging algorithm is introduced with its unique ramp-up and ramp-down mechanism. This mechanism gives our algorithm the ability to respond swiftly to any fluctuation in the overall load by readjusting the number of EVs actively charging at the moment. To examine the performance of our proposed algorithm, a Java tool has been developed for that purpose. The performance of our algorithm in terms of matching the overall load profile to the expected overall load in the system is evaluated. This performance is compared to the performance of a benchmark, Ahead-of-Time scheduling algorithm. On average, our algorithm achieved approximately 50% improvements over the Ahead-of-Time algorithm in terms of mean absolute error (MAE) between the expected overall load and the observed overall load for all three considered penetration levels of wind power: 10%, 20%, and 30%. These improvements have been achieved without any interruption to the charging EVs. Even better MAE has been achieved when our algorithm has the freedom to temporarily interrupt the charging of some EVs. Different levels of EVs penetration have been considered as well. The performance of our algorithm increases as the penetration level of EVs increases which makes our algorithm suitable for high penetration level of EVs. Also, our algorithm has been tested under different intensity levels of fluctuations in the net-load: 15-minutes, 10-minutes, and 5-minutes. The results clearly demonstrate the ability of our algorithm to absorb all these different levels of fluctuations in the system. Throughout all suggested scenarios, our algorithm consistently outperforms the Ahead-of-Time scheduling algorithms in achieving a better MAE between the expected overall load and the observed overall load.

Chapter 6

Using The Flexibility of Electric Vehicles to Provide Regulation Services During Optimum Charging Times

Electric vehicles (EVs) are a potential provider of regulation services in smart grids. A group of EVs connected to the grid can follow the automatic generation control (AGC) signal from the independent system operator (ISO) to regulate-up and regulate-down by decreasing and increasing their charging rates from an optimal charging level, respectively. In this chapter, we introduce a new regulation method that uses the flexibility of EVs to provide the regulation service. Our method uses binary on-off commands to guide the EVs in order to provide the regulation service as opposed to adjusting the charging rates of the EVs to any value between zero and the maximum charging rate in most of the other studies in the literature. A unidirectional regulation method has been used as a benchmark in this study to show the superiority of our method. Also, real data from the US Department of Transportation (DOT) and California ISO have been used in the testing scenarios. Results show that our method has achieved better performance compared to the benchmark method in terms of meeting the requested charging energy by the EVs within the imposed deadline times by the customers. Also, the average number of charging interruptions per EV has been reduced by our method compared to the benchmark method, and, consequently, the active charging times of the EVs are shortened. The performance of our method has been evaluated using 200 EVs. Three different scenarios for the regulation period are considered. In all the scenarios, our method shows that more than 94% of the EVs are charged with the requested charging energy compared to only 50% when using the benchmark method. Also, the average active charging time of the EVs is shortened by 5.3% compared to the benchmark method.

6.1 Introduction

The regulation service is defined as the act of restoring the supply-demand balance in the system and, thus, helping maintain the system frequency at its nominal value (60 Hz/50 Hz). Any gap between the supplied power and the load in the system including the losses would result in deviation in the power frequency. Traditionally, the regulation services are provided by adjusting the supplied power to match the demand in the system. However, EVs can be used to provide regulation services to the grid as well [83].

Many studies used a vehicle-to-grid (V2G) approach to provide a regulation service to the grid [15,40]. In this approach, the energy in the batteries of EVs is used to supply power to the system when needed. The problem with this approach is the need to discharge the batteries of EVs, which leads to decrease in the lifetime of the batteries. Also, most of the battery manufacturers do not honor their warrantee for the batteries which are discharged frequently to provide regulation services [95].

However, a grid-to-vehicle (G2V) approach can be used to provide regulation services as explained in reference [13]. In this approach, EVs maintain a specific level of charging called preferred operating point (POP) during the active charging period. When regulation-up is needed, EVs reduce their charging from the POP accordingly. Similarly, when regulation-down is needed, EVs increase their charging rates from POP accordingly. In this approach, there is no discharging of the batteries. In fact, the EVs will only gain energy during the active period of the regulation. Thus, such an approach is expected to be more attractive to the customers since it prevents the undesirable discharging of the batteries as well as it allows the customers to charge their depleted batteries during the same period. For these reasons, our work in this chapter will use the G2V approach. In this chapter, we introduce a new regulation method that uses the flexibility of the EVs load in order to optimize the charging time of the participating EVs as well as providing a regulation service to the grid during the active charging period. Although many works in the literature used the EVs to provide regulation services to the grid [50, 76, 79, 86, 87, 94], our proposed method provides the regulation service while considering the following points:

- *Optimizing the charging time*: The charging time of the participating EVs is first optimized to flatten the overall load in the distribution system. Then the EVs are used to provide regulation services during that optimum time. This combines the benefit of charging during an optimum charging time (*e.g.,* off-peak period) and providing regulation services to the grid.

- *Only charging*: The EVs are subjected to charging only (*i.e.,* no discharging of the batteries) in order to provide the regulation service. Thus, there will be no effect on the lifetime of the batteries and no violation of the manufacturers' warranties which often do not cover repetitive discharging of the batteries.

- *Flexibility metric*: We define a flexibility metric to prioritize the charging of the EVs according to their availability in the system. This guarantees the maximum use of the flexibilities of the EVs in order to maximize the number of EVs which get their requested energy by the deadlines assigned by the customers.
- *Binary on-off commands*: Our proposed method uses only on-off commands to either switch on or switch off the smart charger in order to accomplish the charging and regulation tasks. This simple mechanism can be carried out by simple smart chargers that are only capable of following binary on-off commands. Therefore, our method does not require smart chargers with a capability of adjusting the charging rates to any value between zero and a maximum charging rate as it is needed in most of the methods in the literature. Further, the on-off mechanism will reduce the number of charging interruptions per EV compared to the methods that allow the charging rates to be adjusted to any value between zero and a maximum charging rate. Consequently, the reduction in the charging interruptions per EV leads to shorter active charging periods per EV.

To evaluate the performance of the proposed method, real data from the US Department of Transportation (DOT) have been used to generate more realistic plug-in and plug-off times of the EVs. Also, the daily load profile of our distribution system example has been generated from real data taken from California ISO website. A case study of 200 EVs is used to evaluate the performance of the proposed method. Three different scenarios for the regulation time are considered. In all scenarios, our method shows that more than 94% of the EVs are charged with the requested charging energy compared to only 50% when using the benchmark method. Also, the average active charging time of the EVs is shortened by 5.3% compared to the benchmark method.

6.2 System Model

Figure 6.1 shows the system model considered in this chapter. The aggregator server receives the regulation signal also known as automatic generation control (AGC) signal from the independent system operator (ISO) in real time. According to the AGC and the predetermined POP of the charging EVs, the server issues an appropriate on-off command to EVs to perform the needed regulation. Also, all charging parameters of the EVs (*e.g.,* plug-in time, deadline time, required amount of energy by the EVs) should be collected by the aggregator server from all participating EVs. Thus, a two-way communication link between the EVs and the aggregator server is needed. In this study, we assume that the charging times of the EVs are optimized ahead-of-time in order to flatten the overall load in the electric distribution system (*i.e.,* shifting the EVs load to the off-peak periods). During that charging period, the EVs will be used further to provide the regulation service. Thus, we assume that a day-ahead forecast of the load in the distribution system is available.

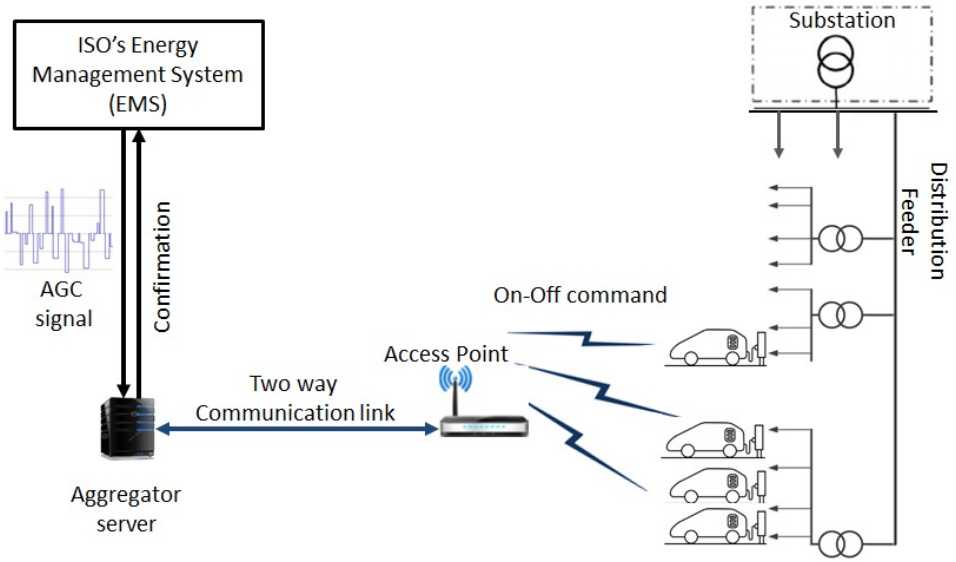

Figure 6.1: The System Model

6.3 Problem Formulation and Description

This section is divided into three subsections. First, we *optimize the charging times* of the EVs ahead of time in order to flatten the overall load in the distribution system. The optimization shifts the EVs load to off-peak periods which benefits both the distribution system and the customers. Second, in order to provide regulation service by *only charging* the EVs (*i.e.,* no discharging of the batteries), an appropriate POP of the EVs is estimated taking into consideration the optimum charging period of the EVs obtained from the ahead of time optimization. Third, we explain the problems when the EVs simply follow their optimum charging profiles and respond at the same time to the AGC signal.

To overcome these problems, a new regulation method will be introduced in Section 6.4. The proposed method defines *flexibility metric* to precisely estimate the EVs' flexibilities. Also, *binary on-off commands* will be used to guide the EVs to start or stop charging according to their flexibilities.

6.3.1 Optimizing The Charging Times of The EVs

As explained earlier, we assume that the EVs are connected to the grid to charge their batteries. During that period, the EVs are used to provide the regulation service to the grid. Further, in this work, the charging time of the EVs will be optimized in order to flatten the overall load in the distribution system. Flattening the overall load benefits

the distribution system as it shifts the flexible load (the EVs load) from peak periods to off-peak periods. Also, this will benefit the customers since the energy cost during off-peak periods is less.

To formulate the optimization problem, we consider a scenario where n EVs are set to be charged. The time over which the optimization will be performed, T, is divided into m time slots, $t = 1, 2, , m$, with slot length of Δt. We assume that the i^{th} EV is plugged into the charger at the time slot $plug_i$ and the customer demands his EV to be charged with the requested amount of energy by a deadline time slot $dead_i$. Also, we assume that the utility (or the aggregator) has the knowledge of the load forecast, $\hat{L}(t)$, $\forall t$, in the system during the optimization period. Flattening the overall load in the system is equivalent to minimizing the square difference between the overall load, ($\hat{L}(t)$+EVs load), and a constant (*i.e.,* perfectly flat) load profile, $G(t)$, where, $G(t) = c, \forall t$. Note that the only variables in this minimization function are the EVs load. Therefore, the optimizer can only adjust the EVs load in order to achieve the flattening overall objective. Thus, we formulate the optimization problem as follows:

$$\begin{aligned} \underset{r_i(t),\forall i}{\text{minimize}} & \sum_{t=1}^{m} \Big((\hat{L}(t) + \sum_{i=1}^{n} r_i(t)) - G(t) \Big)^2, \\ \text{subject to} & \\ & \sum_{t=plug_i}^{dead_i} (r_i(t) \times \Delta t) = C_i, \forall i \\ & 0 < r_i(t) < r_{max}, \forall i \forall t, \end{aligned} \tag{6.1}$$

where, C_i represents the amount of energy to be charged to the i^{th} EV. The decision variables, $r_i(t), \forall i$, represent the charging profiles of the EVs. The first constraint in the optimization problem means that the requested amount of energy, $C_i, \forall i$, have to be met. The second constraint means that the charging rates during any time slot should not exceed the maximum allowed charging rate, r_{max}. The solution of this optimization problem yields the optimum charging profiles for the EVs, $r_i^*(t) \forall i$.

6.3.2 The Appropriate POP to Provide Regulation Service

During this optimum charging time, the EVs are used further to provide a regulation service to the grid. Thus, we need to decide on the appropriate POP for our EVs. In our case, we choose the POP as the collective charging load obtained from the optimization

problem in Equation (6.1) as follows.

$$POP(t) = \sum_{i=1}^{n} r_i^*(t), t = 1, 2, ..., m, \tag{6.2}$$

where, $r_i^*(t)$ represents the optimum charging profile for the i^{th} EV obtained from solving Equation (6.1). In this work, we assume that the EVs are participating in regulation-up and regulation-down with the same capacity as it is allowed in some ISOs (*e.g.,* PJM) [95]. In other words, the amount of energy taken from the EVs to provide regulation-up is approximately equal to the amount of energy given to the EVs to provide regulation-down and, therefore, the overall amount of energy taken from the EVs is zero [9]. Thus, it is assumed that the i^{th} EV ensures the delivery of C_i when it charges according to its optimum charging profile and fully follows the regulation signal from the aggregator server.

6.3.3 The Problems of Directly Following The AGC Signals by The Actively Charging EVs

During the regulation period, when an EVs aggregator receives AGC signal from the grid operator, it responds by sending the appropriate command to the actively charging EVs [13]. For instance, if the grid operator sends a regulation-up signal of 20 kW to an EVs aggregator, the aggregator will signal the currently charging EVs to collectively reduce their charging by 20 kW. Thus, if 20 EVs are charging at the moment, each EV will be commanded to decrease its charging rate by 1 kW. Similarly, when the grid operator sends a regulation-down signal of 20 kW to the aggregator, each EV will be commanded to increase its charging rate by 1 kW. However, such a simple mechanism has two problems.

First, the charging rate of the i^{th} EV in time slot t, $r_i^*(t)$, can be any value between 0 and r_{max} as shown in Equation (6.1). Thus, treating all charging EVs equally is not always appropriate. For example, if the optimum charging rate of the i^{th} EV during the time slot t is the maximum charging rate, $r_i^*(t) = r_{max}$, then this EV will not be able to respond to the regulation-down command from the aggregator at that time slot. Figure 6.2 shows an example of a response of an EV to the regulation signals during two time slots. In the first time slot, the EV responded to both regulation-up and regulation-down signals. However, in the second time slot, it only responded to regulation-up (*i.e.,* decrease charging) but not to the regulation-down since it already charges at the maximum charging rate, 3 kW in this example. Similarly, if the optimum charging rate for an EV is smaller than what the aggregator commanded the EV to decrease, that EV will not be able to fully satisfy the command.

Nevertheless, the aggregator server could solve this problem by using the other EVs which can tolerate more increase or decrease in their charging rates to compensate for those

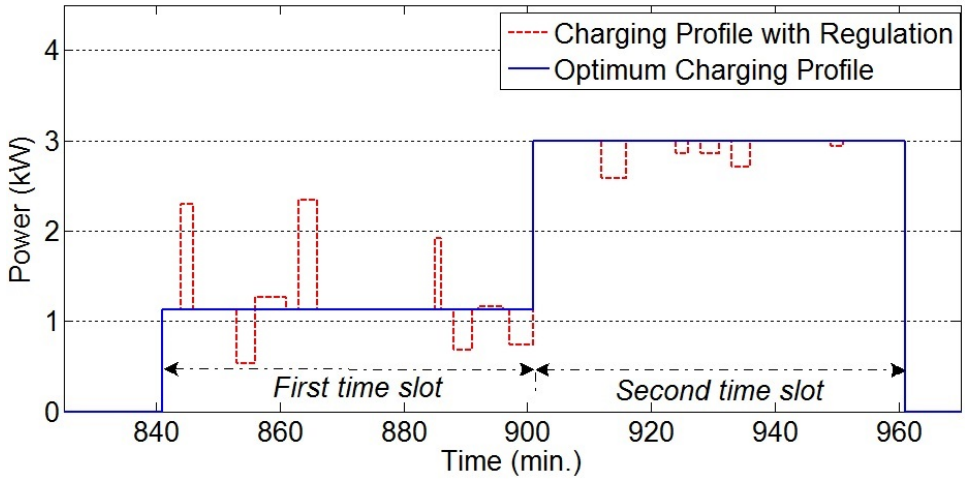

Figure 6.2: Charging profile with and without regulation

which cannot respond fully to the command. This solution leads us to the second issue with the mentioned approach which is the fairness among the charging EVs. We should remember that when all participating EVs respond evenly and fully to the regulation-up and regulation-down commands, they will finish their charging time with the required charging energy, C_i, since the give up energy for the regulation-up is compensated by the regulation-down energy gain. For example, the charging profile in Figure 6.2 shows that during the first time slot, the EV fully responded to both regulation-up and regulation-down. That means if the total energy taken by regulation-up is equal to the total energy given up by regulation-down, as our assumption is, then, during that time slot, the EV is charged with the expected amount of energy dictated by the optimum charging profile. However, during the second time slot, the EV only responded to regulation-up commands. This means that the EV will not be charged with the complete amount of energy during that time slot as dictated by the optimum charging profile. Consequently, by the end of charging time, some of EVs might not get their requested energy, C_i, according to their optimum charging profile. Similarly, some of the EVs might get the full requested energy, C_i, before the end of charging time when their participation in regulation-down service is more than their participation in the regulation-up service. Thus, they withdraw from participating in the charging process when they are supposed to be still charging.

This simple regulation method will be evaluated further in Section 6.5 as it will be used as a benchmark to quantify the improvements in the performance offered by our proposed method.

6.4 The Proposed Method to Respond to Regulation Signal

In this section, we introduce our method in responding to the regulation commands. This method will use the optimum charging profiles obtain from Equation (6.1) to determine the $POP(t)$ as in Equation (6.2). However, the EVs will not use their optimum charging profiles, $r_i^*(t)$, for charging as in the traditional approach. Instead, the aggregator server will guide the EVs to start charging or stop charging based on $POP(t)$, the regulation signal, and the EVs flexibilities.

To explain this approach, we first define a *flexibility metric* to precisely estimate the flexibilities of the EVs. As in Chapter 5, we define the flexibility of an EV as the amount of time the EV can afford to wait before it should start charging in order to get the requested charging energy by the deadline. Thus, we define the flexibility of the i^{th} EV, $F_i(t)$, as follows:

$$F_i(t) = (dead_i - t)\Delta t - \frac{E_i(t)}{r_{max}}, \quad plug_i \leq t \leq dead_i, \tag{6.3}$$

where, $E_i(t)$, represents the remaining amount of energy at time slot t needed to charge the i^{th} EV with the requested energy C_i. It should be noted that at the plug-in time, the remaining amount of energy needed by the i^{th} EV is the same amount of energy originally requested by that EV, $E_i(plug_i) = C_i$. However, once the EV starts charging, $E_i(t)$ starts to decrease until it reaches zero by the deadline time when the EV is completely charged with C_i.

In our method, when an EV is commanded to start charging, it charges with the maximum charging rate, r_{max}. Unlike traditional charging methods where the charging rates can be any value between 0 and r_{max}, we choose to fix the charging rate to r_{max} for the following reasons. First, charging at different rates will impose extra technical requirements on the smart chargers. Thus, by charging at fixed rate, r_{max}, our method relaxes this technical requirement, and, consequently, makes our method suitable for simpler smart chargers that are capable of only following *binary on-off commands*. Second, since the charging EVs will be charging at r_{max}, this will decrease the number of EVs needed to meet the targeted $POP(t)$ at any moment. Consequently, the number of EVs communicating with the server at any moment of time will be minimum. Also, as we will show in Section 6.5.4, the number of charging interruptions for an EV during the whole charging period will be reduced compared to the traditional approach as a result of using r_{max} to charge all EVs.

The flow chart in Figure 6.3 explains the main steps taking by the aggregator server to command the EVs. The steps numbers from 0 through 4 are labeled on the flow chart. In **Step (1)**, $POP(t), \forall t$, is calculated ahead of time from Equations (6.1) and (6.2) based on the charging parameters of the participating EVs which are sent to the aggregator server

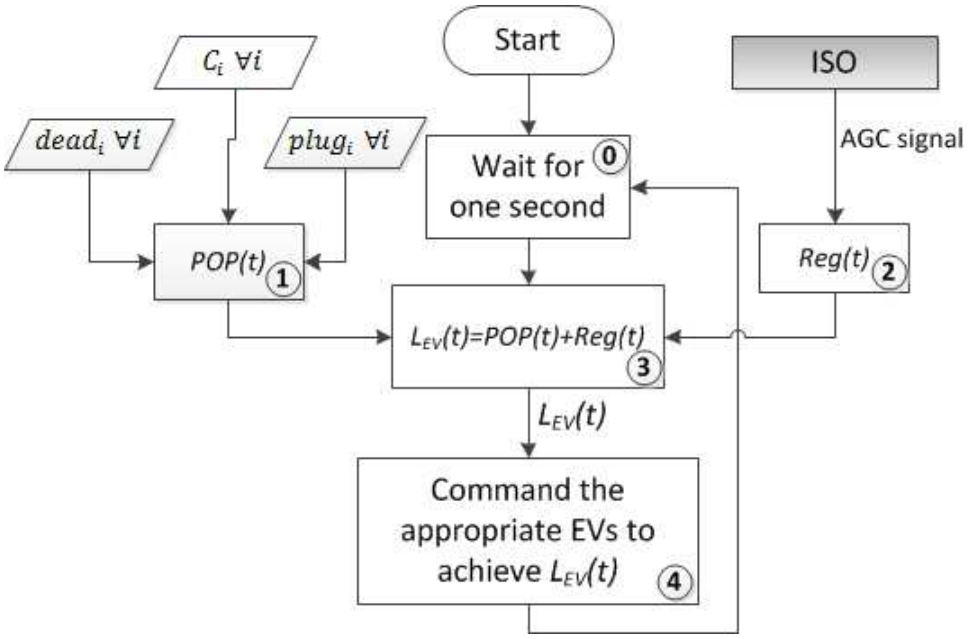

Figure 6.3: Server flow chart

before the start of the charging period. On the other hand, the regulation signal, $Reg(t)$, in **Step (2)** represents how much load need to be added or removed to or from the system as a response to the regulation command. Unlike $POP(t)$, $Reg(t)$ is received at real time from the ISO. In **Step (3)**, the server determines the appropriate EVs load, $L_{EV}(t)$, to be in the system given the optimum $POP(t)$ and the regulation signal, $Reg(t)$, as follows:

$$L_{EV}(t) = POP(t) + Reg(t). \tag{6.4}$$

Note that the amount of energy consumed by the EVs load, $(\sum_{\forall t} L_{EV}(t) \cdot \Delta t)$, can be calculated from Equation (6.4) as follows:

$$\begin{aligned} & L_{EV}(t) = POP(t) + Reg(t) \\ \Rightarrow & \int_T L_{EV}(t)\, dt = \int_T POP(t)\, dt + \int_T Reg(t)\, dt \\ \Rightarrow & \sum_{\forall t} L_{EV}(t) \cdot \Delta t = \sum_{\forall t} POP(t) \cdot \Delta t, \end{aligned} \tag{6.5}$$

Remember that the average energy taken by the regulation signal is assumed to be zero, $\int_T Reg(t)\, dt = 0$. The result from Equation (6.5) means that the amount of energy received by the EVs at the end of the charging period is equal to $(\sum_{\forall t} POP(t) \cdot \Delta t)$. This amount of energy is exactly the amount of energy requested originally by the EVs as shown from

Equations (6.1) and (6.2). Therefore, dispatching the EVs load according to Equation (6.4) ensures the delivery of the whole amount of energy requested by the EVs by the end of charging period.

After computing $L_{EV}(t)$, the server compares $L_{EV}(t)$ to the current EVs load in the system. Based on that, the server decides how many EVs are needed to start charging or stop charging in order to achieve the new $L_{EV}(t)$ in the system as shown in **Step (4)**. Computing the number of EVs to start or stop charging is straightforward since the charging rate in this proposed method is fixed at r_{max} for all EVs. Importantly, the server will choose the EVs with the least flexibility, $F_i(t)$, to command them to start charging (using on-command) when a new load has to be added. Similarly, when the EVs load needs to be reduced, the server will choose the EVs with the largest $F_i(t)$ among those which are charging at the moment to command them to stop charging (using off-command). This allows the EVs with the least $F_i(t)$ to be charged first. Since the EVs with the least $F_i(t)$ are charged first, this will keep the overall flexibility of the EVs which still need to be charged, $\sum_{\forall i} F_i(t)$, at the highest. This is crucial in the mechanism of our method. As the overall charging level of the EVs, $L_{EV}(t)$, is kept on average at $POP(t)$, we know that the total delivered energy to the EVs by the end of the optimization period will be equal to the total requested amount of energy by all EVs, $\sum_{\forall i} C_i$. Thus, all EVs can get their requested amount energy during their availability time if the charging order is managed properly. For this reason, we charge the EVs with the least flexibility first leaving the EVs with the larger flexibility to be called for charging at a later time. After all, the flexibility of the EVs load is the main reason why the server can delay charging of the EVs and, thus, provide a regulation to the system and charge the EVs with their requested amount of energy without violating the customers' deadlines.

Additionally, our method should act promptly to keep the appropriate $L_{EV}(t)$ in the system. This is shown the transition from **Step (4)** to **Step (0)**. In **Step (0)**, the server will wait for only one second to check if there is a need to adjust the $L_{EV}(t)$ in the system or not. Three reasons invoke the need for adjusting $L_{EV}(t)$: First, a change in $POP(t)$ which happens every Δt (*e.g.,* every 60 minutes). Second, a change in $Reg(t)$ which is updated every 2-6 seconds by ISO (*e.g.,* every 4 seconds in California ISO) [95]. Third, a withdrawal of an actively charging EVs from the system due to achieving the requested amount of energy which can happen at any point of time. Note that it is not in every loop from **Step (0)** to **Step (4)** $L_{EV}(t)$ will be adjusted. But when the adjustment is needed, the action will be taken quickly.

6.5 Performance Evaluation

In this section, we evaluate the performance of our proposed method against the performance of the described benchmark method in Section 6.3. A special Java tool has been

developed to simulate our proposed method. As explained earlier, our method takes three inputs: the charging parameters of the EVs (*e.g.,* $plug_i$, $dead_i$, C_i $\forall i$), $POP(t)$, and the regulation signal $Reg(t)$. The details of these inputs are described in the following subsections.

6.5.1 Charging Parameters

For a realistic scenario of plug-in times and deadline times of the EVs, we have used real data from the US Department of Transportation (DOT) report describing the public mobility in USA [73]. In that study, the vehicle trips are categorized according to their purposes (*e.g.,* commuting trips, schools/churches trips, and family trips). Obviously, the plug-in time and deadline time of a vehicle will be influenced by the time of driving of this vehicle which is directly related to the daily vehicle's trip purposes. In this work, we assume that the daily use of the participating EVs is to commute to and from the work place. As shown in the DOT report, these vehicles are generally used twice during the day. One trip is from home to the work place and the other is back from the work place. Figure 6.4 shows the histogram of the trips' starting time from home to work and back from work as reported by the DOT [73]. Although the reported histogram in reference [73] did not explicitly distinguish between the trips from home to work and the trips back from the work place, we assumed that the morning trips represent the trips from home to work and the afternoon trips represent the trips back from work places. Thus, the dashed line in Figure 6.4 evenly breaks the histogram into the two groups of trips accordingly. In this work, we will use the histogram in Figure 6.4 to generate samples of the departure time of EVs (deadline times) and the arrival times of EVs (plug-in time). However, since the second part of the histogram in Figure 6.4 represents the start time of trip from work to home, and since that the average commute travel time is 22.85 minutes as reported by the DOT [73], we have added 30 minutes to the sampled time to account for the delays before the customer actually plug-in the vehicle for charging.

6.5.2 $POP(T)$

As mentioned in Section 6.4, $POP(t)$ is determined from Equations (6.1) and (6.2). To solve the optimization problem in Equation (6.1), we first define all needed parameters. A scaled down version of daily load profile of California ISO (CAISO) is used as the expected load profile of our utility example, $\hat{L}(t)$. The daily load profile data have been taken from CAISO web site [1] from 12:00 PM, 15 Dec 2013 to 12:00 PM, 16 Dec 2013. Also, we assume that there are 200 EVs to be charged during this period. As explained in Section 6.5.1, the plug-in time and deadline time for each EV have been sampled randomly from the histograms in Figure 6.4. The amount of energy needed by each EV, C_i, is randomly selected from the interval of (8 kWh, 3.2 kWh). Also, we assume that the EVs are connected

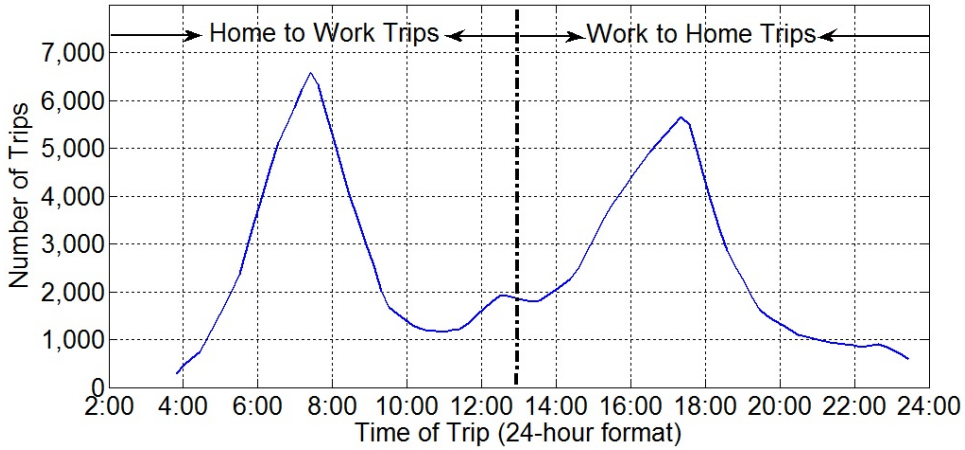

Figure 6.4: The histogram of trips' start time

to smart chargers with the maximum charging rate of $r_{max} = 3$ kW, complying with level II charging standard [61]. Finally, Δt is set to 60 minutes.

Based on these settings, the optimization problem in Equation (6.1) has been solved using the linear least-square solver in MATLAB. Figure 6.5 shows the expected daily load

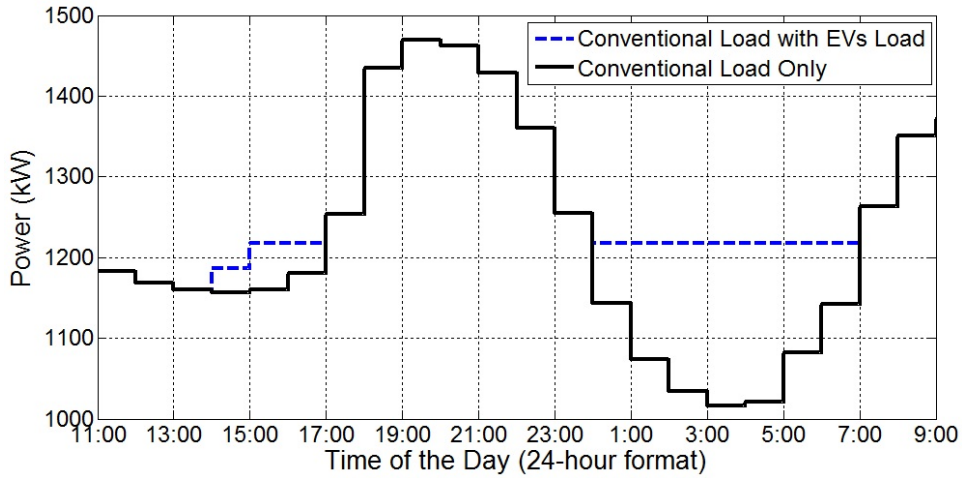

Figure 6.5: The optimized EVs load

in the system along with the optimized EVs load. Clearly, the charging time of EVs has been shifted to fill the load valley as expected. Also, Figure 6.6 shows $POP(t)$ for each hour calculated directly from the optimum charging profiles, $r_i^*(t)$, $\forall i \forall t$, using Equation (6.2).

6.5.3 Regulation Signal ($Reg(T)$)

In some ISOs (*e.g.,* PJM, New England, and Ontario), regulation is a 5-minute service [44]. That is, the regulation resource can be held for regulation-up or regulation-down for up to five minutes. Based on that, we have randomly generated a regulation signal with maximum capacity of ±50 kW. Although the maximum capacity is chosen to be ±50 kW in this scenario, it can be increased with the increase in the number of participating EVs. The magnitude of the signal is randomly generated between 0 and 50 kW. Also, the width of the signal is randomly generated between 0 and 5 minutes. Sample of this signal is shown in Figure 6.7. It should be noted that the average amount of energy taken by this regulation signal over a long period of time is approximately zero.

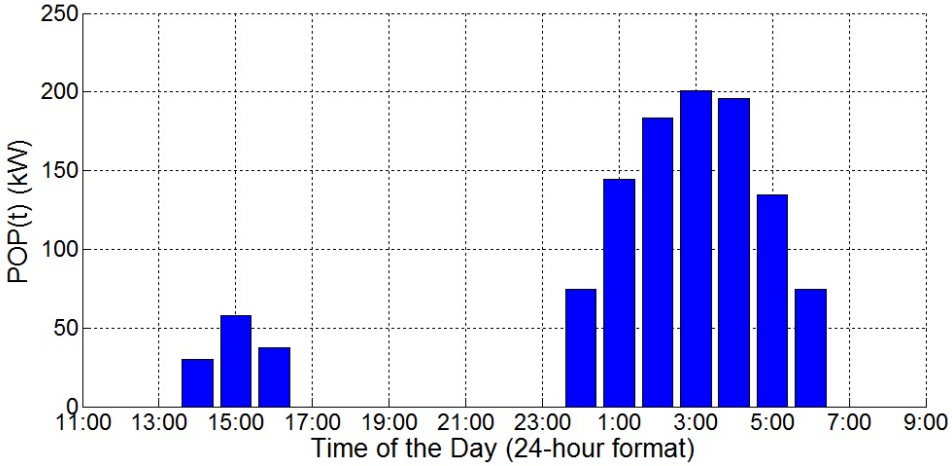

Figure 6.6: The optimum $POP(t)$

6.5.4 Results and Discussions

Figure 6.6 shows the optimum $POP(t)$ for each hour according to the results from the optimization problem. Each hour has different $POP(t)$ since the number of charging EVs in each hour is different and the optimum charging rate, $r_i^*(t)$, for each EV is different. Table 6.1 lists the number of EVs actively charging at each hour along with the value of $POP(t)$ for that hour. Also, the maximum accumulative charging level which can be reached when all actively charging EVs charge at their maximum charging rate, $r_{max} = 3$ kW, is calculated. Clearly, the maximum regulation-up signal that the EVs can successfully respond to is governed by the value of $POP(t)$ in each hour. However, the same maximum value for regulation-down is not necessarily achievable by the same group of actively charging EVs. Recall that only the actively charging EVs are responding to the regulation signal in the

Table 6.1: Optimum $POP(t)$ and maximum possible charging level for all active EVs

Time	Number of active EVs	Optimum $POP(t)$ (kW)	Maximum charging level (kW)
14:00	10	30	30
15:00	27	57.58	81
16:00	19	37.2	57
00:00	37	74.4	111
01:00	59	144.3	177
02:00	80	183.7	240
03:00	85	200.6	255
04:00	80	195.9	240
05:00	57	134.7	171
06:00	37	74.8	111

case of the benchmark method explained in Section 6.3. This limitation should always be taken into consideration. For instance, at time 16:00 in Table 6.1, 19 EVs are scheduled to charge during that hour with $POP(t)$=37.2 kW. These EVs can ramp-down their load to 0 when all of them stop charging to provide a regulation-up of 37.2 kW. However, the same group of EVs cannot respond to the same capacity of regulation-down, 37.2 kW, since they cannot double their load to 74.4 kW. The maximum achievable load of these EVs is 57 kW as shown in Table 6.1. In comparison, our method can always increase the load of EVs as needed as long as there are EVs plugged in and ready to start charging. Remember, our method does not command the EVs to follow their optimum charging profiles obtained from solving the optimization problem. Instead, it commands EVs to start charging or stop charging according to their flexibility, $POP(t)$, and the regulation signal at any point of time.

Figure 6.8 illustrates the deficit and surplus in the charged energy compared to required energy, C_i, $\forall i$, when using the benchmark method in Section 6.3. In this experiment, regulation signal has been applied through different time spans: three hours from 00:00 to 03:00 (Figure 6.8(a)), five hours from 00:00 to 05:00 (Figure 6.8(b)), and seven hours from 00:00 to 07:00 (Figure 6.8(c)). When this signal is applied to the charging EVs, some of EVs received more energy than requested by users while others received less energy than requested. That means, when practically such a regulation method is used, some of these EVs will get fully charged before its calculated optimum time. Consequently, $POP(t)$, $\forall t$, which are calculated based on the optimum time and optimum charging rates of EVs cannot be maintained especially during the later hours since some of these EVs will not be able to charge anymore. Also, as shown from the results, some other EVs have not received the complete amount of energy requested by the users by the deadline. These issues are a direct consequence of the unfairness problem in the benchmark method

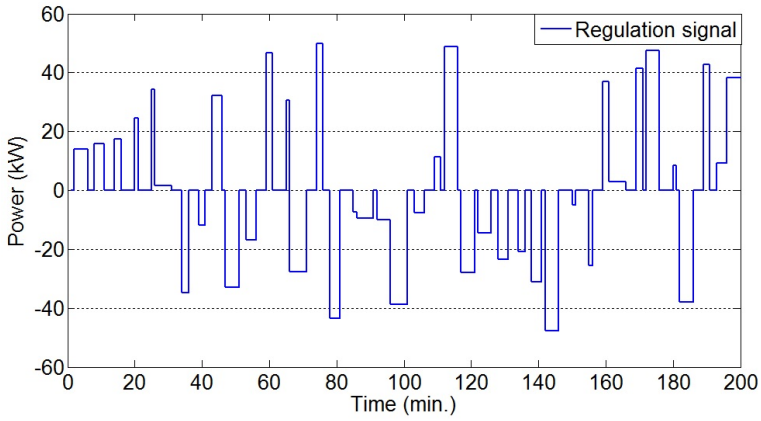

Figure 6.7: Regulation Signal

explained in Section 6.3. However, it should be noted that the overall amount of energy deficit and energy surplus are approximately equal especially when the time of regulation is long enough as in Figure 6.8(c). This means that there is room for improvement if the mechanism of charging considers the flexibility of the EVs, as our proposed method does.

In comparison, Figure 6.9 shows the results from our regulation method with the same experiment settings. Clearly, the number of EVs which did not get their requested energy is significantly less compared to the number of EVs which did not get their requested energy in the benchmark method. Only 8, 10, and 7 EVs from the 200 participating EVs did not get the 100% of their requested energy when the regulation signal is applied for 3 hours, 5 hours, and 7 hours, respectively. On the other hand, most of the 200 participating EVs deviated from their requested energy when applying the benchmark method as shown in Figure 6.8. Also, in our method, the number of EVs with deficit energy is not increasing as the time of regulation is increased as one would expect. Remember that the capacity of regulation-up is assumed to be equal to the capacity of regulation-down. Thus, as time goes by, the amount of energy taken from EVs for regulation-up is compensated by the amount of energy given to EVs for regulation-down.

Further, Table 6.2 shows the average number of charging interruptions per EV for the three scenarios. Note that the charging interruption for an EV in the benchmark method is happening every time the aggregator server adjusts the charging rate of that EV. In our method, the charging interruption is happening every time the aggregator server switches the charging of an EV from on to off. Clearly from the results, an EV in our method is subjected to less charging interruptions as expected in Section 6.4. Given that the average number of charging interruptions in our method is less and all EVs are charging at the maximum charging rate, r_{max}, when they are on, the average active charging time for the EVs is less. In our experiment, the average requested energy by the EVs is 5.6 kWh.

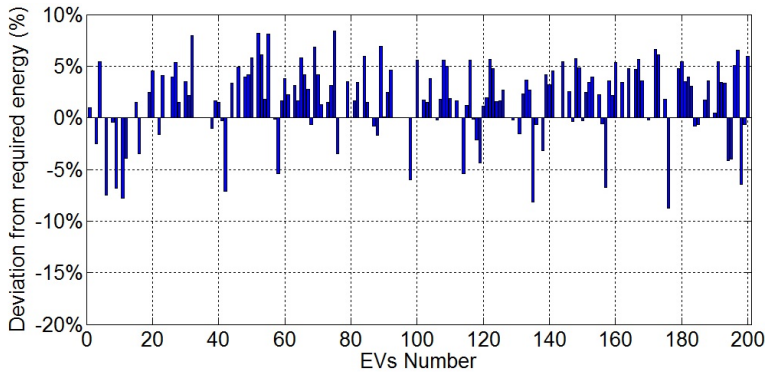

(a) Time from 00:00 to 03.00

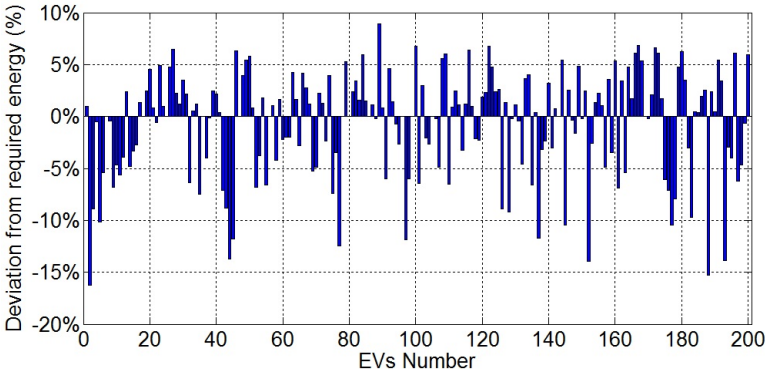

(b) Time from 00:00 to 05.00

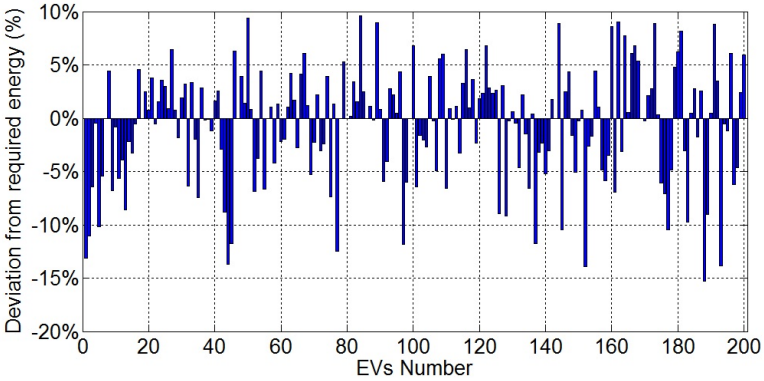

(c) Time from 00:00 to 07.00

Figure 6.8: Percentage of energy deficit and surplus in the requested energy due to regulation using the benchmark method

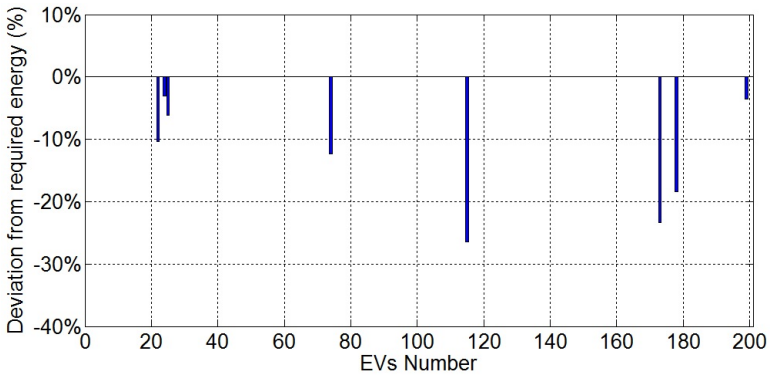

(a) Time from 00:00 to 03.00

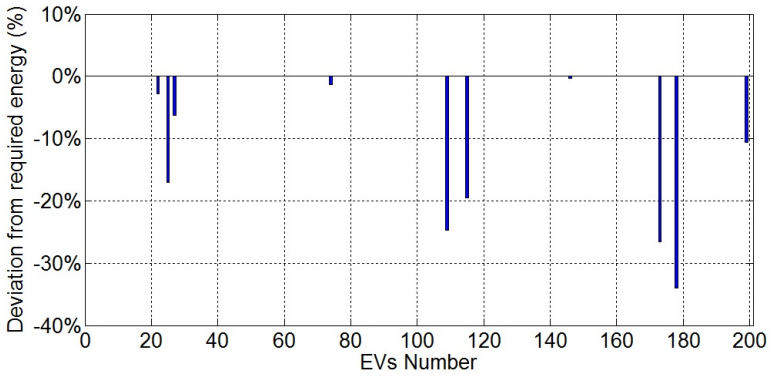

(b) Time from 00:00 to 05.00

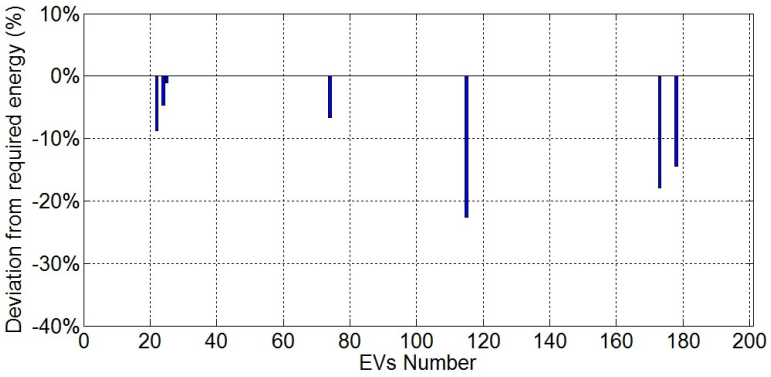

(c) Time from 00:00 to 07.00

Figure 6.9: Percentage of energy deficit and surplus in the requested energy due to regulation using our method

Table 6.2: Average number of charging interruptions per EV during the charging period

Time	Benchmark method (Interruptions per EV)	Our method (Interruptions per EV)
00:00-03:00	17.6	9.9
00:00-05:00	34.1	14.8
00:00-07:00	43.5	16.2

The average active charging time for the EVs in the benchmark method is 5 hours and 4 minutes. On the other hand, in our method, the average active charging time for the EVs is 4 hours and 48 minutes. This results in 5.3% improvement in the charging time of the EVs achieved using our method compared to the benchmark method.

6.6 Summary

In this chapter, we have proposed a dynamic method to manage the charging of EVs in order to provide a regulation service to the grid. The EVs need not to be connected to the grid to only provide a regulation service. Instead, the EVs can be used to provide this service when they are connected to the grid to get their batteries charged. Further, the batteries of EVs will be only charged — no discharging, yet provide regulation-up and regulation-down service to the grid. To evaluate the performance of our method, real data from US department of transportation (DOT) have been used to estimate the plug-in time and deadline time of the EVs. Also, California ISO daily load has been used to realistically create a scenario of the daily load profile of our example distribution system. The results from our method have been compared with results from unidirectional regulation method used as a benchmark. Our method shows better performance compared to the benchmark in delivering the requested energy to the EVs by the deadline assigned by the customers. Also, our method decreases the number of charging interruptions per EV compared to the benchmark method and, thus, shortens the time of active charging for the EVs. Additionally, our method uses only on-off signals to command the EVs to either start charging with fixed charging rate (r_{max}) or stop charging. In comparison, the benchmark method commands the EVs to adjust their charging rates for any value between zero and r_{max}. Consequently, our method imposes less technical requirements on the smart chargers compared to the benchmark method which requires the smart chargers to be capable of adjusting the charging rates to arbitrary values between zero and maximum charging rate.

Chapter 7

Evaluating Electric Vehicles Response Time to Regulation Signals

.

Electric vehicles (EVs) are considered as a flexible load in smart grids. This flexibility promotes the EVs to be good candidates for providing the grid with ancillary services, such as regulation services. A group of EVs controlled by an aggregator can collectively work as a regulation reserve in the electric grid. However, a fast response to the regulation commands is crucial to providing reliable regulation service. In this chapter, we precisely evaluate the expected time delay from the instant when an aggregator server sends a regulation command to n EVs to the instant when all the EVs' responses are received successfully by the server. To achieve this goal, first, a realistic communication structure between the aggregator server and the EVs is considered. Second, the wireless link between the access point (AP) and the EVs is accurately modeled in order to estimate the average delay. The model is based on Markov chain representation for the wireless IEEE 802.11 MAC protocol. Two important factors are considered in this model. First, the packet loss probability due to the lossy wireless environment has been incorporated into the model. Second, the transition stages for the contention window size of 802.11 MAC protocol to reach the saturation stage is taken into account. The model has been validated by means of extensive simulation using the well-known Network Simulator 2 (NS2) tool. Our analysis shows that one AP is capable of handling up to 1000 EVs without violating the four second latency limit when the probability of packet loss is 0.01. However, this number decreases significantly, less than 500 EVs, when the wireless link is experiencing a significant packet loss probability of 0.2. Further, we show that by commanding a sub-group of the charging EVs, it is possible to achieve the same regulation service but with a faster response time, compared to commanding all charging EVs every time.

7.1 Introduction

The flexibility of EVs' load can be used to provide ancillary services to the electric grid, such as regulation reserve as shown in Chapter 6. However, the response time of the EVs to the regulation signal is important in this service. An EV aggregator should maintain the required maximum delay limit imposed by the Independent System Operator (ISO) to be certified as a provider for this service. For instance, California ISO's requirement for the communication delay between the service provider (the aggregator) and the generating unit (the EVs) is to be within 4 seconds [16]. One study suggests that this delay should be in the range of 1-2 seconds [13]. Additionally, the Federal Energy Regulation Commission (FERC) has issued Order 755 in October 2011 [25] in which FERC requests ISOs to implement a compensation scheme in their regulation markets. In this scheme, regulation resources (*e.g.,* EVs) which follow the regulation command more closely and more quickly should be paid more. Nonetheless, most of the studies about providing regulation services to the electric grid by an EV aggregator either did not mention the communication requirements at all or assumed that the links between the aggregator and the EVs are fast enough [15,40].

In this work, we assume that the last-mile link between the EVs and their aggregator server is a wireless link as will be explained in Section 7.2. The regulation command is delivered to the smart chargers of the EVs through an Access Point (AP) using the IEEE 802.11 MAC protocol. Therefore, it is important to accurately model the delay over this wireless link in order to estimate the overall delay between the aggregator server and the EVs. Specifically, the model should be able to answer two related questions. First, if n EVs are covered by one AP and the packet loss probability is p_e, what is the average delay from the instant when the aggregator server sends the first regulation command to these EVs to the instant when all n EVs' responses are received successfully by the server? Second, given a delay limit and a packet loss probability p_e, what is the maximum number of EVs which can be supported by only one AP without violating the delay limit? Although significant efforts have been made to investigate the performance of 802.11 MAC protocols led by novel works in references [8, 81], these works modeled the performance of the protocol in the saturation state which is not the state of the protocol in our scenario. Also, these works assume that the data packet collision due to the contention nature of 802.11 MAC protocol is the only reason for transmission failure– ignoring the packet loss probability due to the lossy wireless environment. In this context, this work makes the following contributions:

1. To suit our (non-saturated) scenario, we have developed a new model, which takes the transient stages of the contention window into account, to accurately model the latency in the wireless link between the AP and the EVs.

2. This model takes into account probability of packet error due to possible interference and potential deteriorating of the wireless signal in the outdoor area.

3. The model has been validated by comparing its numerical results with results from the Network Simulator 2 (NS2) tool.

4. After validating the wireless link latency model, the overall delay between the aggregator server and the EVs is formulated.

5. This overall delay formula has been used to put an upper bound for the number of EVs covered by one AP in order to achieve a specific maximum delay.

Thus, the two important questions of evaluating the response time of n EVs covered by one AP and calculating the maximum number of EVs which can be supported by one AP without violating the imposed delay limit have been answered.

The rest of the chapter is organized as follows. The communication model is described in Section 7.2. The model for the wireless link latency between the AP and the EVs is described in Section 7.3. The model validation is shown in Section 7.5. The estimation for the maximum number of EVs covered by one AP when the maximum latency for their response is restricted is evaluate in Section 7.6. Finally, we summarize this chapter in Section 7.7.

7.2 Communication System Model

Figure 7.1 shows the communication system model considered in this work. In this model, the communication path between ISO' Energy Management System (EMS) and EVs can be divided into two segments: the first segment from ISO's EMS to the aggregator server and the second segment is from the aggregator server to the EVs. The link from ISO to the aggregator server is usually deployed by the ISO itself, and the communication quality of this link is guaranteed by ISO. On the other hand, the aggregator should ensure that the communication quality between the aggregator's server and the EVs as dictated by ISO's communication standards. In this work, the performance of the communication link between the aggregator's server and EVs in terms of latency is accurately modeled. We examine the time delay between sending a command from the aggregator to a specific group of EVs and receiving confirmations back from these EVs. In order for the aggregator to participate in providing regulation service, this delay should be within the ISO communication delay requirements (*e.g.,* California ISO's maximum delay allowed is 4 seconds) [16].

In fact, the aggregator can use existing internet service providers to reach to the EVs. Usually, this link can be Digital Subscriber Line (DSL), coaxial cable, or fiber optic, for example. All these technologies can reliably deliver the command from the aggregator server to the EVs, say in a parking lot, within few milliseconds. However, in the parking

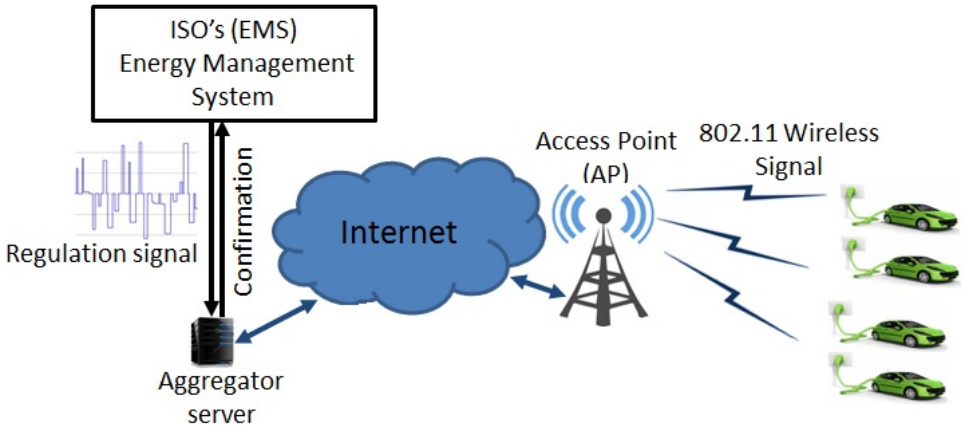

Figure 7.1: The system model

lots, we assume that the command is wirelessly delivered to EVs through a Wi-Fi Access Point (AP) since it is less expensive to equip these places with Wi-Fi compared to other means. However, this wireless link between the AP and the EVs can be considered as the bottleneck in the communication path between the aggregator server and the EVs. Thus, evaluating this link in terms of latency is crucial to understand the overall latency between the aggregator server and the EVs.

7.3 The Wireless Link Between The AP and The EVs

Now we describe the method of communication between the aggregator server and the EVs. Upon receiving the regulation command from the ISO, the aggregator server specifies a group of EVs (say, n EVs) which should increase or decrease their charging rate in response to that command. Then, the aggregator server prepares a data packet containing all the needed information for these n EVs and broadcast it to all the EVs. Only the intended EVs, *i.e.,* the n EVs, will respond to this message by sending a confirmation message back to the aggregator server and then they increase or decrease their charging rate as commanded. Thus, as the intended EVs receive the command from the AP, they will compete on the channel to send back their confirmations to the AP. In this analytical model, we estimate the average delay , $\overline{D(n)}$, taken by n EV from the point they receive the broadcast packet from the AP to the point they successfully send their confirmation messages back to the AP. Mainly, two variables will affect this delay:

(i) The number of EVs which are competing on the channel to send back their confirmation messages.

(ii) And the quality of the channel represented by the packet loss probability (p_e) of the wireless link between the EVs and the AP.

Our analysis follows the same approach in reference [8] where the scenario of n stations continuously sending packets to an AP using 802.11 MAC protocol has been modeled as a Markov chain. However, there are important differences between our model and the model in reference [8]. First, in our model, we consider the impact of probability of packet error, p_e, on the average delay time. In contrast, the model presented in [8] does not take p_e into consideration. Our scenario is an outdoor scenario where the wireless links between the EVs and the AP can easily be affected by the noisy environment and by physical obstacles. Thus, we believe that the consideration of p_e in our model is important. Second, in our scenario, all stations start with contention window of W_{min} as it will be explained in Subsection 7.3.1. Before the average contention window of all the stations reaches the average contention window of the saturation state, the system goes through transient stages where the average delay to transmit the confirmation packet is different than average delay in saturation case. These transient stages and their effect on the average delay have been taken into consideration in our model. On the other hand, the model in reference [8] estimates the delay in saturation state.

7.3.1 IEEE 802.11 MAC Protocol

In this section, we briefly describe the basic access method of IEEE 802.11 MAC protocol, namely the Distributed Coordination Function (DCF) which is used by the wireless stations to transmit their frames in the wireless environment. Since the communication between the stations and the AP in our scenario is brief with only one packet at a time, we assume that IEEE 802.11 MAC protocol is operating in without-handshake mode, *i.e.,* there is no request to sent (RTS) or clear to send (CTS) control frames prior to the data packet transmission. Complete description of 802.11 MAC protocol's operating modes and mechanism can be found in reference [38].

When a station has a new data packet to send, it monitors the channel for a period of time equal to a distributed interframe space (DIFS). If the channel is idle during that DIFS, it sends its packet. Otherwise, it waits until the channel is sensed idle for DIFS; then it chooses a random period of time, called back-off time, from a contention window W_{min} and it starts to count down from that chosen back-off time when the channel is idle, but freezes that counter when the channel is busy. When the counter reaches zero, the station sends the packet. After a short interframe space (SIFS) time, smaller than DIFS, the station should receive acknowledgement (ACK) from the receiver. If no ACK is received, the station assumes that there was a collision and it tries once again. Every time a collision happens, the contention window size is doubled starting from W_{min} until

it reaches W_{max} as follows:

$$W_i = \begin{cases} 2^i \times W_{min}, & \text{if } 2^i \times W_{min} < W_{max} \\ W_{max}, & \text{Otherwise} \end{cases} \tag{7.1}$$

where i represents the number of collisions encountered by the packet. W_i represents the contention window size after the i^{th} collision.

7.3.2 Markov Chain Model

In this study, we adopt the Markov chain representation of the back-off time from reference [8]. As shown in Figure 7.2, the states of the Markov models represent the possible back-off time taken by a station before it attempts to send a packet. For example, state $(i, W_i - 1)$ means that the packet has experienced $i-1$ unsuccessful sending attempts (*i.e.,* collisions) so far, and the current state is the i^{th} attempt. In this state, the MAC protocol has randomly chosen back-off time of $W_i - 1$ slots. A transition from state $(i, W_i - 1)$ to state $(i, W_i - 2)$ happens when the channel is sensed idle for one time slot. When the back-off time reaches zero, *i.e.,* state $(i, 0)$, the packet is sent. The sent packet could collide with another packet sent by another station with probability p or it will be successfully sent with probability $1 - p$. When the packet is successfully delivered, the protocol moves to the next packet to be sent starting with minimum contention window size, $W_{min}(W_0)$. In case of collision, the station will double the contention window size from W_i to W_{i+1} as shown in Equation (7.1). Then, a back-off time will be randomly chosen from that back-off window W_{i+1}. Since doubling the contention window size from W_i to W_{i+1} is with probability p, and the chance of choosing a specific back-off time from that window size is uniformly distributed on the interval $[0, W_{i+1} - 1]$, then the transition from the state $(i, 0)$ to $(i + 1, k)$, $k \in [0, W_{i+1} - 1]$, has probability of p/W_{i+1}. Finally, W_m in the model represents W_{max} in Equation (7.1). From this model, the work in reference [8] concluded that the probability (τ) of transmitting a packet at any given time slot can be expressed as follows:

$$\tau = \frac{2(1-2p)}{(1-2p)(W_{min}+1) + pW_{min}(1-(2p)^m)}, \tag{7.2}$$

where m represents the maximum back-off stage such that $W_{max} = 2^m W_{min}$. Therefore, given that n stations are competing on the channel to send their packets, one of these stations will avoid collision and successfully send its packet if the other $n - 1$ stations are not sending at that time slot. Thus, the collision probability, p, can be expressed in terms of τ as follows:

$$p = 1 - (1 - \tau)^{n-1} \tag{7.3}$$

Finally, the Equations (7.2) and (7.3) can be numerically solved to determine the two unknowns p and τ.

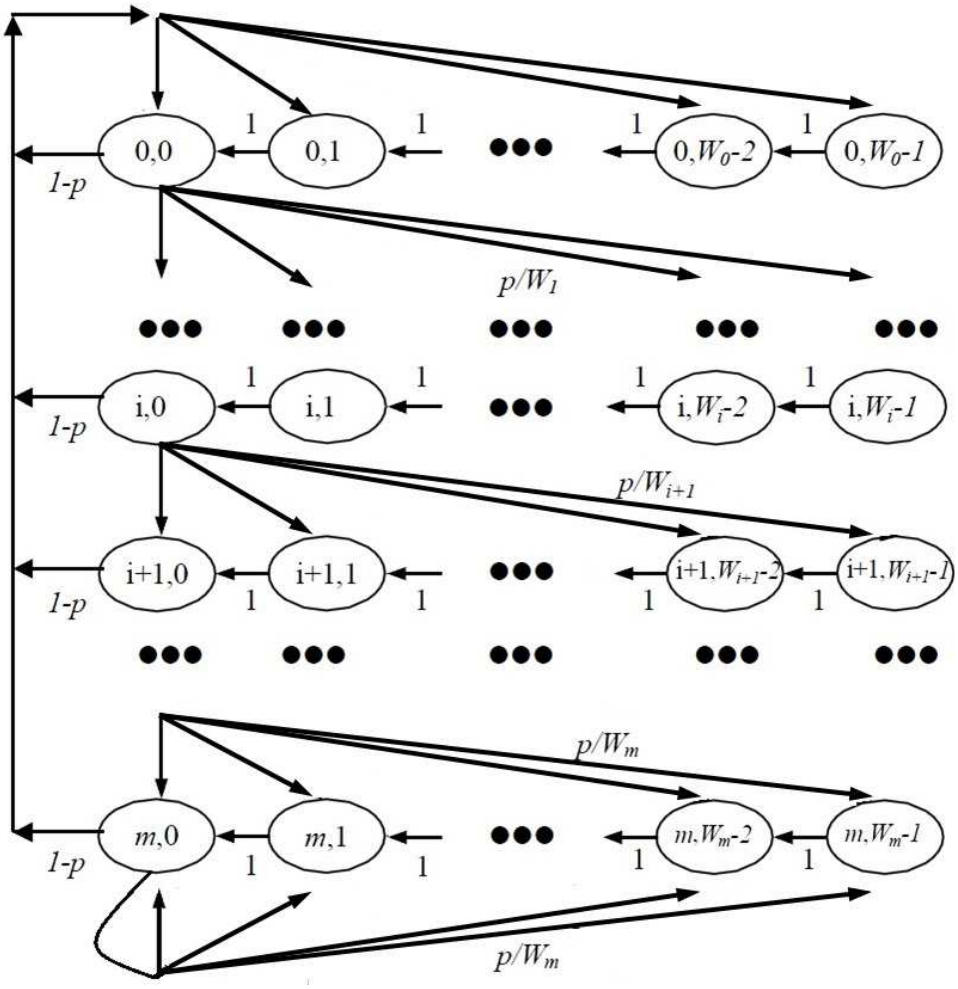

Figure 7.2: Markov chain model [8]

7.4 Model Adjustments

In this section, we explain how the model in Figure 7.2 is extended to suit our scenario. As explained in Section 7.3, there are two differences in our scenario compared to the saturation scenario in reference [8]. First, our scenario considers the impact of the lossy wireless environment on the estimated delay—contrary to the scenario in reference [8], where the probability of packet loss due to the wireless environment is assumed to be zero. Second, the contention window size of the stations in our scenario goes through transient stages before it reaches the average contention window size in the saturation state, while the scenario in reference [8] assumes the stations are already in the saturation state. For simplicity, these two changes in the model will be tackled one at a time.

7.4.1 Lossy Wireless Environment

The assumption in the model in Figure 7.2 is that the failure of transmission can be caused only by a collision with another packet. However, in our scenario, the failure of transmission can be caused by a collision with another packet from other station, but also it can be caused by packet loss due to lossy wireless environment represented by a probability of packet loss, p_e. Note that, in this work, we assume that all nodes (EVs) are uniformly subjected to the same probability of loss (p_e). Nonetheless, our model can still be used to evaluate the average response time even in the case of different p_e due to different positions of EVs from AP, for example. That is, we can assume that all EVs are subjected to the worst case of p_e and compute the response time based on that assumption. In this case, the resulted average response time from the model represent a very good upper bound of the response time instead of the exact average response time.

While a collision can only happen for the data packet, the wireless lossy environment can affect both the data packet and the MAC acknowledgment. We assume that both data frames and the acknowledgement frames can be lost with the same probability p_e. Therefore, in our scenario, the failure of transmission probability p can be formulated as follows:

$$p = 1 - (1 - p_c)(1 - p_e)^2, \tag{7.4}$$

where, p_c represents the probability of collision. In the previous work in reference [8], the probability of failure, p, shown in Figure 7.2 is only driven by p_c , *i.e.,* $p = p_c$. In this work, we keep the same chain in Figure 7.2 but with a different representation for p as shown in Equation (7.4). Consequently, the formulation of the probability τ in Equation (7.2) remains unchanged, but with the *new* failure probability p shown in Equation (7.4). Additionally, the failure probability p can be expressed in terms of τ and p_e as follows:

$$p = 1 - (1 - \tau)^{n-1}(1 - p_e)^2. \tag{7.5}$$

Thus, the two Equations (7.5) and (7.2) can be numerically solved to determine the two unknowns p and τ given the loss probability p_e and the number of competing nodes n. Once we estimated τ, we can express the probability of having at least one transmission by n stations, P_{tr}, during any randomly selected time slot as follows:

$$P_{tr} = 1 - (1 - \tau)^n. \tag{7.6}$$

However, P_{tr} represents the probability of having a transmission whether it is successful or not. The probability of successful transmission given that we have a transmission, $P_{s|tr}$, can be expressed as follows:

$$P_{s|tr} = \frac{n.\tau.(1-\tau)^{n-1}(1-p_e)^2}{1-(1-\tau)^n}. \tag{7.7}$$

Now we can use the result from the work in reference [8] to calculate the average length of time slots for all stations , $E[SlotLen]$, as follows:

$$E[SlotLen] = (1 - P_{tr}).\sigma + P_{tr}.P_{s|tr}.T_s + P_{tr}.(1 - P_{s|tr}).T_f, \tag{7.8}$$

where, σ is the duration of an empty time slot, T_s is the average transmission time for a successful packet, and T_f is the average time the channel is busy due to unsuccessful transmission. According to the mechanism of 802.11 MAC protocol, T_s can be estimated as follows:

$$\begin{aligned} T_s =& DIFS + Hd + FrameSize/DataRate + \\ & SIFS + ACK + \sigma, \end{aligned} \tag{7.9}$$

where, Hd is the time needed to transmit the physical header of the frame, $FrameSize$ is the size of the frame in bits, $DataRate$ is the data rate of the transmission, and ACK is the time needed to transmit the acknowledgment. On the other hand, an unsuccessful packet transmission can be caused by any one of these three factors: a collision of the packet, loss of the packet due to the lossy wireless link, or loss of the acknowledgement. To calculate T_f, the probability of each one of these factors should be estimated. First, the probability of having a collision given that the transmission is a failure, $Pr(c|f)$, can be formulated as follows:

$$Pr(c|f) = \frac{Pr(c \cap f)}{Pr(f)} = \frac{Pr(c)}{Pr(f)} = \frac{p_c}{p}. \tag{7.10}$$

Similarly, the probability of having a failure due to the loss of the data packet, $Pr(Pkt_l|f)$, and the probability of having a failure due to the loss of the acknowledgement, $Pr(Ack_l|f)$,

can be expressed as follows:

$$\begin{aligned} Pr(Pkt_l|f) &= \frac{(1-p_c)p_e}{p} \\ Pr(Ack_l|f) &= \frac{(1-p_c)(1-p_e)p_e}{p}. \end{aligned} \tag{7.11}$$

It should be noted that the channel will be kept busy for T_s when the failure is due to an acknowledgement loss. Otherwise, *i.e.,* with probability of $(1 - Pr(Ack_l|f))$, the channel will be kept busy only for time T_{data} which can be estimated as follows:

$$T_{data} = DIFS + Hd + FrameSize/DataRate + \sigma. \tag{7.12}$$

Based on that, we formulate the average time the channel is busy due to an unsuccessful transmission, T_f, as follows:

$$\begin{aligned} T_f =& Pr(Ack_l|f) \times T_s + (1 - Pr(Ack_l|f)) \times T_{data} \\ =& \frac{(1-p_c)(1-p_e)p_e}{p} \times T_s \\ &+ (1 - \frac{(1-p_c)(1-p_e)p_e}{p}) \times T_{data}. \end{aligned} \tag{7.13}$$

So far, we have all the parameters to calculate the average length of a slot, $E[SlotLen]$, from Equation (7.8). However, to calculate the average delay of the confirmation packet, we have to find the average number of time slots, $E[\#Slots]$, before the station successfully transmits its confirmation packet. Since we know that the transmission probability in any time slot is τ and the probability of success when we have a transmission is $1 - p$, we can define the probability of success, p_s, in any time slot for any station as follows:

$$p_s = \tau(1-p). \tag{7.14}$$

Clearly, the sequence of transmission failures until the transmission is successful is mimicking a geometrical distribution with a success probability of p_s. Therefore, the expected number of time slots needed to transmit one packet is $1/p_s$. Thus, from Equations (7.14) and (7.2), we get:

$$\begin{aligned} E[\#Slots] &= \frac{1}{\tau(1-p)} \\ &= \frac{(1-2p)(W_{min}+1) + pW_{min}.(1-(2p)^m)}{2(1-2p)(1-p)} \end{aligned} \tag{7.15}$$

Finally, we estimate the average delay to transmit a packet, $E[d(n)]$, by a randomly chosen station among n competing stations as follows:

$$E[d(n)] = E[\#Slots] \times E[SlotLen] \tag{7.16}$$

It is important to note that this average delay, $E[d(n)]$, is estimated in the saturation case. This means, any randomly selected station will, on average, send one packet every $E[d(n)]$ second. Therefore, during this window of time, on average, n packets are successfully sent from the n stations to the AP. Since each station in our scenario has only one confirmation packet to send, then the average time needed for all n stations to successfully send their packets to the AP in saturation state is $E[d(n)]$.

7.4.2 Considering The Time For Transient Stages

It is important to note that the estimation of $E[d(n)]$ in Equation (7.16) is formulated by assuming the saturation condition. However, in our scenario, all stations start with the lowest contention window size, W_{min}, in their first try to send the confirmation packet. With each transmission failure, the contention window size is doubled, as shown in Equation (7.1), until the packet is successfully sent or the maximum contention widows size, W_{max}, is reached. In this work, we assume that although the contention window size starts at W_{min}, eventually, the average window size will reach the average window size of the saturation case especially when number of stations is large. The average contention window size in saturation state, $\overline{W}$, given p can be estimated as follows [81]:

$$\overline{W} = \frac{1 - p - p(2p)^m}{1 - 2p} \frac{W_{min}}{2}, \tag{7.17}$$

where, m represents the number of times the contention window size can double before it reaches W_{max}. Since the contention window size starts at W_{min} and go through some stages till it reaches $\overline{W}$, we should account for these transient stages in our model. In the first stage, all stations have their contention window size set to W_{min}. Thus, the average window size at this stage of all stations is $W_{min}/2$. If $\overline{W} > W_{min}/2$, then the first stage, stage (0), will be considered as a transit stage. In general, stage (i) is considered a transient stage if $\overline{W} > 2^i W_{min}/2$. In each transient stage (i) the transmission failure probability p and the average length of time slots $E[SlotLen]$ are calculated from our previous results but with $W_{max} = 2^i W_{min}$, *i.e.,* $m = i$. We denote p and $E[SlotLen]$ for stage (i) with p_i and $E[SlotLen]_i$, respectively. It should be noted that, in transient stage (i), the back off time of all stations is uniformly distributed on the contention window size of $W_{max} = 2^i W_{min}$. Thus, for a randomly selected station, the average number of time slots before the station attempts to transmit its packet is $2^i W_{min}/2$. Consequently, the transient time in stage (i),

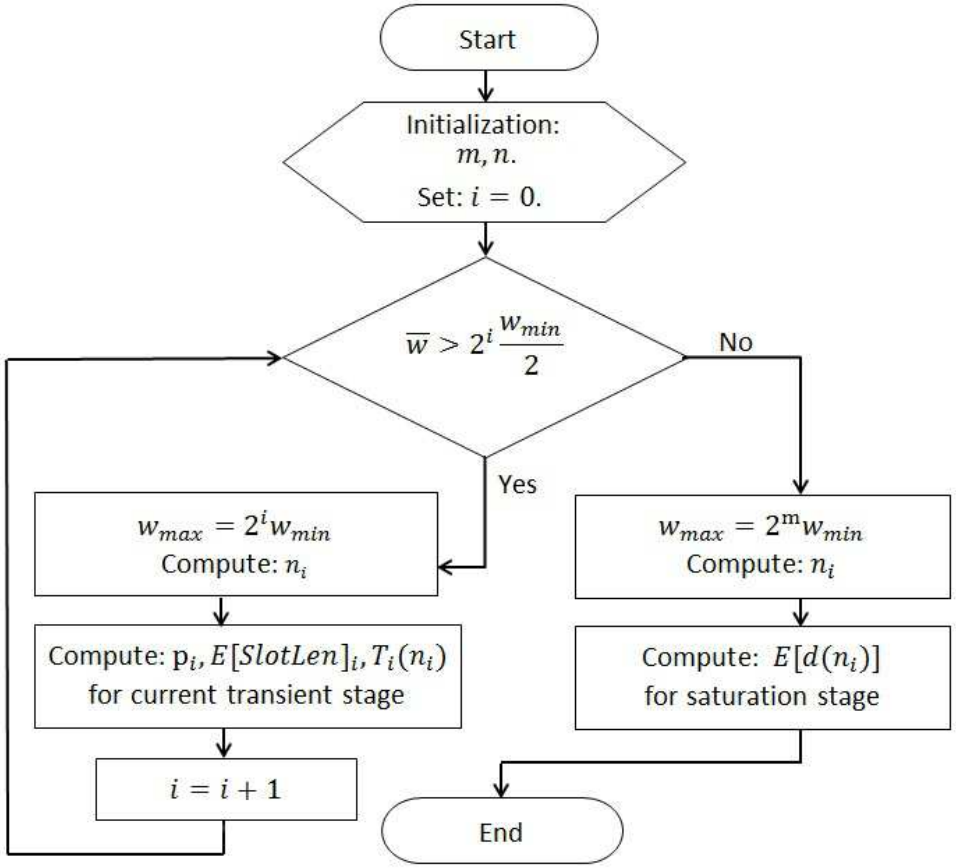

Figure 7.3: Transient stages calculation

$T_i(n_i)$, for a randomly selected station from n_i stations can be formulated as follows:

$$T_i(n_i) = E[SlotLen]_i \times 2^i W_{min}/2 \tag{7.18}$$

Also, the number of stations in each stage is different. Starting with n station in stage (0), the average number of stations in stage (i) can be calculated as follows:

$$n_i = \begin{cases} n, & \text{if } i = 0 \\ n_{i-1} - (n_{i-1}/2)(1 - p_{i-1}), & \text{if } i > 0, \end{cases} \tag{7.19}$$

As shown in Figure 7.3, these $T_i(n_i)$ are calculated for all transient stages until stage (i), at which $\overline{W} \leq 2^i W_{min}/2$, is reached. In this stage, we use Equation (7.16) to calculate $E[d(n_i]$, where, n_i represents the number of stations still trying to send their packet confirmation

packet. Thus, the average delay time, $D(n)$, can be calculated as follows:

$$\begin{aligned} D(n) =& (1-p_0)T_0(n_0) + p_0(1-p_1)T_1(n_1) + ... \\ &+ p_0p_1....p_{i-2}(1-p_{i-1})T_{i-1}(n_{i-1}) \\ &+ p_0p_1.....p_{i-1}E[d(n_i)], \end{aligned} \tag{7.20}$$

Equation (7.20) calculates the average delay to transmit the confirmation packet when n stations receive the broadcasted command packet successfully from the server. However, since the broadcasted packet is susceptible to the lossy wireless environment as well, the number of EVs, k, that will receive the broadcasted packet successfully out of the targeted n EVs follows a binomial distribution as follows:

$$Pr(X=k) = \binom{n}{k} \cdot (1-p_e)^k p_e^{n-k}, \tag{7.21}$$

where, $Pr(X=k)$ represents the probability of k EVs receiving the broadcast command out of the n intended EVs, and p_e is the packet loss probability. Therefore, when the server broadcasts a command to n EVs, the expected number of EVs that will receive the command successfully is $n(1-p_e)$ and the average delay for sending the confirmation packet successfully is as follows:

$$\overline{D(n)} = \sum_{k=1}^{n} [Pr(X=k)(D(k))] \tag{7.22}$$

7.5 Model Validation

To validate our models given in Equations (7.4-7.22), we simulate our scenario using the Network Simulation 2 (NS2) [82] tool. Different group sizes of EVs have been considered in this validation, namely, 20, 40, 60, and 80 EVs. Although there are several standards for IEEE 802.11 MAC protocol (*e.g.,* 802.11b, 802.11a, and 802.11g), 802.11g is considered by far the most popular one. Thus, for the purpose of this validation, we consider that all nodes (EVs and the AP) use 802.11g for their communication. Worth noting that the model is valid for other standards, such as 802.11b and 802.11a, since they use the same MAC protocol. The values of IEEE 802.11g standard parameters which are used in this validation for both the analytical model and the simulation are summarized in Table 7.1. Three different probabilities for data packet loss, $p_e \in \{0.01, 0.1, 0.3\}$, have been considered for validation. The results from the simulation alongside the results from our model are shown in Figures 7.4, 7.5, and 7.6 for each scenario of data packet loss probability. The x-axes represent the number of EVs, n, targeted by the server and the average number of EVs that received the packet successfully. The y-axis represents the average delay of sending a

Table 7.1: IEEE 802.11g parameters

Packet Payload	800 Bytes
MAC header	224 bits
PHY header	136 bits
ACK size	(112+PHY header) bits
Data Rate	54Mbps
Basic Rate	6Mbps
Slot Time (σ)	9 μs
SIFS	16 μs
DIFS	34 μs
W_{min}	31
W_{max}	1023
p_e	0.01, 0.1, 0.3

confirmation packet from those EVs which received the command packet successfully. It may be noted that the expected (average) number of EVs which will receive the command packet successfully out of n targeted EVs is $(n \times (1 - p_e))$. For example, as shown from the results in Figure 7.4, when the server broadcasted a command to 80 EVs with $p_e = 0.01$, on average, 79.2 EVs successfully received the command packet and sent their confirmation packets with average delay of 0.0382 seconds in the simulation and average delay of 0.0398 seconds in the model. In all scenarios of different packet loss probabilities and different number of EVs, the results from our model are accurately matching the results from the simulation.

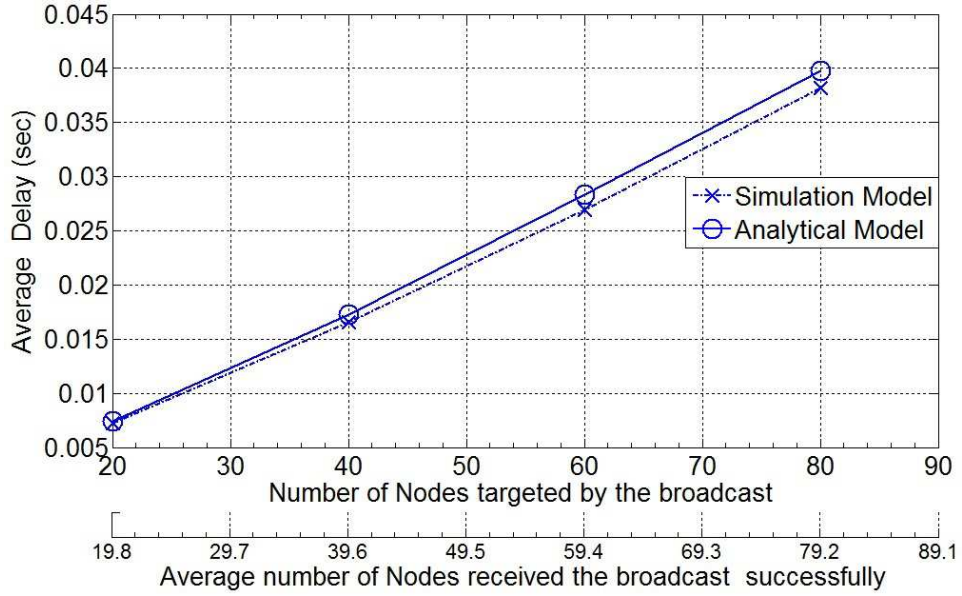

Figure 7.4: Average packet delay for 0.01 loss probability

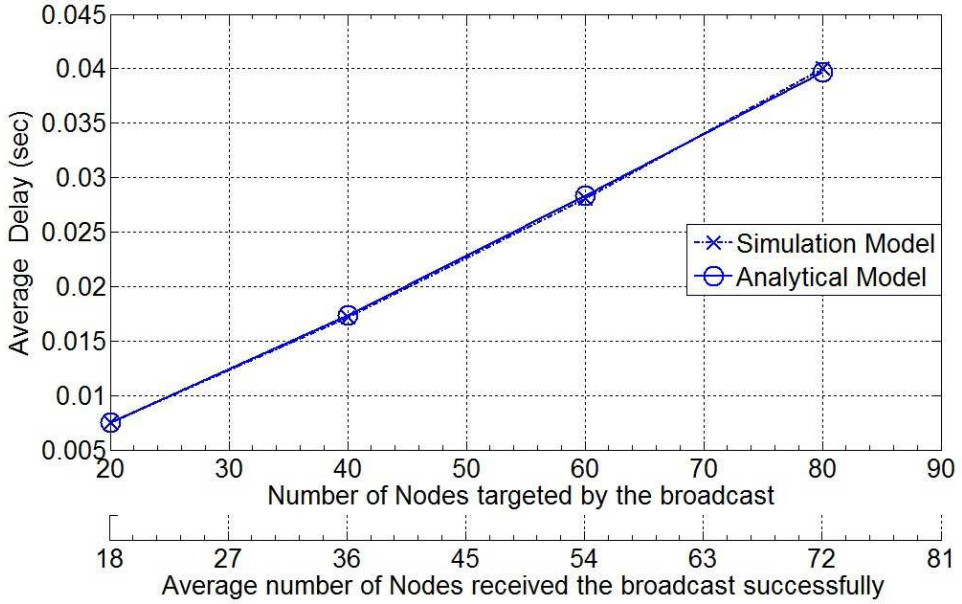

Figure 7.5: Average packet delay for 0.1 loss probability

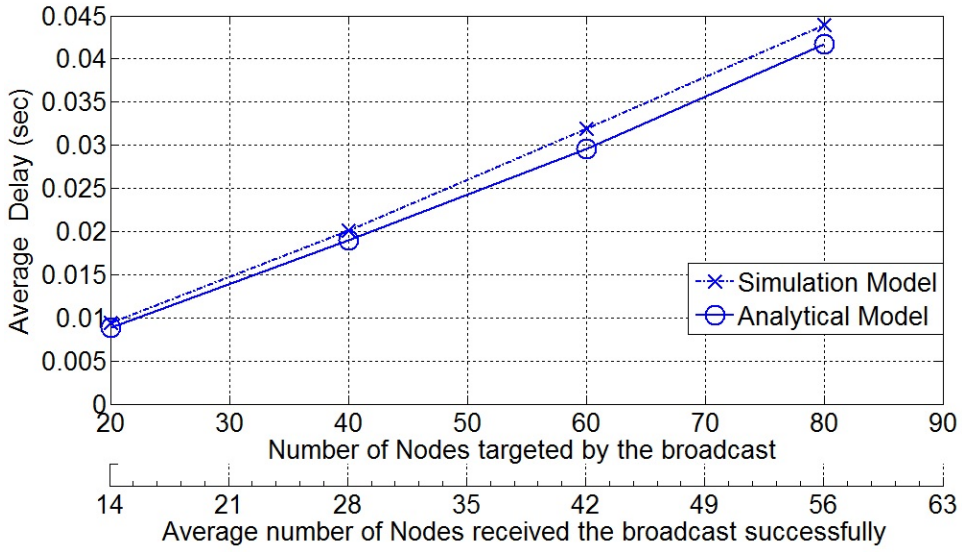

Figure 7.6: Average packet delay for 0.3 loss probability

7.6 The Maximum Number of EVs Supported by One AP

In this section, we answer the question of estimating the average delay from the instant when the aggregator server sends the first regulation command to n EVs to the instant when the responses of *all targeted* n EVs are received successfully by the server? And, consequently, we answer the question of estimating the maximum number of EVs which can be supported by only one AP without violating the delay limit?

In fact, this average delay time can be affected by three factors:

(i) The round trip time (RTT_{int}) of the internet link between the aggregator server and the AP.

(ii) The average delay time for the targeted n EVs to reply to the AP, denoted by $\overline{D(n)}$.

(iii) The average number of broadcasts needed to deliver the broadcast command to all the targeted n EVs.

In this context, we define the overall average delay time, T_D, from the point when an aggregator server sends a command packet to the point of receiving the confirmation

messages back from the EVs that received the command successfully as follows:

$$T_D = RTT_{int} + \overline{D(n)} \tag{7.23}$$

Note that T_D represents the average time for transmission of one command from the aggregator server. However, since we have a packet loss probability of p_e, we probably need more than one transmission to reach all the targeted n EVs. In fact, the probability that any targeted EV received the broadcasted command packet successfully after k broadcast attempts can be defined as follows:

$$Pr(BroadSuccess) = 1 - (p_e)^k \tag{7.24}$$

Thus, we can estimate the number of broadcast, k, needed to reach all EVs with a specific probability, $Pr(BroadSuccess)$, when the loss probability (p_e) is known using Equation (7.24). Also, the server should wait for a specific time after each broadcast before it proceeds to perform the next broadcast when not all the targeted EVs responded. We denote this time as a Retransmission Time-Out (RTO). In this work, we set $RTO = 2T_D$. Although this setting for RTO might be tight especially when the internet link is experiencing a significant RTT variance, we believe this setting is appropriate for two reasons. First, when RTO is tight, the overall delay to reach all EVs when more than one broadcast is needed will be shorter compared to longer RTOs. Second, when another broadcast is not needed but the server sends it due to a tight RTO, that would not affect the mechanism of EVs since they already responded to the earlier broadcast successfully and they will assume that the command is not meant for them. Thus, we calculate the overall time, T_{oa}, taken to get a response from all n targeted EVs with probability of $Pr(BroadSuccess)$ given that the probability of loss is p_e, as follows:

$$T_{oa} = (k-1)RTO + T_D, \tag{7.25}$$

where, k is the number of broadcasts computed from Equation (7.24) given $Pr(BroadSuccess)$ and p_e.
Figure 7.7 shows the results of the estimated overall time delay, T_{oa}, for different numbers of EVs. Three different loss probabilities have been examined; namely, $p_e = 0.01$, $p_e = 0.1$, and $p_e = 0.2$. To determine the number of broadcasts needed (*i.e.,* k in Equation (7.24)), the chance that all EVs receive the command packet successfully is set to be greater than 99.9%, *i.e.,* $Pr(BroadSuccess) = 0.999$. Also, we have set our RTT_{int} to the average internet RTT in Canada (96.43 ms) as reported by Canadian Internet Registration Authority (CIRA) [19].

The results in Figure 7.7 show that the maximum number of EVs which can be managed by one AP differ with different packet loss probabilities. One AP is sufficient to successfully deliver the regulation command to more than 1000 EVs within 4 seconds when $p_e = 0.01$. However, this number decreases significantly, less than 500 EVs, when the wireless link

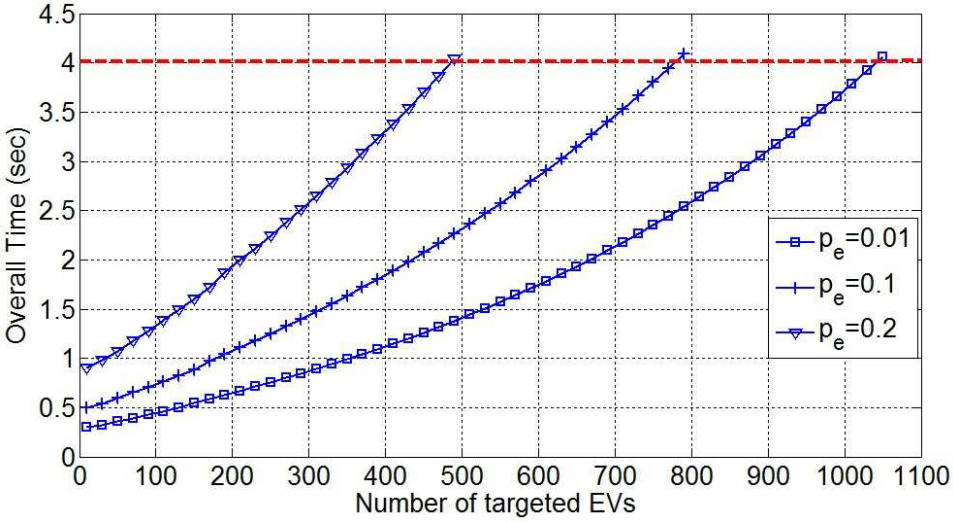

Figure 7.7: The Overall Time Delay (T_{oa})

is experiencing a significant packet loss at $p_e = 0.2$. Further, low latency is generally valued in providing regulation services to the grid. Typically, faster response is better. The aggregator company can even offer less than 4 seconds as a response time to compete with offers from other companies. For example, reference [13] suggests that the round-trip time should be of the order of one or two seconds. In this context, our findings are helpful to the aggregator to decide on how many EVs covered by one AP should be participating in order to ensure their offered latency boundary.

Additionally, the EVs which are assumed to have the capability of providing the regulation services should be connected to Level 2 smart chargers with a maximum charge power of 3.3 kW per EV [61]. Thus, a contract for 1 MW of regulation needs around 606 EVs charging at the rate of 1.65 kW so they can increase their charging by 1 MW when all EVs are charging at maximum charging power (3.3 kW) or decrease their charging by 1 MW when all are off. From our results in Figure 7.7, this number of EVs, when all of them are covered by one AP, is guaranteed (with probability of 0.999) to respond to a command from the server within 2 seconds when $p_e = 0.01$, and within 3 seconds when $p_e = 0.1$. However, when the probability of loss is very bad, *e.g.,* $p_e = 0.2$, the response time cannot be guaranteed to be less than 4 seconds. In the latter case, the aggregator can manage a subset of these EVs at a time to ensure that the maximum response time is within the limit. For example, the 606 EVs can be divided into two groups, each with 303 EVs. The base load can be achieved by having one group charging at the maximum charging power and the other group remaining off. To increase 1 MW load to the base, the off group is commanded to start charging at the maximum charging rate. To decrease 1 MW from the base, the charging group is commanded to stop charging. Since at most

303 EVs are commanded at a time, the maximum response time can be assured to be within 2.5 seconds even when $p_e = 0.2$, as shown by the results in Figure 7.7. In fact, the regulation method proposed in Chapter 6 commands the EVs to either start charging with the maximum allowed charging rate r_{max} or stop charging. Thus, the number of EVs needed to meet the targeted POP(t) at any moment will be the minimum. Consequently, the number of EVs communicating with the with the server at any moment of time will be minimum. This will, definitely, reduce the response time to the regulation signals.

7.7 Summary

In this chapter, we have accurately modeled the average delay time for a group of EVs covered by one Access Point (AP) from the instant when these EVs receive the broadcast command from the AP to the instant when all of these EVs successfully send back their confirmations. The AP and EVs are assumed to use the IEEE 802.11g MAC protocol to communicate. Although our model relies on a previous Markov chain model representation for the contention window size of the 802.11 MAC protocol in saturation state, two additional important factors have been considered in our model. First, the effect of a lossy wireless link between the EVs and the AP has been added to the model, and its impact on the delay has been measured. Second, the transient stages of the contention window size before the average contention window size of the saturation state has been reached are considered in our model. The model is validated by comparing its results to the results obtained from the NS2 simulator. The validation shows that our model is accurately capturing the average delay time of successfully sent confirmation packets for different number of EVs with different wireless link qualities. Further, this model has been used to estimate an upper bound for the number of EVs which can be managed by the aggregator server through one AP in order to comply with a given maximum response time limit (*e.g.,* 4 seconds). Finally, we showed that the regulation method proposed in Chapter 6 achieves the same regulation service but with a better response time compared to commanding all charging EVs every time.

Chapter 8

Conclusion and Future Work

8.1 Summary and Conclusion

Integration of renewable energy sources (RES) into electric grids comes with significant challenges. The intermittency of RES, especially wind and solar, necessitates more operational flexibility in the grid. A direct way to increase the operational flexibility in the electric grid is to increase the capacity of the operational reserve. Clearly, the increase in operational reserve is an expensive option. In **Chapter** 2, the RES represented by wind power have been reviewed. The forecast error of the wind power is investigated. Also, the conventional load in the electric grid has been reviewed. The forecast methods and techniques of the conventional load have been summarized. Additionally, the forecast error behaviour of the conventional load is reviewed. The combined forecast error of the RES and conventional load represent the stochastic behaviour of the net-load in the electric grid. This stochastic behaviour has a direct impact on the amount of the operational reserve needed to maintain reliable services in the grid.

On the other hand, EVs are expected to be more popular in the near future. Fortunately, EVs are considered to be flexible loads. For 90-95% of the time, vehicles are parked somewhere and theoretically available for charging. This gives the opportunity to choose the right time to charge these EVs in order to serve the interest of both the customers (*e.g.,* cheaper energy price) and the electric grid (*e.g.,* flattening the overall load in the system). **Chapter** 3 has been dedicated to investigate the impact of uncontrolled charging of EVs on the distribution system. Also, smart charging algorithms and techniques proposed in the literature to mitigate some of the problems caused by the uncontrolled charging of EVs have been reviewed.

Based on the findings in Chapters 2 and 3, this thesis moved forward to exploit the flexibility of the EVs not only to optimize the charging time of the EVs ahead of time but also to dynamically adjust the charging rates of the EVs at real time to encounter the

stochastic behaviour of the net-load in the system. As first step, the thesis investigated the net-load forecast error in **Chapter** 4. The net-load forecast error is modeled as a normally distributed random variable. This random variable captures the stochastic behaviour of the net-load with different penetration levels of the RES.

In **Chapter** 5, we introduced our novel online charging algorithm for EVs. The algorithm has two stages; offline stage and online stage. In the offline stage, the charging time of the EVs is optimized ahead of time in order to flatten the overall load in the distribution system. However, since the net-load forecast is not accurate as shown in Chapter 4, the online stage of the proposed algorithm deals with this forecast error when it appears at real time by sending commands to the EVs in order to adjust their charging rates accordingly. Results show that our algorithm clearly outperforms the traditional ahead-of-time scheduling algorithm in absorbing the fluctuations in the net-load. This mechanism of absorbing the unexpected fluctuations in the net-load will effectively reduce the dependency on the expensive operational reserve needed otherwise to deal with these fluctuations.

In **Chapter** 6, we used EVs to provide regulation services to the grid. The algorithm maintains approximately the same structure as in Chapter 5. However, instead of reacting to the net-load variability, the algorithm follows the AGC signals from ISO. Compared to a unidirectional regulation approach used as a benchmark, our regulation method shows a better performance in terms of both complying with AGC signals and delivering the requested charging energy by the customers within the dictated deadlines.

Our algorithm uses commands to adjust the charging rates of the EVs at real time. Thus, the response time for these commands critical especially when providing regulation services as explained in Chapter 6. Therefore, **Chapter** 7 in the thesis has been devoted to precisely evaluate the response time of group of EVs to a command from an aggregator server. To achieve this goal, first, a realistic communication structure between the aggregator server and the EVs is considered. Second, the wireless link between the access point (AP) and the EVs is accurately modeled. The model has been validated by means of extensive simulation using the well-known Network Simulator 2 (NS2) tool. The validation shows that our model is accurately capturing the average delay time of successfully responding to a command from the aggregator server by different number of EVs with different wireless link qualities. Further, this model has been used to estimate an upper bound for the number of EVs which can be managed by the aggregator server through one AP in order to comply with a given maximum response time limit (*e.g.,* 4 seconds).

8.2 Summary of Contributions

This thesis makes the following contributions:

- It evaluates the forecast error of the net-load in the system. This error has been

modeled as a random variable, ε. The distribution of this random variable is estimated. Further, the parameters of this distribution are measured against different penetration levels of wind energy.

- The shortcomings of the traditional EVs scheduling algorithms in dealing with the net-load forecast error are explained. In fact, these traditional EVs scheduling algorithms optimize the charging time of the EVs ahead of time based on the forecast of the load in the system assuming that the forecast of the load or the net-load is accurate.

- It shows that the energy consumed by the overall load in the system can be estimated ahead of time despite the stochastic behavior of the net-load and that this estimation gets more accurate as the period of time over which this estimation is done increases. This fact is formulated as a theorem. The theorem proof is provided. This fact is important in designing the mechanism of the proposed online algorithm.

- It proposes a novel online charging algorithm for EVs in electric grids. Unlike traditional charging methods, this algorithm is designed to exploit the flexibility of the EVs load to absorb the unforeseen fluctuations in the net-load caused mainly by the intermittency of the renewable energy sources (wind energy). Also, unlike most of the charging algorithms in literature, the proposed algorithm considers keeping the charging rate constant, thus, imposing less technical and engineering requirements and complexity on the EVs charging infrastructure. To test the performance of the proposed online charging algorithm, a tool has been developed in Java to simulate our algorithm. A comprehensive performance evaluation of the algorithm against a traditional Ahead-of-Time charging algorithm shows clear improvements achieved by our algorithm in absorbing the unexpected fluctuations in the net-load caused mainly by the stochastic behavior of the produced wind power.

- It introduces a new regulation method that uses the flexibility of EVs to provide the regulation service to the grid during the optimum charging period. The method uses binary on-off commands to guide the EVs in order to provide the regulation service as opposed to adjusting the charging rates of the EVs to any value between zero and maximum charging rate in most of the other studies in the literature. A simple unidirectional regulation method has been used as a benchmark in this study to show the better performance of our method. Also, real data from US Department of Transportation (DOT) and California ISO have been used in the testing scenarios. Results show that our method has achieved better performance compared to the benchmark method in terms of meeting the requested charging energy by the EVs within the imposed deadline times by the customers. Also, the average number of charging interruptions per EV has been reduced by our method compared to the benchmark method and, consequently, the active charging times of the EVs are shortened.

- As a fast response to the regulation commands is crucial to providing reliable regulation service to the grid, this thesis precisely evaluates the expected time delay from the instant when an aggregator server sends a regulation command to n EVs to the instant when all the EVs' responses are received successfully by the server. To achieve this goal, first, a realistic communication structure between the aggregator server and the EVs is considered. Second, the wireless link between the access point (AP) and the EVs is accurately modeled. The model is based on Markov chain representation for the wireless IEEE 802.11 MAC protocol. Two important factors are considered in this model. First, the packet loss probability due to the lossy wireless environment. Second, the transition stages for the contention window size of 802.11 MAC protocol to reach the saturation stage is taken into account. The model has been validated by means of extensive simulation using the well-known Network Simulator 2 (NS2) tool. Our analysis shows that one AP is capable of handling up to 1000 EVs without violating the four second latency limit imposed by some ISOs (*e.g.,* California ISO) when the probability of packet loss is 0.01. However, this number decreases significantly, less than 500 EVs, when the wireless link is experiencing a significant packet loss probability of 0.2. Further, we show that by commanding a sub-group of the charging EVs, it is possible to achieve the same regulation service but with a shorter delay, compared to commanding all charging EVs every time.

8.3 Future Research Work

The overall objective of this research is to use the flexibility of EVs load in order to provide services to the electric grid and to satisfy the customers' requirements at the same time. This objective has been achieved through the design and implementation of a dynamic online charging algorithm capable of adjusting the overall charging rate of the EVs at real time. The work presented in this thesis, however, still has the potential for various extensions and directions for future work, as listed in the following bullet points:

- Although the technical constraints of the distribution system (*e.g.,* the maximum allowed current in the cables and the maximum transformers load) are not violated in normal operating conditions, our algorithm should take these constraints into consideration to protect the system during unexpected operational conditions, such as too many EVs charging at the same time.

- The algorithm uses communication infrastructure such as internet to deliver information and control commands between the aggregator server and the EVs. Therefore, cybersecurity should be a concern. For instance, if an attacker gains a control of large number of EVs and commands them to start charging at the same time, that can possibly over load the distribution system and results in electricity outages. Thus, a secure channel between the aggregator server and the EVs is needed.

- In Chapter 6, the EVs have been used to provide regulation services to the grid. It has been, however, assumed that the AGC signals' average is zero. In other words, it has been assumed that the amount of energy taking from the EVs to provide regulation-up is equal to the amount of energy taken by the EVs to provide regulation-down during the regulation period. However, the algorithm can easily be extended to provide regulation-up only as some ISOs require. This can be achieved by readjusting the preferred operating point (POP) of the EVs to include both the requested energy for charging the EVs' batteries and the amount of energy needed to provide the regulation-up services.

References

[1] California Independent System Operator area, CAISO. http://www.oasis.caiso.com/. Accessed: 2017-01-20.

[2] EIA, U.S. Energy Information Administration. http://www.eia.gov. Accessed: 2014-07-20.

[3] EPA, The United States Environmental Protection Agency . http://www.epa.gov/. Accessed: 2014-04-21.

[4] Pathways to high penetration of electric vehicles 2013. http://www.theccc.org.uk. Accessed: 2014-04-23.

[5] RWE npower renewables, the royal academy of engineering. http://www.raeng.org.uk/education/diploma/maths/pdf/exemplars_advanced/23_Wind_Turbine.pdf. Accessed: 2014-07-30.

[6] S. Amjad, S. Neelakrishnan, and R. Rudramoorthy. Review of design considerations and technological challenges for successful development and deployment of plug-in hybrid electric vehicles. *Renewable and Sustainable Energy Reviews*, 14(3):1104 – 1110, 2010.

[7] R. Barth, H. Brand, P. Meibom, and C. Weber. A stochastic unit-commitment model for the evaluation of the impacts of integration of large amounts of intermittent wind power. In *Probabilistic Methods Applied to Power Systems, 2006. PMAPS 2006. International Conference on*, pages 1–8. IEEE, 2006.

[8] G. Bianchi. Performance analysis of the IEEE 802.11 distributed coordination function. *IEEE Journal on selected areas in communications*, 18(3):535–547, 2000.

[9] A. Bilh, K. Naik, and R. El-shatshat. A novel online charging algorithm for electric vehicles under stochastic net-load. *IEEE Transactions on Smart Grid*, to be published, accepted in 2016.

[10] A. Bilh, K. Naik, and R. El-Shatshat. An adaptive charging algorithm for electric vehicles in smart grids. In *Vehicular Technology Conference (VTC Spring), 2015 IEEE 81st*, pages 1–7. IEEE, 2015.

[11] F. Bouffard and F. D. Galiana. Stochastic security for operations planning with significant wind power generation. In *Power and Energy Society General Meeting-Conversion and Delivery of Electrical Energy in the 21st Century, 2008 IEEE*, pages 1–11. IEEE, 2008.

[12] A. Boulanger, A. Chu, S. Maxx, and D. Waltz. Vehicle electrification: Status and issues. *Proceedings of the IEEE*, 99(6):1116–1138, 2011.

[13] A. Brooks, E. Lu, D. Reicher, C. Spirakis, and B. Weihl. Demand dispatch. *IEEE Power and Energy Mag.*, 8(3):20–29, 2010.

[14] A. Brooks and S. H. Thesen. PG&E and tesla motors: Vehicle to grid demonstration and evaluation program. In *Proc. 23rd Elect. Veh. Symp*, pages 1–10, 2007.

[15] A. N. Brooks. *Vehicle-to-grid demonstration project: Grid regulation ancillary service with a battery electric vehicle*. California Environmental Protection Agency, Air Resources Board, Research Division, 2002.

[16] California ISO. ISO generation monitoring and control requirements for AGC/Regulation Units. *URL: http://citeseerx.ist.psu.edu*, 2007. Accessed: 2016-12-20.

[17] Y. Cao, S. Tang, C. Li, P. Zhang, Y. Tan, Z. Zhang, and J. Li. An optimized ev charging model considering tou price and soc curve. *Smart Grid, IEEE Transactions on*, 3(1):388–393, 2012.

[18] H. Chen, C. A. Canizares, and A. Singh. Ann-based short-term load forecasting in electricity markets. In *Power Engineering Society Winter Meeting, 2001. IEEE*, volume 2, pages 411–415. IEEE, 2001.

[19] CIRA. CANADAS INTERNET PERFORMANCE: NATIONAL, PROVINCIAL AND MUNICIPAL ANALYSIS. *URL: https://cira.ca/sites/default/files/canadas-internet-performance-report.pdf*, 2016.

[20] K. Clement, E. Haesen, and J. Driesen. Coordinated charging of multiple plug-in hybrid EVs in residential distribution grids. In *Power Sys. Conf. and Expo. PSCE'09. IEEE/PES*, pages 1–7. IEEE, 2009.

[21] K. Clement-Nyns, E. Haesen, and J. Driesen. The impact of charging plug-in hybrid electric vehicles on a residential distribution grid. *Power Systems, IEEE Transactions on*, 25(1):371–380, 2010.

[22] A. Costa, A. Crespo, J. Navarro, G. Lizcano, H. Madsen, and E. Feitosa. A review on the young history of the wind power short-term prediction. *Renewable and Sustainable Energy Reviews*, 12(6):1725–1744, 2008.

[23] R. Doherty and M. O'Malley. A new approach to quantify reserve demand in systems with significant installed wind capacity. *Power Systems, IEEE Transactions on*, 20(2):587–595, 2005.

[24] K. J. Dyke, N. Schofield, and M. Barnes. The impact of transport electrification on electrical networks. *IEEE Transactions on Industrial Electronics*, 57(12):3917–3926, Dec 2010.

[25] Federal Energy Regulatory Commission. Frequency regulation compensation in the organized wholesale power markets. *Order*, (755), 2011.

[26] E. A. Feinberg and D. Genethliou. Load forecasting. In *Applied mathematics for restructured electric power systems*, pages 269–285. Springer, 2005.

[27] E. A. Feinberg, J. Hajagos, and D. Genethliou. Load pocket modeling. In *Proceedings of the 2nd IASTED International Conference: Power and Energy Systems*, pages 50–54. Citeseer, 2002.

[28] E. A. Feinberg, J. Hajagos, and D. Genethliou. Statistical load modeling. In *Proceedings of the 7th IASTED International Multi-Conference: Power and Energy Systems*, pages 88–91, 2003.

[29] L. Gan, U. Topcu, and S. Low. Optimal decentralized protocol for electric vehicle charging. *Power Systems, IEEE Transactions on*, 28(2):940–951, May 2013.

[30] L. Gan, U. Topcu, and S. H. Low. Stochastic distributed protocol for electric vehicle charging with discrete charging rate. In *Power and Energy Society General Meeting, 2012 IEEE*, pages 1–8. IEEE, 2012.

[31] J. Gomez and M. Morcos. Impact of ev battery chargers on the power quality of distribution systems. *Power Delivery, IEEE Transactions on*, 18(3):975–981, 2003.

[32] R. C. Green II, L. Wang, and M. Alam. The impact of plug-in hybrid electric vehicles on distribution networks: A review and outlook. *Renewable and Sustainable Energy Reviews*, 15(1):544–553, 2011.

[33] A. Halbleib, M. Turner, and J. Naber. Control of battery electric vehicle charging for commercial time of day demand rate payers. In *Innovative Smart Grid Technologies (ISGT), 2012 IEEE PES*, pages 1–5, Jan 2012.

[34] R. Halvgaard, N. K. Poulsen, H. Madsen, J. Jorgensen, F. Marra, and D. E. M. Bondy. Electric vehicle charge planning using economic model predictive control. In *Electric Vehicle Conference (IEVC), 2012 IEEE International*, pages 1–6. IEEE, 2012.

[35] U. Helman. Resource and transmission planning to achieve a 33% rps in California–ISO modeling tools and planning framework. In *FERC Tech. Conf. on Planning Models and Software*, volume 2010, 2010.

[36] B. Hodge, A. Florita, K. Orwig, D. Lew, and M. Milligan. A comparison of wind power and load forecasting error distributions. In *2012 World Renewable Energy Forum*, pages 13–17, 2012.

[37] W. Hu, C. Su, Z. Chen, and B. Bak-Jensen. Optimal operation of plug-in electric vehicles in power systems with high wind power penetrations. *Sustainable Energy, IEEE Transactions on*, 4(3):577–585, 2013.

[38] IEEE Computer Society LAN MAN Standards Committee. Wireless LAN medium access control (MAC) and physical layer (PHY) specifications, 1997.

[39] W. Kempton and J. Tomić. Vehicle-to-grid power fundamentals: calculating capacity and net revenue. *Journal of power sources*, 144(1):268–279, 2005.

[40] W. Kempton, V. Udo, K. Huber, K. Komara, S. Letendre, S. Baker, D. Brunner, and N. Pearre. A test of vehicle-to-grid (V2G) for energy storage and frequency regulation in the PJM system. *Results from an Industry-University Research Partnership*, 32, 2008.

[41] M. E. Khodayar, L. Wu, and M. Shahidehpour. Hourly coordination of electric vehicle operation and volatile wind power generation in scuc. *Smart Grid, IEEE Transactions on*, 3(3):1271–1279, 2012.

[42] A. Khotanzad, R. Afkhami-Rohani, and D. Maratukulam. Annstlf-artificial neural network short-term load forecaster generation three. *Power Systems, IEEE Transactions on*, 13(4):1413–1422, 1998.

[43] B. Kirby. Ancillary services: Technical and commercial insights. 2007.

[44] B. J. Kirby. *Frequency regulation basics and trends*. United States. Department of Energy, 2005.

[45] L. Landberg, G. Giebel, H. A. Nielsen, T. Nielsen, and H. Madsen. Short-term predictionan overview. *Wind Energy*, 6(3):273–280, 2003.

[46] M. Lange and D. Heinemann. Accuracy of short term wind power predictions depending on meteorological conditions. In *CD-Proc. of the 2002 Global Windpower Conference, Paris, France*, 2002.

[47] E. Lannoye, D. Flynn, and M. O'Malley. Evaluation of power system flexibility. *Power Systems, IEEE Transactions on*, 27(2):922–931, 2012.

[48] M. Lei, L. Shiyan, J. Chuanwen, L. Hongling, and Z. Yan. A review on the forecasting of wind speed and generated power. *Renewable and Sustainable Energy Reviews*, 13(4):915–920, 2009.

[49] Q. Li, T. Cui, R. Negi, F. Franchetti, and M. D. Ilic. On-line decentralized charging of plug-in electric vehicles in power systems. *arXiv preprint arXiv:1106.5063*, 2011.

[50] J. Lin, K.-C. Leung, and V. O. Li. Online scheduling for vehicle-to-grid regulation service. In *Smart Grid Communications (SmartGridComm), 2013 IEEE International Conference on*, pages 43–48. IEEE, 2013.

[51] J. P. Lopes, F. J. Soares, P. Almeida, and M. M. da Silva. Smart charging strategies for electric vehicles: Enhancing grid performance and maximizing the use of variable renewable energy resources. In *EVS24 Intenational Battery, Hybrid and Fuell Cell Electric Vehicle Symposium, Stavanger, Norveška*, 2009.

[52] J. Lopes, F. Soares, and P. Almeida. Integration of electric vehicles in the electric power system. *Proceedings of the IEEE*, 99(1):168–183, 2011.

[53] H. Madsen, G. Kariniotakis, H. A. Nielsen, T. S. Nielsen, and P. Pinson. A protocol for standardizing the performance evaluation of short-term wind power prediction models. *Technical University of Denmark, IMM, Lyngby, Denmark, Deliverable ENK5-CT-2002-00665*, 2004.

[54] A. Majumder et al. Power line communications. *Potentials, IEEE*, 23(4):4–8, 2004.

[55] Y. V. Makarov, C. Loutan, J. Ma, and P. de Mello. Operational impacts of wind generation on california power systems. *Power Systems, IEEE Transactions on*, 24(2):1039–1050, 2009.

[56] F. Marra, E. Larsen, and C. Træholt. *Electric Vehicles Integration in the Electric Power System with Intermittent Energy Sources-The Charge/Discharge infrastructure*. PhD thesis, Technical University of DenmarkDanmarks Tekniske Universitet, Department of Electric Power EngineeringInstitut for Elteknik, 2013.

[57] F. Marra, G. Y. Yang, C. Traholt, E. Larsen, C. N. Rasmussen, and S. You. Demand profile study of battery electric vehicle under different charging options. In *Power and Energy Society General Meeting, 2012 IEEE*, pages 1–7. IEEE, 2012.

[58] B. K. Mauch. Managing wind power forecast uncertainty in electric grids. 2012.

[59] C. Moehrlen. Uncertainty in wind energy forecasting. 2004.

[60] C. Monteiro, R. Bessa, V. Miranda, A. Botterud, J. Wang, G. Conzelmann, et al. Wind power forecasting: state-of-the-art 2009. Technical report, Argonne National Laboratory (ANL), 2009.

[61] K. Morrow, D. Karner, and J. Francfort. Plug-in hybrid electric vehicle charging infrastructure review. *US Department of Energy- Vehicle Technologies Program*, 2008.

[62] P. Moses, M. A. S. Masoum, and S. Hajforoosh. Overloading of distribution transformers in smart grid due to uncoordinated charging of plug-in electric vehicles. In *Innovative Smart Grid Technologies (ISGT), 2012 IEEE PES*, pages 1–6, Jan 2012.

[63] Y. Mou, H. Xing, Z. Lin, and M. Fu. Decentralized optimal demand-side management for phev charging in a smart grid. *Smart Grid, IEEE Transactions on*, 6(2):726–736, 2015.

[64] R. F. Nelson. Power requirements for batteries in hybrid electric vehicles. *Journal of power sources*, 91(1):2–26, 2000.

[65] M. A. Ortega-Vazquez and D. S. Kirschen. Estimating the spinning reserve requirements in systems with significant wind power generation penetration. *Power Systems, IEEE Transactions on*, 24(1):114–124, 2009.

[66] G. Putrus, P. Suwanapingkarl, D. Johnston, E. Bentley, and M. Narayana. Impact of electric vehicles on power distribution networks. In *Vehicle Power and Propulsion Conf., 2009. VPPC'09.*, pages 827–831. IEEE.

[67] K. Qian, C. Zhou, M. Allan, and Y. Yuan. Modeling of load demand due to ev battery charging in distribution systems. *Power Systems, IEEE Transactions on*, 26(2):802–810, 2011.

[68] K. Qian, C. Zhou, M. Allan, and Y. Yuan. Modeling of load demand due to ev battery charging in distribution systems. *Power Systems, IEEE Transactions on*, 26(2):802–810, 2011.

[69] S. Rahman. Formulation and analysis of a rule-based short-term load forecasting algorithm. *Proceedings of the IEEE*, 78(5):805–816, 1990.

[70] S. Rahman and G. B. Shrestha. An investigation into the impact of electric vehicle load on the electric utility distribution system. *IEEE Transactions on Power Delivery*, 8(2):591–597, Apr 1993.

[71] S. Rahman and G. B. Shrestha. An investigation into the impact of electric vehicle load on the electric utility distribution system. *IEEE Transactions on Power Delivery*, 8(2):591–597, Apr 1993.

[72] A. Y. Saber and G. K. Venayagamoorthy. Resource scheduling under uncertainty in a smart grid with renewables and plug-in vehicles. *IEEE Systems Journal*, 6(1):103–109, March 2012.

[73] A. Santos, N. McGuckin, H. Y. Nakamoto, D. Gray, and S. Liss. Summary of travel trends: 2009 national household travel survey. Technical report, 2011.

[74] S. Shafiee, M. Fotuhi-Firuzabad, and M. Rastegar. Investigating the impacts of plug-in hybrid electric vehicles on power distribution systems. *Smart Grid, IEEE Transactions on*, 4(3):1351–1360, 2013.

[75] S. Shao, T. Zhang, M. Pipattanasomporn, and S. Rahman. Impact of tou rates on distribution load shapes in a smart grid with phev penetration. In *Transmission and Distribution Conference and Exposition, 2010 IEEE PES*, pages 1–6. IEEE, 2010.

[76] E. Sortomme and K. W. Cheung. Intelligent dispatch of electric vehicles performing vehicle-to-grid regulation. In *2012 IEEE International Electric Vehicle Conference*, pages 1–6, March 2012.

[77] E. Sortomme, M. M. Hindi, S. J. MacPherson, and S. Venkata. Coordinated charging of plug-in hybrid electric vehicles to minimize distribution system losses. *Smart Grid, IEEE Transactions on*, 2(1):198–205, 2011.

[78] W. Su, H. Eichi, W. Zeng, and M.-Y. Chow. A survey on the electrification of transportation in a smart grid environment. *Industrial Informatics, IEEE Transactions on*, 8(1):1–10, 2012.

[79] S. Sun, M. Dong, and B. Liang. Real-time welfare-maximizing regulation allocation in dynamic aggregator-evs system. *IEEE Transactions on Smart Grid*, 5(3):1397–1409, 2014.

[80] O. Sundstrom and C. Binding. Flexible charging optimization for electric vehicles considering distribution grid constraints. *Smart Grid, IEEE Transactions on*, 3(1):26–37, March 2012.

[81] Y. Tay and K. C. Chua. A capacity analysis for the IEEE 802.11 MAC protocol. *Wireless networks*, 7(2):159–171, 2001.

[82] The VINT Project. The UCB/LBNL/VINT Network Simulator-ns (version 2). *URL: http://www.isi.edu/nsnam/ns/*, 1999.

[83] J. Tomić and W. Kempton. Using fleets of electric-drive vehicles for grid support. *Journal of power sources*, 168(2):459–468, 2007.

[84] A. Tuohy, P. Meibom, E. Denny, and M. O'Malley. Benefits of stochastic scheduling for power systems with significant installed wind power. In *Probabilistic Methods Applied to Power Systems, 2008. PMAPS'08. Proceedings of the 10th International Conference on*, pages 1–7. IEEE, 2008.

[85] J. Usaola, O. Ravelo, G. Gonzalez, F. Soto, M. C. Dávila, and B. Díaz-Guerra. Benefits for wind energy in electricity markets from using short term wind power prediction tools; a simulation study. *Wind Engineering*, 28(1):119–127, 2004.

[86] S. I. Vagropoulos and A. G. Bakirtzis. Optimal bidding strategy for electric vehicle aggregators in electricity markets. *IEEE Transactions on power systems*, 28(4):4031–4041, 2013.

[87] S. I. Vagropoulos, D. K. Kyriazidis, and A. G. Bakirtzis. Real-time charging management framework for electric vehicle aggregators in a market environment. *IEEE Transactions on Smart Grid*, 7(2):948–957, 2016.

[88] O. Van Vliet, A. S. Brouwer, T. Kuramochi, M. van Den Broek, and A. Faaij. Energy use, cost and co 2 emissions of electric cars. *Journal of Power Sources*, 196(4):2298–2310, 2011.

[89] D. Wu, D. Aliprantis, and K. Gkritza. Electric energy and power consumption by light-duty plug-in electric vehicles. *Power Systems, IEEE Transactions on*, 26(2):738–746, May 2011.

[90] D. Wu, D. Aliprantis, and K. Gkritza. Electric energy and power consumption by light-duty plug-in electric vehicles. *Power Systems, IEEE Transactions on*, 26(2):738–746, 2011.

[91] T. Wu, Q. Yang, Z. Bao, and W. Yan. Coordinated energy dispatching in microgrid with wind power generation and plug-in electric vehicles. *Smart Grid, IEEE Transactions on*, 4(3):1453–1463, 2013.

[92] Y.-K. Wu and J.-S. Hong. A literature review of wind forecasting technology in the world. In *Power Tech, 2007 IEEE Lausanne*, pages 504–509. IEEE, 2007.

[93] S. Xu, D. Feng, Z. Yan, L. Zhang, N. Li, L. Jing, and J. Wang. Ant-based swarm algorithm for charging coordination of electric vehicles. *International Journal of Distributed Sensor Networks*, 2013, 2013.

[94] E. Yao, V. W. Wong, and R. Schober. A robust design of electric vehicle frequency regulation service. In *Smart Grid Communications (SmartGridComm), 2014 IEEE International Conference on*, pages 698–703. IEEE, 2014.

[95] E. Yao, V. W. Wong, and R. Schober. Robust frequency regulation capacity scheduling algorithm for electric vehicles. *IEEE Transactions on Smart Grid*, 8(2):984–997, 2017.

[96] M. Yilmaz and P. T. Krein. Review of the impact of vehicle-to-grid technologies on distribution systems and utility interfaces. *Power Electronics, IEEE Transactions on*, 28(12):5673–5689, 2013.